A novel function of the endothelial thrombomodulin-protein C

system for cellular function in the CNS

Dissertation

zur Erlangung des akademischen Grades

doctor rerum naturalium

(Dr. rer. nat.)

genehmigt durch die Fakultät für Naturwissenschaften

der Otto-von-Guericke-Universität Magdeburg

von   Dipl. biol. Juliane Wolter

geb. am 30.10.1981   in Salzwedel

Gutachter: Prof. Dr. med. Berend Isermann

Prof. Dr. med. Triantafyllos Chavakis

eingereicht am: 26.10.2015

verteidigt am: 04.04.2016

Aus dem Institut für Klinische Chemie und Pathobiochemie

der medizinischen Fakultät

der Otto-von-Guericke-Universität Magdeburg

A novel function of the endothelial thrombomodulin-protein C system for cellular function in the CNS

Dissertation

der Fakultät für Naturwissenschaften
der Otto-von-Guericke-Universität Magdeburg
zur Erlangung des akademischen Grades

doctor rerum naturalium
(Dr. rer. nat.)

am
26.10.2015

eingereichte Dissertation,

vorgelegt von

Dipl. biol. Juliane Wolter

geb. am 30.10.1981 in Salzwedel, Deutschland

Magdeburg, 2015

Bibliographische Beschreibung

Wolter, Juliane:

A novel function of the endothelial thrombomodulin-protein C system for cellular dysfunction in the CNS. – 2015. –90 Bl., 26 Abb.

Dipl. biol. Wolter Juliane

Title: A novel function of the endothelial thrombomodulin-protein C system for cellular function in the CNS

Abstract:

Loss of endothelial thrombomodulin (TM) function is associated with macrovascular, microvascular, and inflammatory diseases. Loss of TM function impairs the generation of the anticoagulant protease activated protein C (aPC), which conveys important neuroprotective effects. Yet, the physiological relevance and the mechanism through which the TM-aPC system maintains nerve function remain unknown. Using mice expressing a mutant TM (TM$^{Pro/Pro}$) resulting in markedly reduced aPC generation we uncover a previously unknown function of TM-mediated aPC-generation for physiological nociception. While conductivity of isolated peripheral nerves is normal in TM$^{Pro/Pro}$ mice, loss of TM-dependent aPC generation impairs myelination, increases ROS generation, and disrupts mitochondrial function within the CNS in unchallenged (non-diseased) mice. Substitution of aPC in TM$^{Pro/Pro}$ mice normalises nociception as well as myelination, reduces ROS-generation, and ameliorates mitochondrial function within the CNS.

To evaluate whether functional impairment of the TM-PC system is of pathophysiological relevance we evaluated the impact of impaired aPC-generation on peripheral neuropathy and on demyelinating disease models within the CNS. In experimental diabetic neuropathy, a disease of the peripheral nerve system, impaired TM-dependent aPC-generation does not aggravate the disease progression, consistent with a primary myelination defect within the CNS. Contrary, in a murine model of experimental autoimmune encephalitis (EAE) impaired TM-dependent PC-generation aggravates the disease progression. Impaired endogenous aPC generation enhances ROS generation and reduces markers reflecting mitochondrial mass (porin) and biogenesis (PGC1α). This establishes that endogenous aPC generation protects from neuronal demyelination and mitochondrial dysfunction in EAE. Restoring endogenous aPC levels or genetically restraining mitochondrial ROS generation partially reverses the disease severity in TM$^{Pro/Pro}$ mice. Intriguingly, therapeutic application of soluble TM (solulin) conveys pronounced neuroprotection, delaying the disease onset and diminishing the disease severity in TM$^{Pro/Pro}$ mice. The effect of soluble TM is superior to that of aPC or ROS-inhibition. A similar effect of soluble TM is apparent in TM wild-type mice, corroborating the therapeutic potential of soluble TM. Of note, soluble TM improves myelination even in a non-immunological mediated demyelination model (cuprizone-induced demyelination), establishing that soluble TM protects myelin independent of its known immune-modulatory function. Our results identify TM-dependent aPC activation as a new physiological pathway regulating neuronal function and as an important pharmacological target to alleviate impaired nociception and demyelinating diseases of the CNS.

Dipl. biol. Wolter Juliane

Title: A novel function of the endothelial thrombomodulin-protein C system for cellular function in the CNS

Zusammenfassung

Der Funktionsverlust von endothelialen Thrombomodulin (TM) ist kennzeichnend für makro- und mikrovaskulären Erkrankungen. Der Funktionsverlust von TM beeinträchtigt die Aktivierung des gerinnungshemmenden aPC (aktiviertes Protein C). aPC vermittelt zell-protektive Effekte in verschiedenen Zellsystemen und Erkrankungsmodellen. Insbesondere die nephro- und neuroprotektiven Eigenschaften des aPC sind durch zahlreiche Arbeiten belegt. Dis physiologische Bedeutung des TM-PC Systems für die neuronal Funktion sowie der genaue Wirkungsmechanismus des TM-PC Systems auf die Funktion der Nerven ist jedoch nach wie vor unbekannt.

Unter Verwendung von Mäusen, die eine Punktmutation im TM (TM$^{Pro/Pro}$) aufweisen, was zu deutlich reduzierter aPC-Aktivierung führt (< 1% im Vergleich zu wt Tieren), haben wir eine bisher unbekannte Funktion der TM-vermittelten aPC Generation für die physiologische Schmerzwahrnehmung aufgedeckt. Während die Leitfähigkeit von isolierten peripheren Nerven in TM$^{Pro/Pro}$-Mäusen normal ist, zeigen sich durch den Verlust der TM-abhängigen aPC Generation Beeinträchtigtigungen in der Myelinisierung, erhöhte ROS (reactive oxygen species) Produktion und gestörte Funktionen der Mitochondrien innerhalb des ZNS in bereits nicht erkrankten Mäusen. Durch Substitution von aPC in TM$^{Pro/Pro}$ Mäusen (i.p. Applikation) normalisiert sich die Schmerzwahrnehmung sowie auch die Myelinisierung, es wird vermindert ROS generiert und die mitochondrialen Dysfunktionen innerhalb des ZNS werden geringer. Anhand dieser Studien identifizieren wir einen neues und physiologisch relevantes System, das TM-PC-System, das die Schmerzwahrnehmung reguliert.

Um zu beurteilen, in wie weit die Funktionsstörungen innerhalb des ZNS bei Mäusen mit eingeschränkter aPC Generation von pathophysiologischer Relevanz sind, untersuchen wir im weiteren Verlauf die Auswirkungen von eingeschränkter PC-Aktivierung auf die periphere Neuropathie und auf demyelinisierende Erkrankungsmodelle, wie EAE, innerhalb des ZNS.
In Tiermodellen zur experimentellen diabetischen Nephropathie trägt die beeinträchtigte TM-abhängige aPC Generation nicht zum beschleunigten Fortschreiten der Erkrankung bei, was im Einklang mit einem primären Myelinisierungsdefekt innerhalb des ZNS ist. Im Gegensatz dazu steht das Mausmodell der Multiplen Sklerose, die **e**xperimentelle **a**utoimmunene **E**nzephalitis (EAE). In diesem Erkrankungsmodell beschleunigt die beeinträchtigte TM-abhängige PC-Generation das Fortschreiten der Krankheit. Beeinträchtigte endogene aPC-

Erzeugung führt zu erhöhter ROS-Produktion und zur Störungen der mitochondrialen Funktion, was durch die Verringerung der mitochondrialen Masse (Porin) und der mitochondrialen Biogenese (PGC1α) wiedergespiegelt wird. Diese Ergebnisse zeigen, dass die endogene aPC-Generation vor neuronalen Demyelinisierungserkrankungen und vor mitochondrialen Dysfunktionen im EAE-Modell schützt. Durch Ersetzen von endogenem aPC (aPC Injektion) oder durch genetisches Ausschalten der mitochondrialen ROS-Erzeugung (p66^{Shc} Mangel) ist die Schwere der EAE-Erkrankung in TM$^{Pro/Pro}$ Mäusen teilweise umkehrbar.

Interessanterweise vermittelt die therapeutische Anwendung von löslichem TM (Solulin) ausgeprägte Neuroprotektion, gekennzeichnet durch eine Verzögerung des Erkrankungsausbruchs und eine Verringerung der klinischen Erkrankungssymptome in TM$^{Pro/Pro}$-Mäusen. Ein ähnlicher Effekt von löslichem TM zeigt sich in TM-Wildtyp-Mäusen, was das therapeutische Potential von löslichem Thrombomodulin belegt.

Des Weiteren ist zu beobachten, dass lösliches Thrombomodulin die Myelinisierung ebenfalls in einem nicht-immunologischen Demyelinisierungsmodell (Cuprizon induzierte Demyelinisierung) verbessert. Cuprizon (bis-Cyclohexanon-Oxaldihydrozon) ist ein Kupfer-Chelator, der bei 5-wöchiger Beigabe im Futter zu Demyelinisierungserscheinungen im Corpus callosum des Gehirns führt. Diese neuen Erkenntnisse zeigen erstmals, dass lösliches TM Myelin unabhängig von seiner immun-modulatorischen Funktion vor demyelenisierenden Erkrankungen schützt.

Zusammenfassend identifizieren unsere Ergebnisse die TM-abhängige PC-Aktivierung als ein neues physiologisch relevantes System, dass die neuronale Funktion reguliert, und als eine wichtige pharmakologische Zielstruktur. Die weitere Untersuchung dieses Ansatzes könnte neue Therapieansätze für demyelisierenden Erkrankungen aufzeigen.

TABLE OF CONTENTS

List of abbreviations

aPC	activated protein C
BBB	blood brain barrier
BSA	bovine serum albumin
C	control
cDNA	complementary deoxyribonucleic acid
CL	Cardiolipin
CNS	Central Nervous System
d	days
DAB	3,3'-diaminobenzidine
DAPI	4′,6-Diamidin-2-phenylindol
ddH$_2$O	double destilled water
dH$_2$O	destilled water
DEPC	diethylpyrocarbonat
DMEM	dulbecco´s modified eagle´s medium
DMSO	dimethyl sulfoxide
DNA	deoxyribonucleic acid
DNase	deoxyribonuclease
dNTPs	desoxynucleosid triphosphates
DSPN	diabetic sensorimotoric polyneuropathy
DTT	dithiothreitol
EAE	experimental autoimmune encephalomyelitis
EDTA	ethylenediamine tetraacetic acid
EGTA	ethylene glycol tetraacetic acid
EPCR	endothelial cell protein C receptor
FBS	fetal bovine serum
FCS	fetal calf serum
g	gravitational acceleration
Glu	glutamate
HBSS	hanks' balanced salt solution
HRP	horseradish peroxidase

H_2O_2	hydrogen peroxide
IgG	immunoglobulin G
i.p.	intraperitoneal
kb	kilobase(s)
$MgCl_2$	magnesium chloride
MOG	myelin oligodendrocyte glycoprotein
mRNA	messenger ribonucleic acid
MS	multiple sclerosis
PAR	protease-activated receptor
PBS	phosphate buffered saline
PC	protein C
PCR	polymerase chain reaction
PGC1α	Peroxisome proliferative activated receptor gamma coactivator 1α
Pro	proline
PVDC	Polyvinylidenchloride
rpm	revolutions per minute
RT	room temperature
RT-PCR	reverse transcription polymerase chain reaction
SDS	sodium dodecyl sulfate
s.e.m.	standard error of the mean
SOD1	superoxide dismutase 1
sTM	soluble thrombomodulin
TBE	tris borate EDTA
TE	tris-HCL EDTA
TF	tissue factor
TM	thrombomodulin
U	units
VDAC1	Voltage Dependent Anion Channel 1
Wt	wildtype

1 Introduction

1.1 Coagulation

The blood coagulation system comprises three basic elements: 1. platelet adhesion, activation and aggregation, 2. fibrin formation, and 3. fibrinolysis. These elements interact with each other and under physiological conditions vascular integrity is maintained and blood flow to tissues is unimpaired by clotting [1]. Under pathophysiological conditions, blood coagulation becomes activated through the interaction of three components: an altered vessel wall, an impaired and/or changed pattern of blood flow and/or an altered blood composition (known as the "Virchow's trias").

Injury to the blood vessel wall causes disruption of its endothelial layer, resulting in the exposure of the underlying extracellular matrix. Within the matrix, both von Willebrand factor (vWF) and collagen are present and following exposure they will bind to specific receptors, glycoproteins (GP), present on the surface of the platelets. Dependent on the flow within the vessel other glycoproteins are involved in the adhesion of the platelets to the vessel wall. Formation of the tissue factor-factor VII(a) complex drives the intrinsic pathway of coagulation to form thrombin and fibrin. Platelet adhesion, activation, and interactions with leukocytes accelerate the process of thrombin formation yielding activated coagulation proteases such as factor XIa that amplify thrombin generation (Fig 1).
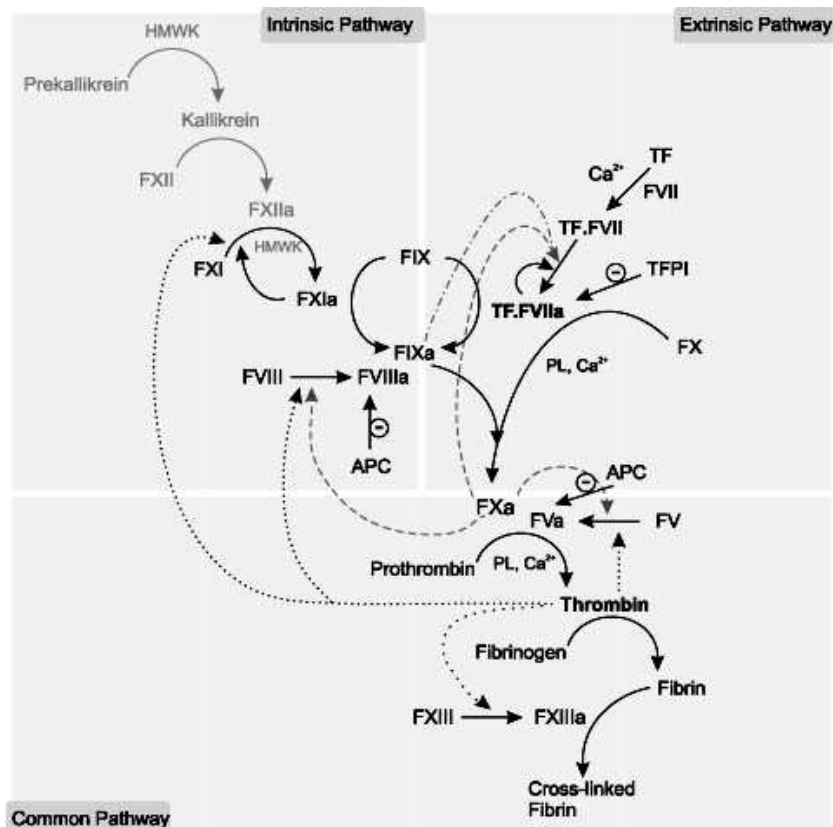
Fig. 1. Schematic overview of the blood coagulation cascade (adapted from Spronk et al., 2003). The model is divided in the intrinsic, extrinsic, and common pathway. Active forms of blood coagulation factors are denoted by a small 'a' added to the roman number. TF, tissue factor; PL, phospholipid; HMWK, high molecular weight kininogen. Positive feedback loops by thrombin (dotted lines), FIXa (dashed-dotted line), and FXa (dashed line) are indicated in grey. Y indicates inhibition by activated protein C (APC) and tissue factor pathway inhibitor (TFPI).

1.2 Thrombomodulin structure

Thrombomodulin (TM), a type 1 transmembrane molecule expressed predominately on endothelial cells, conveys an important function in regulating the coagulation system, inflammation, fibrinolysis and cellular proliferation. TM binds and inhibits the procoagulant function of the key coagulation protease thrombin. When bound to TM thrombin obtains substrate specificity for protein C (PC), generating activated PC (aPC).

Encoded by an intronless gene, the mature single-chain glycoprotein in humans is 557 amino acids long, structurally organized into 5 distinct domains (Fig. 2). TM has a short cytoplasmic tail followed by a well-conserved membrane-spanning region and a serine/threonine-rich domain with sites for O-linked glycosylation, which support the attachment of a chondroitin sulfate (CS). Adjacent to serine/threonine-rich region is the best-characterized domain, which comprises six epidermal growth factor (EGF)-like repeats.

EGF like repeats 3, 4, 5, and 6 (EGF3 to 6) have been studied in detail by several groups. Via its anion-binding site, exosite 1, thrombin binds to EGF5 through EGF6. EGF-like repeats 4-6 are essential in activation of protein C (Fig. 2) by thrombin, while EGF-like repeats 3-6

are required for activation of TAFI (thrombin activatable fibrinolysis inhibitor, also known as carboxypeptidase B2) [2, 3]. At the N-terminus of the molecule and joined to the first EGF-like repeat by a 72- amino acid residue hydrophobic stretch, there is a 154-amino acid residue module with homology to other C-type lectins [4, 5].
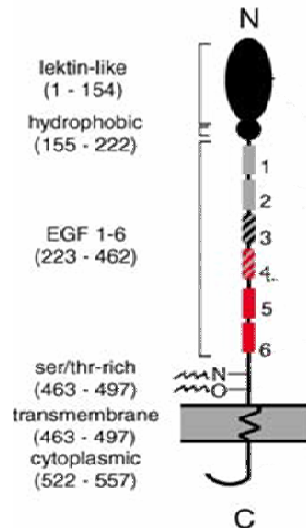
Fig. 2: Structure of thrombomodulin (from Weiler et al., 2003)
See text for more details

1.3 Thrombomodulin and PC-system

The activation of PC by the TM-thrombin complex is about 10-fold accelerated in the presence of the co-receptor EPCR (endothelial protein C receptor). The serine protease aPC initiates a negative feedback mechanism of coagulation activation by inactivating factor Va and VIIIa. Independent of its well-known anticoagulant activity APC acts directly on cells and alters gene expression, inhibits apoptosis, and down-regulates inflammation via protease activated receptor-1 (PAR-1) and EPCR (Fig. 3). PAR-1 is a member of the 7 transmembrane domain G-protein coupled receptor family, and its activation requires cleavage at a specific site within its extracellular amino terminus. This cleavage produces a new aminoterminus, which then acts as its own tethered ligand. PAR-1 was first discovered as a human platelet thrombin receptor [6] and today four homologous PARs (PAR-1, 2, 3, and 4) are known in man and rodents [7-9]. The tissue and cell specific expression as well as different activating proteases allow differential effects, which remain incompletely understood [10]. Direct neuronal protective effects through aPC require signaling via PAR-1 and PAR-3 [11].
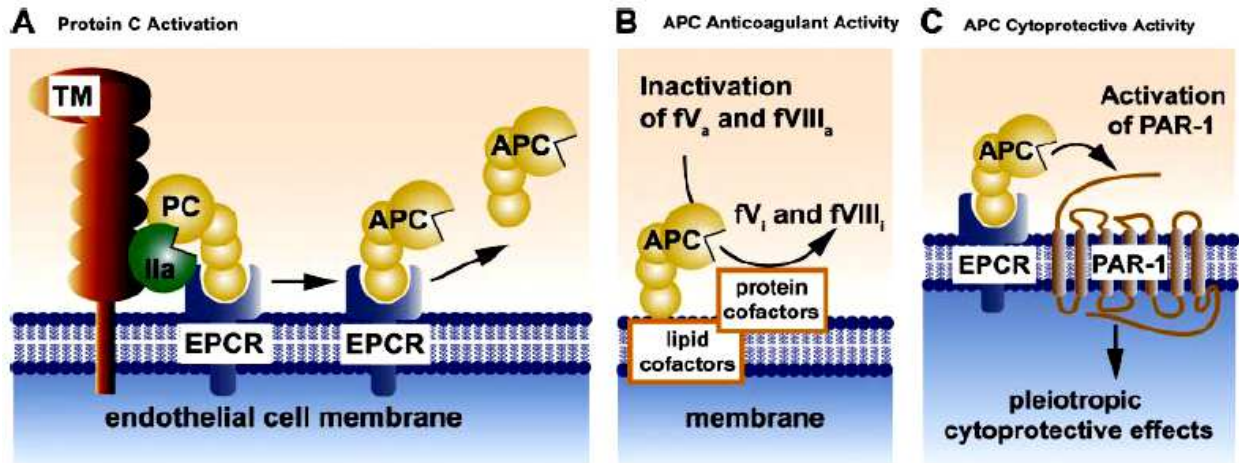
Fig. 3: Schematic models of PC activation and aPC activities (adapted from Mosnier et al., 2007)
Protein C and various cellular receptors are localized to the cell surface where they initiate biochemical signals for transformation. Among these reactions protein C gets activated and conveys it´s either anticoagulant or cytoprotective activity (Fig. 1 A-C). To activate PC, thrombin (IIa) binds to thrombomodulin. Binding of protein C to its endothelial receptor (EPCR), enhances activation of protein C. **(A)**. Dissociation of aPC from EPCR allows anticoagulant activity of aPC only when bound to protein or lipid cofactors. In the presence of cofactors (protein S, fV) aPC cleaves fVa and fVIIIa, thus dampening coagulation activation **(B)**. Retention of aPC bound to EPCR allows various cellular activities. To achieve cytoprotective effects of aPC the cellular receptors EPCR and PAR-1 are required on endothelial cells, but other receptors (e.g. PAR-3, S1P1) are required for its pleiotropic effects on other cell types. APC´s cytoprotective activities include anti-inflammatory and antiapoptotic activities, alterations in gene expression, and protection of endothelial barrier function **(C)**.

1.4 TM-PC system and neuroprotection

1.4.1 TM-PC system and stroke

APC can only act on cells inside the central nervous system by passing the blood brain barrier (BBB). The transport of aPC across the BBB is mediated by EPCR [12]. Cytoprotective efficacy of aPC has been shown in a variety of disease models. In the context of stroke aPC's neuroprotective effect requires signalling via PAR3 and is associated with reduced mitochondrial apoptosis [13]. The cytoprotective properties of aPC in stroke are independent of its anticoagulant activities. An aPC mutant largely devoid of its anticoagulant function but still signaling competent improved neurological scores, reduced bleeding, cerebral infarct area and oedema ratio [14]. Further, the efficacy and safety of an aPC-variant with reduced anticoagulant function (3K3A-aPC) is evaluated in clinical stroke studies (NCT01660230; NCT02222714). However, the intracellular signalling pathways and consequences of aPC signalling within the CNS are sparse at best. Furthermore, it is not known whether TM and / or aPC have a physiological role for neuronal function in the CNS, e.g. in the absence of disease promoting stimuli

1.4.2 TM-PC system in diabetic neuropathy/peripheral neuropathy

Macrovascular and microvascular complications are associated with loss of endothelial thrombomodulin (TM) function [15, 16]. In the context of diabetic nephropathy plasma levels of soluble TM, thought to reflect loss of endothelial TM, and plasma levels of activated protein C (aPC) correlate positively or inversely, respectively, with albuminuria [17, 18]. Studies in mice demonstrated that loss of TM-dependent protein C (PC) activation accelerates diabetic nephropathy [19-21]. Mechanistically, aPC reduces glucose induced ROS-generation in endothelial cells and podocytes, thus dampening glucose mediated glomerular injury. While these effects depend on signalling via PAR1 and EPCR in endothelial cells, signalling via PAR3 and PAR2 (human) or PAR1 (mouse) is required in podocytes (highly specialised epithelial cells within the glomeruli), reflecting the cell-specificity of PAR-dependent signalling [22-24]. While these studies provided mechanistic insight into the role of the TM-PC system for glomerular microvascular injury, the relevance of the TM-PC system for other microvascular complications in the context of diabetes remains unknown.

Reduced expression of TM in perineuronal microvessels of patients with diabetic neuropathy has been reported [25], suggesting that TM-dependent PC activation may modulate neuronal function akin to its role in glomeruli. Diabetic neuropathy is a chronic illness of the peripheral nerves and one of the most frequent and compromising complications of diabetes mellitus (DM) [26]. [27, 28]. International epidemiological data suggest that the incidence of neural dysfunction is about 30% in diabetic patients. The most common manifestation of a neuropathy in DM is the diabetic sensorimotoric polyneuropathy (DSPN) with impaired nociception. DSPN is a mixed neuropathy with involvement of different fibers: sensitive, vegetative and motor neurons. It manifests itself in a symmetrical fashion affecting particularly the distal extremities (predominately the legs). DSPN results in impaired perception of touch, pain and temperature sensation [29, 30]. Deficits with reduction or loss of these qualities of perception are of utmost clinical importance, since they pave the way for neuropathic-related foot complications, which is the most frequent cause of amputation in industrialized countries.

Unfortunately, effective therapeutic options for diabetic neuropathy as well as other peripheral neuropathies are lacking. Hence, new mechanistic insights are required which may pave the ground for future therapeutic developments. Of note, PARs are widely expressed and their functional relevance within the peripheral and central nervous system is established [31-33]. Thus, peripheral PAR2 stimulation results in thermal and mechanical hyperalgesia and increased nociceptor activation, while PAR1 stimulation does not cause hyperalgesia, but increases the nociceptive threshold to mechanical or thermal stimulation [34, 35]. While the relevance of PARs for nociception is established, the impact of

coagulation proteases in general, and the TM-PC system in particular, on nociception remains unknown.

The function of the TM-PC system in nociception may, however, extend beyond its potential impact on peripheral nerves. As mentioned above, PARs are expressed within the CNS. Furthermore, both thrombin and aPC are known to regulate the function of various cell types within the CNS [36-38], including multiple sclerosis (see next section).

1.4.3 TM-PC system and multiple sclerosis

Multiple sclerosis (MS) is a severe inflammatory and neuro-degenerating disease of the central nervous system, resulting frequently in severe illness and long-lasting disabilities [39]. MS affects approximately 0.1 % of the general population [40]. The ratio of women with MS to men with the disease is 2 to 1.

The corresponding animal model "experimental autoimmune encephalomyelitis" (EAE) is well-established in neuroscience research and is used to understand the mechanisms underlying EAE. The morphological hallmark of MS and EAE are disseminated myelination and axonal loss. Several therapeutic approaches have been evaluated with partial success, but efficient medical approaches to contain this disabling disease are still lacking [41-43]. Hence, new and better therapeutic modalities are urgently needed.

EAE is an auto-immunological disease but the precise underlying mechanism remains unresolved. Several contributing factors have been identified, including activation of the coagulation system [44]. Intriguingly, while generally thought to be neuro-protective, the role of aPC in EAE remains controversial. Initially, a proteomic study of plaque tissue from human MS-patients demonstrated induction of TF and the protein C inhibitor in MS, indicating increased coagulation activation paralleled by aPC-inhibition [44]. Subsequent animal studies indeed revealed an anti-inflammatory and neuro-protective effect in mice with EAE [45]. Likewise, the thrombin mutant W215A/E217A, which enhances TM-dependent PC activation, ameliorates EAE severity [40].

The beneficial effect of the thrombin mutant W215A/E217A, which ameliorated EAE severity, suggested that EAE may be therapeutically amendable by targeting the TM-PC system [40]. WE (W215A/E217A) thrombin is a recombinant thrombin analogue that contains two amino acid mutations, generating an enzyme with significantly reduced procoagulant activity. It´s activity toward fibrinogen and the thrombin receptor, protease activated receptor-1 (PAR-1) is reduced 19,000–and 1,200–fold, respectively, *in vitro* [40], [46]. Unlike aPC the thrombin mutant W215A/E217A lacks direct anticoagulant function, reducing the risk of undesirable haemorrhage. However, generation of aPC by W215A/E217A thrombin depends on thrombomodulin (TM), and the impaired function of TM in inflammatory diseases, including

MS [47, 48], may impede the efficacy of WE-thrombin. In addition, W215A/E217A thrombin has not reached clinical studies and hence its translation into the clinic remains uncertain.

Soluble TM and variants thereof, such as solulin, are being used in clinical settings or evaluated in clinical studies [49, 50]. Solulin (**s**oluble human recombinant **t**hrombo**m**odulin) has been optimized by inducing several point mutations (Met388Leu, Arg456Gly, His457Gln, Ser474Ala) and a deletion of the last seven amino acids of carboxy terminus, increasing its resistance to ROS [51]. Similar to W215A/E217A thrombin soluble TM promotes aPC generation on demand, yielding aPC in a temporal and spatial controlled fashion. However, unlike W215A/E217A thrombin, soluble TM compensates for an inflammation associated loss of endogenous TM-function [47]. Pre-clinical studies demonstrated that solulin reduces infarct volume in cerebral artery occlusions models and it decreases infarct volume in thrombotic stroke [50].

A recent study unexpectedly questioned a disease-promoting role of impaired endogenous aPC-generation. Using an antibody (MPC1609) inhibiting binding of protein C and aPC to endothelial phospholipid surfaces the authors demonstrated that inhibiting protein C / aPC improves the outcome of EAE [45, 52]. The amelioration of EAE following protein C / aPC inhibition was associated with an increase of myeloid derived suppressor cells (MDSCs) and suppression of T-cell function [45]. Of note, aPC has been shown to directly interact with numerous non-endothelial cells, including neurons, astrocytes, or immune-modulatory cells such as monocytes and dendritic cells, via a variety of receptors, involving integrins and ApoER2 [53, 54]. The impact of the inhibitory antibody on aPC signalling in these cells is not known. In addition, the exact binding site of the antibody used remains unknown and hence the fate and consequences of the PC- and aPC-antibody complexes remains uncertain. Taken together, this study demonstrated that inhibition of endogenous aPC improves EAE-outcome in rodents, and hence the impact of endogenous aPC generation in EAE and MS remains unknown.

1.4.4 Regulation of ROS by aPC:

The mechanism of how aPC conveys its protective properties in the EAE model is still disputed. Several studies suggest that neurodegenerative MS is linked to mitochondrial dysfunction and ROS [55, 56]. Various pathways leading to mitochondrial dysfunction have been proposed. Interestingly all involve pathologic opening of the permeability transition pore (PTP), which is located in the inner membrane of the mitochondria [57-60]. Specifically, Ca^{2+} overload and mitochondrial ROS exposure (**r**eactive **o**xygen **s**pecies) open the PTP resulting in disruption mitochondrial structure and function, promoting cell death [61, 62]. The mitochondrial p66 isoform of the Shc gene locus (p66^{Shc}) has been proposed to be a

potential pore modulator [63] and in the presence of ROS it is targeted to the intermembrane space, where it serves as a redox enzyme by oxidising cytochrome c and reducing oxygen [64, 65]. It has been shown that p66[Shc] inhibition confers protection against ROS in various disease models including EAE [59, 63, 66].

Considering the controversial data regarding aPC in EAE the pathophysiological role of endogenous TM-mediated aPC generation in EAE remains unresolved [40, 67]. Understanding the pathophysiological relevance of endogenous aPC generation is, however, of high translational relevance considering the recent introduction of small-molecule anticoagulants, some of which interfere with endogenous aPC generation [68], and the evaluation of aPC-variants and soluble TM in clinical studies [49].

1.5 Objectives of this study

The role of endogenous TM-dependent PC activation for neuronal function remains unknown. Hence, we determined the physiological and pathophysiological role of TM-dependent PC activation. Unexpectedly, we identified a physiological role of TM-dependent PC activation for nociception, which is independent of peripheral nerve function but rather linked with impaired myelination and mitochondrial dysfunction in the CNS. While this defect, which is apparent in healthy mice, does not accelerate diabetic nephropathy, it aggravates demyelinating diseases of the CNS. These studies unravel a previously unknown physiological function of the TM-PC system for neuronal myelination within the CNS and provide new insight into pathomechanisms of demyelinating diseases of the CNS.

2 Materials and Methods

2.1 Chemicals and solutions

Chemical/Solution	Company
Acetic Acid	Sigma-Aldrich, Taufkirchen, Germany
Agarose, Ultra Pure	Invitrogen, Karlsruhe, Germany
Ammonium Hydroxide	Sigma-Aldrich, Taufkirchen, Germany
Antigen Unmasking Solution	Vector Labs, Burlingame, CA, USA
Boric acid	Sigma-Aldrich, Taufkirchen, Germany
Bovine Serum Albumin (BSA)	Promega, Mannheim, Germany
Bovine Serum Albumine, fraction V	Sigma-Aldrich, Taufkirchen, Germany
Bradford Reagent	Sigma-Aldrich, Taufkirchen, Germany
Chloroform	Sigma-Aldrich, Taufkirchen, Germany
Citric Acid	Sigma-Aldrich, Taufkirchen, Germany
Crsyl Echt Violet	Sigma-Aldrich, Taufkirchen, Germany
Cytoseal Mounting Medium	Microm, Walldorf, Germany
2´-Deoxynucleoside 5´-triphosphates (dNTPs)	Initrogen, Karlsruhe, Germany
Diethylpyrocarbonat (DEPC)	Roth, Karlsruhe, Germany
Dimethyl Sulfoxide (DMSO)	Roth, Karlsruhe, Germany
EDTA	Sigma-Aldrich, Taufkirchen, Germany
EGTA	Sigma-Aldrich, Taufkirchen, Germany
Eosin Y	Roth, Karlsruhe, Germany
Ethanol	Sigma-Aldrich, Taufkirchen, Germany
Ethidium Bromide	Sigma-Aldrich, Taufkirchen, Germany
Formaldehyde (37–40 %)	Roth, Karlsruhe, Germany
Formalin, 4% Buffered	Roth, Karlsruhe, Germany
Hematoxylin, Gill's Formula	Roth, Karlsruhe, Germany
Hydrogen Peroxide	Sigma-Aldrich, Taufkirchen, Germany
Isopropanol	Becton Dickinson (BD), Heidelberg, Germany
KH_2PO_4	Sigma-Aldrich, Taufkirchen, Germany
KCl (Potassium chloride)	Roth, Karlsruhe, Germany
Ladder, DNA, 100bp – 10kb	Promega, Mannheim, Germany

Lithium Carbonate	Sigma-Aldrich, Taufkirchen, Germany
Luxol Fast Blue	Sigma-Aldrich, Taufkirchen, Germany
Magnesium Chloride	Sigma-Aldrich, Taufkirchen, Germany
Magnesium Sulfate	Sigma-Aldrich, Taufkirchen, Germany
MassRuler, DNA Ladder, Low Range	Fermentas, St. Leon-Rot, Germany
2-Mercaptoethanol	Sigma-Aldrich, Taufkirchen, Germany
Methanol	Roth, Karlsruhe, Germany
Milk Powder	Roth, Karlsruhe, Germany
Na-deoxycholate	Sigma-Aldrich, Taufkirchen, Germany
$Na_2HPO_4(2H_2O)$	Sigma-Aldrich, Taufkirchen, Germany
Na-fluoride	Sigma-Aldrich, Taufkirchen, Germany
Na-orthovanidate	Sigma-Aldrich, Taufkirchen, Germany
Nitric Acid	Roth, Karlsruhe, Germany
Nonidet-p40 (NP40)	Sigma-Aldrich, Taufkirchen, Germany
Percoll	GE Healthcare Europe, Freiburg, Germany
Protease Inhibitor Cocktail	Roche, Mannheim, Germany
Protein Ladder (kDa)	Fermentas, St. Leon-Rot, Germany
Proteinase K	Sigma-Aldrich, Taufkirchen, Germany
Re-Blot Plus Strong Solution (10x)	Merck-Millipore, Darmstadt, Germany
RNAlater	Ambion, Austin, TX, USA
Roti Histo-Kitt II	Roth, Karlsruhe, Germany
Silver Nitrate	Sigma-Aldrich, Taufkirchen, Germany
Sodium Acetate	Sigma-Aldrich, Taufkirchen, Germany
Sodium Chloride	Sigma-Aldrich, Taufkirchen, Germany
Sodium Dodecyl Sulfate (SDS)	Sigma-Aldrich, Taufkirchen, Germany
Sodium Thiosulfate	Sigma-Aldrich, Taufkirchen, Germany
Sucrose	Sigma-Aldrich, Taufkirchen, Germany
TEMED	Sigma-Aldrich, Taufkirchen, Germany
Tetra-Myristoyl Cardiolipin	Avanti Polar Lipids, Alabaster, AL, USA
Tissue Tek, O.C.T. Compound	Sakura, Zoeterwonde, The Netherlands
Tris-HCL	Sigma-Aldrich, Taufkirchen, Germany
TRIZOL	Invitrogen, Karlsruhe, Germany
Vectashield	Vector Labs, Burlingame, CA, USA
Xylol	BD, Heidelberg,Germany

2.2 Hormones, Proteins, Peptides and Adjuvants

Protein, peptide, adjuvant	Company
Freund´s Adjuvant, Complete	Sigma-Aldrich, Taufkirchen, Germany
MOG$_{35-55}$	Bachem, Bubendorf, Germany
Mycobacterium tuberculosis H37 RA	Difco, Detroit, Michigan, USA
Pertussis toxin from *Bordetella*	Merck-Millipore, Darmstadt, Germany
Soluble thrombomodulin (Solulin)	PAION GmbH, Aachen, Germany
aPC	AG Isermann, Magdeburg, Germany [69]

2.3 Antibodies and serum

Antibody	Company	Dilution
rabbit polyclonal anti-mouse Nitrotyrosine	Merck-Millipore, Darmstadt, Germany	1:1000
Mouse monoclonal anti-mouse nitrotyrosine	Santa Cruz Biotechnology, Heidelberg, Germany	1:200
mouse monoclonal anti-mouse GAPDH	Sigma-Aldrich, Taufkirchen, Germany	1:1000
rabbit polyclonal anti-mouse MAP2	Cell Signaling, Danvers, MA, USA	1:100
rabbit polyclonal anti-mouse PGC1 alpha	Abcam, Cambridgeshire, UK	1:250
polyclonal rabbit anti-mouse ß-actin	Cell Signaling, Danvers, MA, USA	1:1000
mouse monoclonal anti-mouse 8-oxo-dG	Trevigen, Gaithersburg, MD, USA	1:250
rabbit polyclonal anti-mouse VDAC1/Porin	Abcam, Cambridgeshire, UK	1:500
goat anti-rabbit IgG-HRP	Abcam, Cambridgeshire, UK	1:2000
rabbit anti-mouse IgG-HRP	Abcam, Cambridgeshire, UK	1:2000
rabbit anti-goat IgG-HRP	Abcam, Cambridgeshire, UK	1:2000
Fluorescein-goat anti-rabbit IgG	Vector Labs, Burlingame, CA, USA	1:400
Fluorescein-horse anti-mouse IgG	Vector Labs, Burlingame, CA, USA	1:400
Texas Red-horse anti-mouse IgG	Vector Labs, Burlingame, CA, USA	1:400
Mito Profile Total OXPHOS rodent WB Antibody Cocktail	Abcam, Cambridgeshire, UK	1:250
Texas Red-goat anti-mouse IgG	Vector Labs, Burlingame, CA, USA	1:400

2.4 Enzymes

Enzyme	Company
GoTaq Flexi DNA Polymerase	Promega, Mannheim, Germany
LongAMP Taq DNA Polymerase	New England Biolabs, Frankfurt/Main, Germany

2.5 Buffers

2.5.1 General Buffers

10x PBS:

- 80 g NaCl
- 2 g KCl
- 14.4 g $Na_2HPO_4(2H_2O)$
- 2.4 g KH_2PO_4

Make up to 1 litre with dH_2O after adjust the pH to 7.4.

10x TBS:

- 24.2 g Tris base
- 80 g NaCl

Make up to 1 litre with dH_2O after adjust the pH to 7.6 with HCl.

0.5 M EDTA:

- 186.1 g EDTA
- 800 ml dH_2O

Make up to 1 litre with dH_2O after adjusting pH to 8.0 with NaOH.

5x TBE:

- 54 g Tris
- 27.5 g Boric acid
- 20 ml EDTA (0.5 M)

Make up to 1 litre with dH_2O. For TBE working solution (0.5 x) dilute stock 1:10 with dH_2O.

2.5.2 Luxol Fast Blue stain

Luxol Fast Blue Solution:

- 1 g Luxol fast blue
- 100 ml 95 % ethanol
- 5 ml 10 % acetic acid

0.05 % Lithium Carbonate:

- 0.5 g Li_2CO_3
- 1000 ml dH_2O

0.25 % Cresyl Echt Violet:

- 0.25 g Cresyl Echt Violet
- 100 ml dH_2O
- 10% Acetic acid

2.5.3 "Karlsson–Schultz" solution [70]:

2.5 % Glutaraldehyde/4 % Formaldehyde in Phosphate Buffer pH 7.3

Paraformaldehyde (16 %) stock solution:

- Mix 80 g paraformaldehyde with 450 ml H_2O.
- Stir at 60 °C for 15–20 min.
- Add droplets of 1 M NaOH until solution turns clear.
- Add H_2O to a final volume of 500 ml.

Filter with a Nalgene^{TM} filter unit and freeze aliquots for storage (-20 °C).

Thaw aliquots at 60 °C for use, the solution should be clear.

Fixative working solution (200 ml):

- 0.36 g $NaH_2PO_4·H_2O$
- 3.1 g $Na_2HPO_4·2H_2O$
- 1 g NaCl
- 130 ml H_2O
- 20 ml glutaraldehyde 25 % in H_2O, EM-grade (end 2.5 %)
- 50 ml paraformaldehyde 16 % in H_2O (end 4 %)

Filter with a Nalgene^{TM} filter unit, adjust pH to 7.3 if necessary

2.5.4 Immunohistochemistry

Permeabilisation buffer:

- 5 % BSA   2 g

- 0.3 % Triton-X 100   120 µl
- Made in 1x PBS   40 ml

Blocking solution:

- 1 % BSA   1 g
- 0.05 % Tween20   250 µl
- Made in 1x PBS   500 ml

Acid rinse solution:

- glacial acetic acid   2 ml
- dH$_2$O   98 ml

Blueing solution:

- NH$_4$OH   1.5 ml
- 70 % EtOH   98.5 ml

2.5.5 Cell lysate total protein

RIPA Buffer (final concentration) for whole cell and tissue lysates

- 50 mM Tris-HCl (pH 7.4)
- 1 % NP-40
- 0.25% Na-deoxycholate
- 150 mM NaCl
- 1 mM EDTA
- 1 mM PMSF
- 1 mM Na$_3$VO$_4$
- 1 mM NaF
- add 40 µl/ml protease inhibitor cocktail (Roche)

Note: Use RIPA buffer with 0.5% Na-deoxycholate for isolation of proteins from tissue.

2.5.6 SDS-PAGE

Electrophoresis resolving-buffer:

- 90.825 g (1.5 M) Tris-HCL
- 20 ml (0.4 %) 10 % SDS
- Adjust pH – 8.8

Make up to **500 ml** with dH$_2$0

Stacking-buffer:

- 30.275 g (1 M) Tris-HCL
- 8 ml (0.4 %) SDS
- Adjust pH – 6.8

Make up to **200 ml** with dH_2O

1 x SDS Sample-buffer:

- 62.5 mM Tris-HCl (pH 6.8 at 25 ^{0}C)
- 2 % w/v SDS
- 10 % Glycerol
- 50 M DTT
- 0.01 % bromophenol blue

5 x SDS Running-buffer:

- 15.1 g (0.125 M) Tris
- 94 g (1.250 M) Glycine
- 50 ml 10 % SDS

Make up to 1 litre with dH_2O

Blot-buffer:

- 2.42 g (0.02 M) Tris
- 11.25 g (0.15 M) Glycine
- 200 ml Methanol

Make up to 1 litre with dH_2O

Blocking buffer:

- 5 g Non-fat dried milk powder
- % or 0.05 % (v/v) Tween 20

Make up to 1 litre with 1xPBS or 1x TBS

2.6 Mouse models and materials

2.6.1 Mouse models

C57BL/6	Charles River Laboratories, Sulzfeld, Germany
$TM^{Pro/Pro}$	Generous gift from Mr. Prof. Dr. H. Weiler, Medical College of Wisconsin, USA [71]
hPC^{high}	Previously established by Prof. Dr. B. Isermann's lab [21]
$p66^{Shc}$	generous gift from E. Migliaccio et al., Milan, Italy [63]

2.6.2 Anesthesia

sodium ketamine	Pfizer, Karlsruhe, Germany
xylazine	Bayer, Leverkusen, Germany

2.7 Cell culture

2.7.1 Cells

Conditionally immortalized rat neuronal PC12 cells were obtained from the Department of Neuropathology, Magdeburg. Cells were routinely grown on plates and maintained at 37°C in a humidified 5% CO_2 incubator in a DMEM medium with 1% L-glutamine, 1 % penicillin/streptavidin and 10 % FBS. After pre-treatment with aPC (20 nM) or solulin (3 µg/ml) for 1 hr, cells were treated with H_2O_2 (500 µM) for 1 hr [72].

2.7.2 Media, sera, buffers and supplements

Media, sera, buffer, supplement	Company
Foetal Bovine Serum Standard Quality	PAA laboratories, Pasching, Austria
Dulbecco´s Modiefied Eagle´s Medium	Sigma-Aldrich, Taufkirchen, Germany
1x Dulbecco's PBS + Ca^{2+} and Mg^{2+}	Sigma-Aldrich, Taufkirchen, Germany
1x HBSS with Ca^{2+} and Mg^{2+}	Sigma-Aldrich, Taufkirchen, Germany
100x Penicillin / Streptomycin	PAA laboratories, Pasching, Austria
0.05 % Trypsin and 0.02 % EDTA	PAA laboratories, Pasching, Austria

200 mM L-Glutamine	PAA laboratories, Pasching, Austria

2.8 Oligonucleotides

2.8.1 PCR primer pairs for RT-PCR in mice

The following primers were purchased from Thermo Electron GmbH, Ulm, Germany.

Primer	Sequence
D-17 loop deletion (mt-DNA)	Fwd.: 5´-ACT AAT CCT AGC CCT AGC CC-3´ Rev.: 5´- AAT AAC CCT ACC CCT AGC CC-3´
ß-actin	Fwd.: 5´-GCTCCTAGCACCATGAAGATCAA-3´ Rev.: 5´-AACGCAGCTCAGTAACAGTC-3´
TEM-1	Fwd.: 5´-AGC GCT GTG CAG CCC TTC AG-3´ Rev.: 5´-CAC AGC TGC CAC GGA GCC AA-3´

2.9 Kits

Kit	Company
BCA reagent	Thermo Scientific, Germany
Bradford reagent	Bio-Rad, München, Germany
DAB Substrate Kit for Peroxidase	Vector Labs, Burlingame, CA, USA
Immobilon Western Chemiluminescent HRP Substrate	Merck-Millipore, Darmstadt, Germany
ReliaPrep™ gDNA Tissue Miniprep System	Promega, Heidelberg, Germany

2.10 Equipment

Equipment	Company
BD Micro-Fine syringes	Becton Dickinson, Heidelberg, Germany
BioDoc Station	Biometra, Göttingen, Germany
Biowizard SilverLine hood	Kojair, Vilppula Finland
Blot chamber	Trans-Blot Electrophoretic Transfer Cell, Biorad Laboratories, Germany
Cell culture flasks and dishes	Becton Dickinson, Heidelberg, Germany
Cell F Imaging Software	Olympus, Hamburg, Germany
Cover slips for cell culture	Paul Marienfeld GMBH & Co.KG, Lauda-Königshofen, Germany
Ecocell Incubator	Schnakenberg Laboratories, Bremen, Germany
FEATHER microtome blades	PFM, Koeln, Germany
Harvester	Tomtec, Unterschleissheim, Germany
HERAcell 150 Incubator	Thermo Scientific, Germany
Heraeus fresco17 centrifuge	Thermo Scientific, Germany
High resolution respirometra	Oroboros, Austria
Image Pro Plus Software	Media Cybernetics, Inc., Bethesda, MD, USA
Immobilon-P Transfer Membrane	Merck-Millipore, Darmstadt, Germany
LiChroCart column	Merck, Darmstadt, Germany
LiChrospher Si60	Merck, Darmstadt, Germany
MICCRA D-1 homogenizer	ART, Process and Lab Technique, Muellheim, Germany
Micro 20 Centrifuge	Hettich Lab Technology Tuttlingen, Germany
MicroChemi 4.2 Developer	Biostep, Jahndorf, Germany
MICROM HM400 microtome	MICROM International, Walldorf, Germany
Nano Drop 2000c	Thermo Scientific, Germany
Olympus BX43 Microscope	Olympus, Hamburg, Germany
Olympus CK40 Microscpoe	Olympus, Hamburg, Germany
Pipettes Gilson Pipetman	Gilson, Germany
Pipettes, pipette tips and falcon tubes	Sarstedt, Germany

pH meter 3110	WTW, Weilheim, Germany
Power supply unit	Biorad Laboratories, Germany
Rotofix 32 Centrifuge	Hettich Lab Technology Tuttlingen, Germany
Spectrophotometer	BIO-TEK-Instruments, Inc, Vermont, USA
Spectrofluorimeter	BIO-TEK-Instruments, Inc, Vermont, USA
Thermomixer	Eppendorf, Germany
Tissue flotation bath	MEDITE, Burgdorf, Germany
TSQ Quantum Discovery Max	Thermo Scientific, Germany
T3000 Thermocycler	Biometra, Göttingen, Germany

2.11 Interventional studies in mice

$TM^{Pro/Pro}$ mutant mice were maintained on a C57BL/6 background. Wild-type (WT) C57BL/6 mice were obtained from Jackson Laboratories, Bar Harbor, ME, USA. $TM^{Pro/Pro}$ have been described previously [59, 71, 73]. Age-matched female and male animals have been used (n = 8-10, each group). In a subset of experiments $TM^{Pro/Pro}$ mutant mice and wt mice were daily injected i.p with aPC (1 mg/kg body weight) or solulin (1 mg/kg body weight, PAION GmbH) for 30 days. A further subgroup of $TM^{Pro/Pro}$ mice were fed with 0.2 % cuprizone for 5 weeks (N = 6) [74]. Littermates were used with at least 98% of the genetic C57BL/6 background. Animals were housed in climate controlled rooms with a regular 12 hours day and night rhythm. Animal experiments were carried out in accordance with the approval of the local Animal Care and Use Committee of the Otto-von-Guericke-University Magdeburg. The approval was given by the Landesverwaltungsamt Halle/Saale, Germany).

2.11.1 Nociception studies

2.11.1.1 Hot plate assay: Mice were placed on a heated plate with a constant temperature of 50°C and time was measured until the animal showed a reaction towards the temperature stimulus like shaking or licking the hind paw or jumping. Mice were kept on the hot plate for maximum 60 seconds to avoid burnings. Analyses were done in triplicates taken in a 30 minutes time intervals. Minimum 8 mice were used per group.

2.11.1.2 Tail flick assay: Tail retraction time was recorded after targeting the tail with a hot light beam. For these experiments mice were put in a restrainer and the tail was

exposed to the light beam for a maximum of 10 seconds to avoid burnings. Mean value were calculated from triplicate measurements. Minimum 8 mice were used per group.

2.11.2 Afferent recordings in skin nerve preparation

An *in vitro* skin nerve preparation was used to study the properties of mechanosensitive C fibers that innervate the skin of the hind paw following previously established protocols [75, 76]. Experiments were performed on dissected skin of control wt mice and TM$^{Pro/Pro}$ mice. Animals were sacrificed by CO_2 inhalation, the saphenous nerve excluding the dorsal root ganglion was dissected with the skin of the dorsal hind paw attached and the tissue was mounted in an organ bath inside-up to expose the dermis. The preparation was perfused with an oxygen-saturated modified synthetic interstitial fluid solution containing (in mM) 123 NaCl, 3.5 KCL, 0.7 $MgSO_4$, 1.5 NaH_2PO_3 $2CaCl_2$, 9.5 sodium gluconate, 5.5 glucose, 7.5 sucrose and 10 HEPES at a temperature of 32 °C and a pH 7.4. Fine filaments were teased from the desheathed nerve and placed on a recording electrode. Nerve fibers were classified according to their conduction velocities, von Frey threshold, and firing properties. Electrical stimulation of the nerve fiber was employed to calculate conduction velocities of individual nerve fibers. Fibers which conducted <1 m/s were considered to be unmyelinated C-fibers. The threshold for each unit was tested using calibrated von Frey filaments; the thinnest filament that elicited three action potentials in the time of approximately 2 seconds of pressing the filament on the units was taken as a threshold. Once the receptive field was identified using a glass rod, a computer-controlled linear stepping motor (Nanomotor Kleindiek Nanotechnik, Reutlingen, Germany) was used to apply standardized mechanical stimuli. Each fiber was tested with a series of displacement mechanical stimuli ranging from 6 to 384 µm for both control and TM$^{Pro/Pro}$ mice. Electrophysiological data were collected with a Powerlab 4.0 system (ADInstrumentsm Spechbach, Germany) and analysed off-line with the spike histogram extension of the software.

2.11.3 Preparation of MOG$_{35-55}$ –emulsion and induction of EAE in mice

For induction of EAE in mice a 200 µl emulsion with a 1:1 ratio of myelin oligodendrocyte glycoprotein peptide (MOG$_{35-55}$) and complete Freund´s adjuvant was prepared. It contained 100 µl Complete Freund´s Adjuvant (CFA + 10 mg/ml *Mycobacterium tuberculosis* H37RA) and 400 µg MOG$_{35-55}$ –peptide dissolved in 100 µl PBS. EAE was induced in 8 to 12 weeks old mice by subcutaneous immunization using the above 1:1 emulsion. Each animal received 200 ng Pertussis toxin diluted in 100 µl PBS on days 0 and 2 post-immunization. Animals were assessed daily for 30 days and scored for clinical symptoms of EAE according:

0 = healthy, no clinical symptoms

1 = tail weakness

2 = definite tail paralysis and hind limb weakness

3 = partial paralysis of hind limb

4 = complete paralysis of hind limbs

5 = complete paralysis of hind limbs with incontinence and partial/complete paralysis of forelimbs

6 = moribund or dead

Animals with 25 % loss of weight were taken out of the experiments and scored as 6.

2.12 Animal sacrifice and tissue processing

Mice were sacrificed at two defined time-points:

a) 1 week after EAE onset

b) 30 days after EAE induction

Mice were anesthetized with sodium ketamine (100 mg/kg body weight i.p.) and xylazine (10 mg/kg body weight, i.p.) , blood was taken from the inferior vena cava into a syringe pre-filled with 150µl anticoagulant solution (0.38% sodium citrate and 50 mM benzamidine HCl final concentration), and mice were perfused with PBS. The spinal cord and brain were dissected from all mice and further divided for specific use. For histological analyses, EM, and frozen sections the spinal cord was prepared from the intact cervical region of the upper spinal cord whereas for protein isolation the crushed lower part of the spinal cord was used. Samples were either fixed in 4 % formalin for histological analyses, flash frozen for protein isolation, or stored in Karlsson-Schultz solution for further EM analyses.

2.12.1 Preparation of mitochondria

Bain mitochondria were prepared from mice in ice-cold medium containing 250 mM sucrose, 20 mM Tris (pH 7.4), 2 mM EGTA, and 1% (w∕v) bovine serum albumin using a standard procedure [77]. In detail, brain tissue was homogenised and washed twice in 14 ml isolation medium (containing BSA). The homogenised solution was centrifuged for 5 minutes at 1000 g (3386 h/min, 4 °C). Supernatant was further centrifuged for 10 minutes at 14000 g (12670 h/min, 4 °C). Pellet was resuspended in 6 ml isolation medium (+BSA and 0.7 ml percoll). After homogenising solution was again centrifuged (10 minutes at 14000 g at 4 °C) and the pellet was resuspended in 7 ml isolation medium (- BSA). Finally the pellet was dissolved in 700 µl isolation medium (- BSA) and homogenised for further purification. After the initial isolation, Percoll was used for purification of mitochondria from a fraction containing some endoplasmatic reticulum, Golgi apparatus and plasma membranes [78, 79].

Isolation medium (1 l, pH 7.4):

250 mM mannitol

1 mM EGTA

1 mM EDTA

0.3 % BSA

2.12.2 Mitochondrial respiration

Brain samples were homogenized to permeabilise plasma membranes in order to allow the substrates free access to the mitochondria. To this end, 20 mg of tissue were homogenized in a medium containing 25 mM methanol, 20 mM Tris, 1 mM EGTA and 0.3 % bovine albumin (pH 7.4) using a potter-elvehjem homogeniser. To enrich mitochondria the homogenate was centrifuged for 5 minutes at 10000 x g. Afterwards, the pellet was resuspended in 15 ml of a medium containing 120 mM KCl, 60 mM Tris, 35 mM mannitol, 5 mM $MgCl_2$, 15 mM NaCl, 10 mM KH_2PO_4 and 0.5 mM EGTA (pH 7.4). An aliquot of 4 ml of this suspension was used for the measurement of oxygen consumption at 30 °C applying high resolution respirometry (Orobos oxygraph, Paar Systems, Austria). Before measurement, the measuring system was calibrated according to the instructions of the manufactor. There were 2 experimental set-ups:

a) 2 ml cell homogenate, 5 mM glutamate, 5 mM malate (basal respiration), 500 µM ADP (respiration with glu/mal, relating to mitochondrial respiration complex I)

b) 2 ml cell homogenate, 10 mM succinate, 500 µM ADP (respiration with succinate, relating to mitochondrial respiration complex II)

2.12.3 Incubation of mitochondria

Mitochondria (about 0.5 mg protein/ml) were incubated in a medium containing 10 mM sucrose, 120 mM KCl, 20 mM Tris, 5 mM potassium phosphate, 0.5 mM EGTA and 1 mM free Mg^{2+} at pH 7.4. Oxygen consumption of mitochondria was analysed by using the method of high resolution respirometra (Oroboros, Austria).

2.12.4 Cardiolipin (CL) analyses

2.13.4.1 Extraction of Cardiolipins

For the extraction of cardiolipins 50 ng of tetra-myristoyl-CL [(C14:0)4-CL; Avanti Polar Lipids Inc., Alabaster, AL] was added as internal standard to 10 µl mitochondrial suspension. For extraction of CL chloroform/methanol (2/1, v/v) containing 0.05% BHT as antioxidant was added. The lipid and aqueous phases were separated by adding 0.01 M HCl and intensive shaking and centrifugation. Afterwards, the lower lipid phase was collected and dried under nitrogen atmosphere and acidified. Ice-cold methanol (2 ml), chloroform (1 ml) and 0.1 M HCl

(1 ml) were added and the solution was intensively mixed. After 5 minutes of incubation on ice the samples were separated by the addition of chloroform (1 ml) and 0.1 M HCl (1 ml). The chloroform/ methanol phase was recovered as CL-containing sample. The samples were dried under nitrogen again and dissolved in 0.8 ml chloroform/methanol/water (50/45/5, v/v/v). After mixing and filtering the mixture over 0.2 µm PTFE membranes the samples were ready for analysis.

2.13.4.2 HPLC-MS/MS analysis

For measuring the molecular CL species a TSQ Quantum Discovery Max (Thermo Fisher Scientific GmbH, Dreieich, Germany) was used in the negative ion electrospray ionization (ESI) mode. The HPLC system consisted of a Surveyor MS quaternary narrow bore pump with integrated vacuum degasser and a Surveyor auto sampler. Auto sampler tray temperature was hold at 8°C. In partial loop mode a sample of 10 µl of lipid extract dissolved in chloroform/methanol/water (50/45/5, v/v/v) was injected and CL was separated by using a LiChroCart column (125 mm × 2 mm), LiChrospher Si60 (5 µm particle diameter; Merck, Darmstadt, Germany) and a linear gradient between solution A (chloroform) and solution B (methanol/water 9:1, v/v). All solutions contained 25% aqueous ammonia (0.1 ml/l). The gradient was as follows: 0–0.2 minutes 92% solution A, 8% solution B; 0.2–4.5 minutes 92–30% solution A, 8–70% solution B; 4.5–6 minutes 30% solution A, 70% solution B; 6–6.5 minutes 30–92% solution A, 70–8% solution B; 6.5–11 minutes 92% solution A, 8% solution B. The flow rate was 200 µl/min. Total time of analyses was 11 minutes. The eluate between 0.3 and 6 minutes was introduced into the mass spectrometer. Nitrogen was used as the nebulizing gas and argon as collision gas at a pressure of 1.5 mTorr. The spray voltage was 3.5 kV, the ion source capillary temperature was set at 375°C and the cone-voltage was 30 V. Daughter fragments from the doubly charged parent derived from $(C18:2)_4$-CL with m/z 723.6 $((M–2H)2–/2)$ were obtained using a collision energy of 36 eV. This molecular CL species and the internal standard (m/z 619.6) were analysed by mass transfer reaction monitoring their doubly charged ions and their respective fatty acids linoleic acid m/z 279.2 and myristic acid m/z 227.2 using the selected reaction monitoring (SRM) mode. The same approach was used for parent and daughter fragments of other molecular species of CL. The quantity of these molecular species was related to the content of $(C18:2)_4$-CL. Oxidized CL [$(C18:2)3$monohydroxylinoleic acid-CL] was measured in the SRM mode as a transition from m/z 731.6 to m/z 279.2 (linoleic acid).

2.13.4.3 Determination of protein

The protein content of the mitochondrial suspension was measured according to the Bradford method [80] using bovine serum albumin as the standard.

2.13 Histology and immunohistochemistry

For all histological analyses 4 µm or 10 µm (LFB) thick paraffin section from spinal cord were cut with the microtome. All immunhistochemical and immunofluorescence stainings were performed in a wet chamber.

2.13.1 Luxol Fast Blue (LFB) stain

The LBF stain was used to identify myelinated fibers, which stain blue, while the parenchyma and demyelinated areas appear white. To this end sections were dewaxed and hydrated to 96 % ethanol and incubated in 0.2 % LFB solution over night at 58°C. The next day slides were washed in dH$_2$O, differentiated repeatedly in lithium carbonate solution for 10-15 seconds and in 70 % ethanol until there was a sharp contrast between the blue of the white-matter and the white/colourless grey-matter of the spinal cord. After washing for 10 minutes in tap water the sections were transferred into cresyl violet solution for 30 minutes and then rinsed in dH$_2$O. Afterwards slides were dehydrated through 96 % and 100 % ethanol for 1 minute, moved to xylol for 10 minutes and covered with mounting medium. The myelinated and demyelinated areas of the spinal cord sections were analysed by a blinded investigator using the cellSense Dimension Imaging software.

2.13.2 Immunofluorescence

For immunofluorescence the spinal cord sections were dewaxed, dehydrated and then fixed in ice cold acetone for 1 minute. The antigens were unmasked by boiling for 30 minutes in antigen retrieval solution according to the manufacturer´s instructions. Further the slides were incubated in permeabilisation buffer (PBS + 0.3 % Triton-X 100 + 5 % BSA) for 10 minutes, blocked for 1 h and incubated with the primary antibody over night at 4°C. The next day the slides were rinsed twice in PBS and the secondary fluorescein labelled anti-IgG antibody (3.75 µg/ml) was added for 1 hour at room temperature followed by rinsing the tissue sections twice in PBS. Slides were covered with DAPI containing vectashield mounting medium and sealed with nail polish. Slides were analysed for MAP2/nitrotyrosine co-expression by a blinded investigator using the cellSense Dimension Imaging software.

2.13.3 Mitotracker – 8-deHO-G staining:

Frozen sections of spinal cord or PC12 cells, grown on cover slips, were incubated in the presence of 200 mM MitoTracker® Mitochondrion-Selective Probes (Invitrogen) at 37°C for 20 minutes. After being washed with DPBS (Gibco) sections/cells were fixed with 99.5 % acetone (Roth) for 1 minute. Sections/cells were then incubated with 8-hydroxy-2'-deoxyguanosine antibody (1:100 diluted in DPBS) at 4°C overnight. After washing with DPBS slides were incubated with FITC labeled secondary antibody (1:400 diluted in DPBS) for 1 hr at room-temperature. Finally slides were counterstained with vectashield containing DAPI.

Colocalisation of mitotracker (red) and 8-hydroxy-2'-deoxyguanosine (green) reflects oxidatively damaged mitochondrial DNA. Fluorescence slides were analysed for mitochondrial ROS, by a blinded investigator using the cellSense Dimension Imaging software.

2.13.4 MitoSOX staining:

PC12 cells were cultured on cover slips and incubated in the presence of 5 µM MitoSOX (Invitrogen) at 37°C for 10 minutes. After being washed with DPBS (Gibco) cells were fixed with 100 % methanol (Roth) for 20 minutes at -20 °C. Fixed cells were then counterstained with vectashield containing DAPI. Fluorescence slides were analysed for mitochondrial ROS by a blinded investigator using the cellSense Dimension Imaging software.

2.13.5 Peroxidase immunohistochemistry for 8-hydroxy-2'-deoxyguanosine, nitrotyrosine, PGC1α and VDAC1

Paraffin sections were dewaxed, dehydrated and then fixed in ice cold acetone for 1 minute and washed in PBS. Antigen-retrieval (incubation in boiling antigen unmasking solution for 30 minutes) was performed followed by inactivation of the endogenous peroxidase activity in 0.3% hydrogen peroxide diluted in PBS for 30 minutes at room temperature. Tissue samples were blocked for 1 hour incubated at room temperature and incubated with the primary antibody over night at 4°C. The following day slides were rinsed twice in PBS and incubated with the according secondary antibody (IgG-HRP). After washing twice in PBS, DAB substrate kit for peroxidase was added until the negative control started to develop colour. To stop the reaction tissue samples were immediately transferred to PBS. Counterstain was performed using Gill's formula hematoxylin for 1 minute. Afterwards tissue samples were rinsed in water, dipped in acid rinse solution, then in water and stained in blueing solution for 1 minute. An additional washing step followed. Tissue samples were dehydrated and fixed in xylol, followed by covering them in Roti Histo-Kitt II. Slides were analysed for oxidative damage (8-hydroxy-2'-deoxyguanosine), formation of peroxynitrite (ROS, nitrotyrosine), mitochondrial biogenesis (PGC1α) and outer mitochondrial membrane channel protein (VDAC1, reflecting mitochondrial mass) by a blinded investigator using the cellSense Dimension Imaging software.

2.14 Transmission electron microscopy

Deeply anesthetized mice were transcardially perfused with ice-cold PBS and followed by perfusion with fixative (2.5% glutaraldehyde, 2.5% polyvidone 25, 0.1 M sodium cacodylate pH 7.4). Spinal cords were dissected and washed with 0.1 M sodium cacodylate buffer (pH 7.4). Samples were then post-fixed in the same buffer containing 2% osmium tetroxide and 1.5% potassium ferrocyanide for 1 hour, washed in water, contrasted on bloc with uranyl

acetate, dehydrated using an ascending series of ethanol and embedded in glycidyl ether 100-based resin. Ultrathin sections were cut with a Reichert Ultracut S ultramicrotome (Leica Microsystems, Wetzlar, Germany), contrasted with uranyl acetate and lead citrate, and were viewed with an EM 10 CR electron microscope (Carl Zeiss NTS, Oberkochen, Germany).

2.15 Western blot (WB)

Spinal cord tissue homogenates were prepared from frozen spinal cord tissues using RIPA buffer containing 50 mM Tris (pH7.4), 1 % NP-40, 0.5 % sodium-deoxycholate, 150 mM NaCl, 1 mM EDTA, 1 mM Na_3VO_4, 1 mM NaF supplemented with protease inhibitor cocktail (Roche). After centrifuging for 10 minutes at 1300 g at 4 °C the supernatants were quantified and protein concentrations were measured using BCA reagent (Pierce, Germany). Equal amount of protein samples (20 µg) were electrophoretically separated on 10 % or 12.5 % SDS polyacrylamide gel, transferred to PVDF membrane (Millipore) and probed with desired primary antibodies or primary OXPHOS antibody cocktail (Abcam, UK) at recommended dilutions shaking over night at 4°C. The next day the membrane was washed with PBST and incubated with the secondary anti-mouse IgG (1:2000) or anti-rabbit IgG (1:2000) horseradish peroxidase conjugated antibody. Blots were developed using the enhanced chemiluminiscence system (Merck-Millipore, Darmstadt, Germany). To compare and quantify levels of proteins, the density of each band was measured with ImageJ software. Equal loading was confirmed by actin or GAPDH western blot.

2.16 Polymerase Chain Reaction (PCR)

To visualize expression of various genes in murine spinal cord primer pairs listed under 2.9.1 were used. PCRs with a final volume of 25 µl were setup as followed:

1.0 µl undiluted cDNA

5.0 µl 5x Green GoTaq Flexi Buffer

2.5 µl 25 mM $MgCl_2$

0.2 µl 25 mM dNTPs

0.5 µl 10 nM forward primer

0.5 µl 10 nM reverse primer

15.2 µl sterile ddH_2O

0.1 µl GoTaq Flexi DNA Polymerase

PCRs were run on the Biometra T3000 Thermocycler under conditions optimized for each primer pair.

To visualize the D17-loop deletion of mitochondrial DNA total DNA isolated from mouse brain was used and the primer pair listed under 2.9.1.

Gel electrophoresis

Amplified DNA was detected by running 10 µl of the reaction on a 1 % TBE agarose gel containing ethidium bromide. To prepare a 1 % gel, 100 ml of 0.5 x TBE buffer were added to a 250 ml bottle containing 1 g of agarose. The agarose was heated in a microwave to boiling at which point it melted readily. Ethidium bromide was added to a final concentration of 0.5 µg/µl. The agarose was then poured into a gel electrophoresis box with a well comb large enough to accommodate both, sample size and number. After the gel cooled down, 0.5 x TBE buffer was added to the buffer chambers and the comb removed.

The DNA samples were then loaded into the wells. A marker with known molecular weight was loaded alongside the DNA in separate lane. A power supply was then connected to the electrophoresis box delivering a current of 100 volts. The DNA migrated down through the gel toward the anode because of its negative charge. The separation of the DNA was documented by taking a photo of the gel under a BioDoc station. Expression was normalized to β-actin. Reactions lacking reverse transcriptase served as controls.

2.17 Amplification of mitochondrial DNA by PCR

To visualize the expression of mitochondrial DNA of murine brain total DNA from mouse brain tissue was isolated.

2.17.1 Total DNA isolation from tissue

Total DNA (DNA) was isolated following instructions of ReliaPrep™ gDNA Tissue Miniprep System (Promega). The frozen brain tissue (25 mg) was homogenized by using a chilled mortar and pestle. To the powder-like solution 160 µl PBS and 20 µl Proteinase K were added. Next, 200 µl cell lysis buffer (all buffers are provided with the kit) was added to each sample and vortexed for at least 10 seconds. Afterwards, samples were incubated at 56 °C for up to two hours shaking. Then, 20 µl RNase A solution was added, mixed and vortexed for 10 seconds and placed at 56°C for 10 minutes. After adding 250 µl of binding buffer tubes were mixed and vortexed again. Then, a binding column was placed inside a collection tube. After centrifuging for 1 minute at maximum speed the liquid portion was discarded and the column was washed twice. Finally the eluant was collected by adding 200 µl nuclease-free water and centrifugation at maximum speed for 1 minute. Samples were stored at -20 °C until analyses.

2.18 Statistical analysis

All *ex vivo* experiments were performed at least in triplicates. The data are summarized as the mean ± s.e.m. (standard error of the mean). Number of damaged myelin/axon per image branching mitochondria were counted from at least 10 images per mouse. Data are shown as arbitrary units. Statistical analyses were performed using Student's t test or Kruskal-Wallis test (as indicated in the figure legend or in the text). StatistiXL (http://www.statistixl.com) and Prism Version 5 software (GraphPad) was used for statistical analyses. Statistical significance was accepted at the $P < 0.05$ level.

3 Results

3.1 Thrombomodulin-mediated protein C activation maintains neuronal function and myelin structure

To determine the consequence of impaired TM-mediated PC activation for diabetic neuropathy we used mice with severely impaired PC activation secondary to a point mutation in TM (Glu404Pro, TM$^{Pro/Pro}$ mice) [71]. Unexpectedly, the nociceptive sensitivity was already reduced in non-diabetic TM$^{Pro/Pro}$ mice when compared to non-diabetic wt control mice (matched for age, sex, and background) (Fig. 3.1.1 A-B). This uncovers a previously unknown phenotype in mice with reduced anticoagulant capacity and impaired PC activation due to a point mutation in TM. Following 26 weeks of persistent hyperglycaemia the nociceptive sensitivity decreased further in the hot-plate and the tail flick assay (increased latency) in TM$^{Pro/Pro}$, as reflected by an increased reaction time compared to non-diabetic TM$^{Pro/Pro}$ and diabetic wt mice. However, the difference between non-diabetic and diabetic mice was comparable in wt (Δt = 7,0 sec. and Δt = 1,7 sec. for the hot plate and the tail-flick assay, respectively) and TM$^{Pro/Pro}$ mice (Δt = 5,6 sec. and Δt = 1,2 sec.; *P*<0,05 for both comparisons, Fig. 3.1.1 A, B). Thus, in mice with impaired TM-dependent PC activation nociceptive sensitivity is reduced already in the absence of persistent hyperglycaemia. Superimposed hyperglycaemia has an additional additive effect in TM$^{Pro/Pro}$ mice on nociceptive sensitivity, which, however, is comparable to the hyperglycaemia dependent effect in wt diabetic mice. This indicates that loss of TM function does not aggravate hyperglycaemia induced impairment of nociceptive sensitivity, but constitutes and additive factor diminishing nociceptive sensitivity independent of hyperglycaemia induced nociceptive dysfunction.
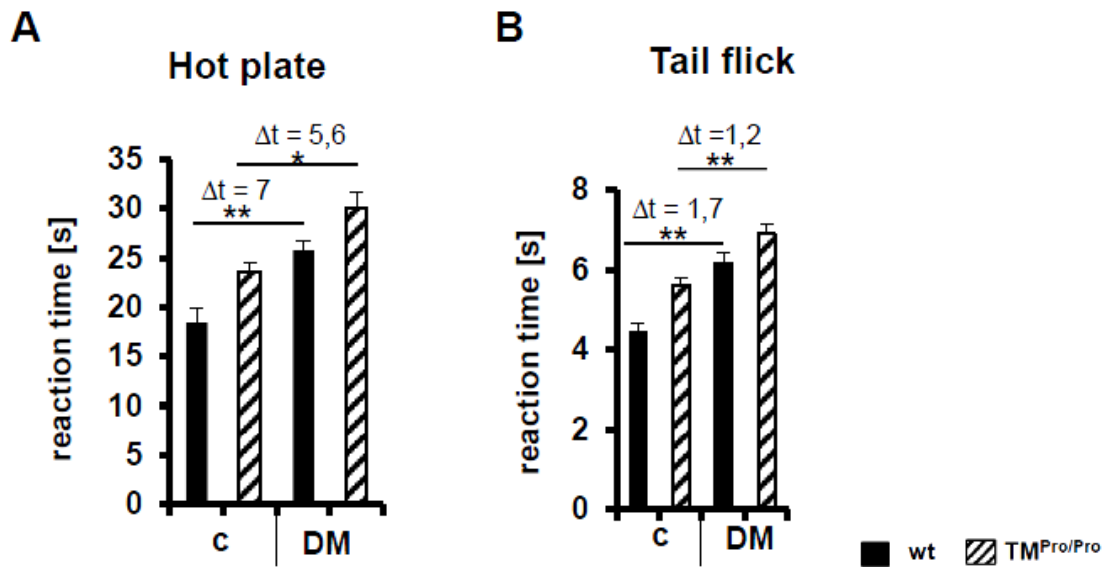
Fig. 3.1.1: Impaired nociception in TM^{Pro/Pro} mice

A-B: Nociception is impaired in TM^Pro/Pro^ mice compared to background-, age- and sex-matched wt mice. The latency in the hot plate (A) and tail flick (B) assay is increased in TM^Pro/Pro^ as compared to wt mice. Persistent hyperglycaemia impairs nociception in wt and TM^Pro/Pro^ mice to the same extend, as indicted by a comparable delta of the latency in the hot-plate assay (A). In the tail-flick (B) assay no differences were visible. Bar graphs summarise results of at least three repeat measurements in 10 (A, B,) different mice per group. *$P < 0.05$; **$P < 0.01$; Student's t-test.

In order to characterise the impaired nociception in non-diabetic TM^Pro/Pro^ mice we analysed firing properties of peripheral afferent fibres. Skin-nerve preparation of the saphenous nerve from non-diabetic wt and TM^Pro/Pro^ mice were prepared and stimulated. Intriguingly, stimulus-response functions of various fibres, including C-fibers (Fig. 3.1.2), showed no difference between wt and TM^Pro/Pro^ mice, indicating that the impaired nociception observed in TM^Pro/Pro^ mice is not caused by an impaired function of the peripheral nerve and may be related to a defect of second-order neurons in the spinal cord.

C

Firing rate of C-fiber nociceptors
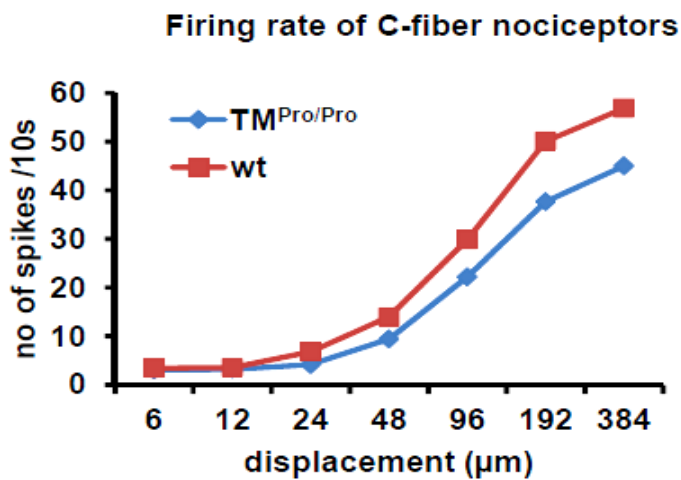
Fig. 3.1.2: Peripheral nerve function is not impaired in TM^{Pro/Pro} mice

The stimulus response of peripheral nerves is similar in TM$^{Pro/Pro}$ and wt mice. Electrophysical analyses of skin-nerve preparation obtained from paws of healthy wt (red, n= 4) and healthy TM$^{Pro/Pro}$ mice (blue, n = 4). Firing rates of C-mechanociceptors (C-fibers) were evoked by application of increasing, 10 seconds lasting pressure via a nanomotor (expressed in terms of displacement).

Ultrastructural analyses of the upper spinal cord using TEM revealed an altered morphology in TM$^{Pro/Pro}$ mice. In contrast to an intact dense axonal arrangement with dark multi-layer myelin structures of spinal cord axons in wt control mice (Fig. 3.1.3) loosening of the myelin sheath and a pale axoplasm devoid of organelles was readily visible in spinal cord axons of TM$^{Pro/Pro}$ mice (Fig. 3.1.3). Of note, healthy TM$^{Pro/Pro}$ mice lack signs of spontaneous inflammation [71, 81]. These data suggest that the impaired nociception in TM$^{Pro/Pro}$ mice is not caused by a defect of the peripheral nerves, but linked with dysfunctional neurons in the CNS independent of spontaneous inflammation.
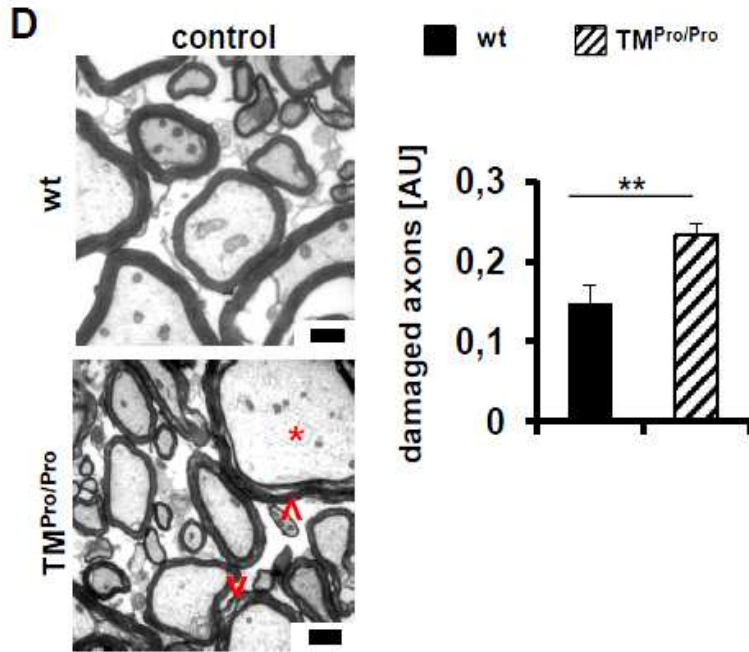
Fig. 3.1.3: Impaired myelin structure in TM^Pro/Pro mice

Myelination defect in the upper spinal cord of TM^Pro/Pro mice. TEM images of mouse spinal cord showing loosening of the myelin sheath [arrow heads] and pale axoplasm devoid of organelles [asterix] in TM^Pro/Pro mice compared to wt mice. Scale bars: 500 nm. Bar graphs summarising results obtained from 3 mice per group. ** $P < 0.01$; Student's t-test.

3.2 Loss of endogenous PC activation increases markers of oxidative stress

As neurons are sensitive to ROS (reactive oxygen species) induced damage and as aPC has been shown to reduce ROS generation [19, 82-84] we next analysed markers reflecting ROS generation in spinal cord (immunohistochemistry) and brain (immunoblotting) tissue. Nitrotyrosine (ONOO⁻), a marker of peroxynitrite formation, and 8-hydroxy-2'-deoxyguanosine, reflecting ROS induced DNA-damage, were both increased in TM^Pro/Pro mice as compared to wt mice (Fig. 3.2.1 A-C).
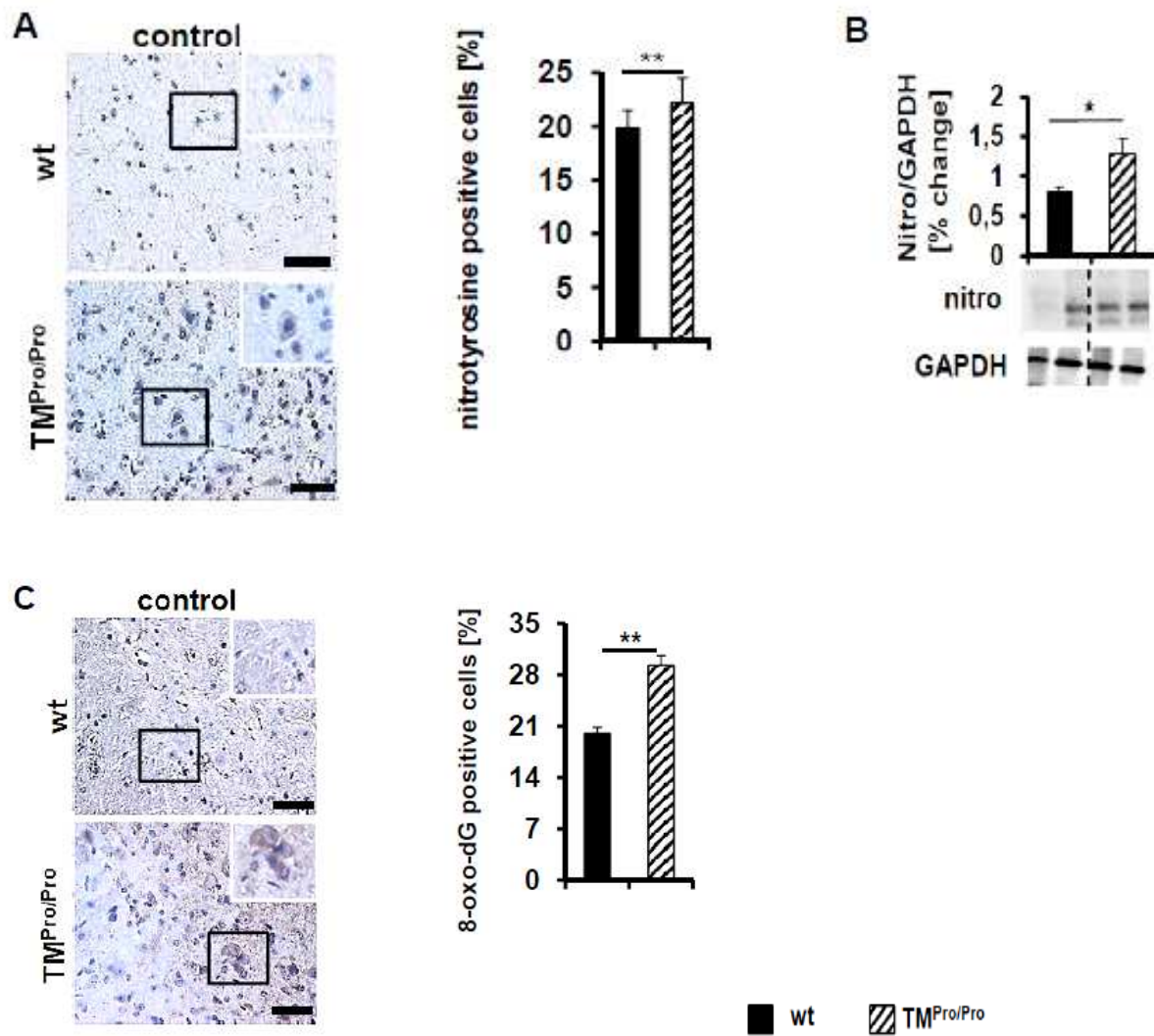
Fig. 3.2.1: Increased oxidative stress markers in the CNS of mice with impaired endogenous PC activation

A: Representative immunohistochemical images (left) and bar graphs (right) showing an increased staining intensity of nitrotyrosine in TM$^{Pro/Pro}$ mice as compared to wt mice. **B:** Representative immune-blots (bottom) and bar graphs (top) showing nitrotyrosine levels in mouse spinal cord tissue samples. Bar graphs summarise semi-quantitative results obtained from eight different mice per group. **C:** Representative immunohistochemical images (left) and bar graphs (right) showing an increased staining intensity of 8-hydroxy-2'-deoxyguanosine in mouse spinal cord in TM$^{Pro/Pro}$ mice as compared to wt mice. Brown, nitrotyrosine (A) or 8-hydroxy-2'-deoxyguanosine (C) positive cells detected by horseradish peroxidase-3,3´-diaminobenzidine reaction; blue, haematoxylin counterstain. Black squares (A, C) indicate areas shown at higher magnification in the inset in the right corner (white frame). Scale bars (A, C): 20 µm. N = 8. *$P < 0.05$; **$P < 0.01$; Student´s t-test.

To determine whether impaired PC activation increases mitochondrial ROS generation we determined the co-localization of 8-hydroxy-2'-deoxyguanosine with mitochondria using immunofluorescence analyses. In TM^{Pro/Pro} mice co-localization 8-hydroxy-2'-deoxyguanosine with mitochondria in spinal cord tissue was increased as compared to wt mice (Fig. 3.2.2), suggesting that in mice with defective PC-activation mitochondrial ROS generation is increased in the CNS.
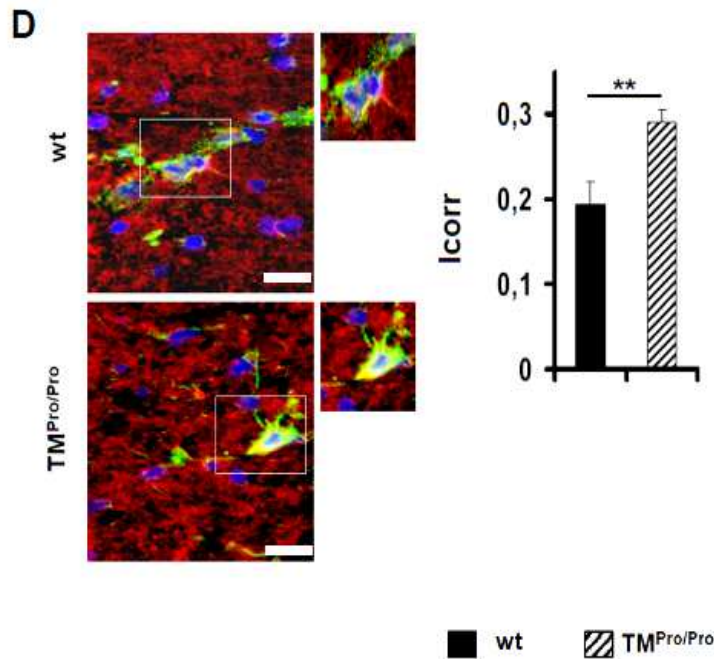
Fig. 3.2.2: increased mitochondrial ROS in TM^{Pro/Pro} mice

Representative co-immunofluorescence images (left) and summarising bar graphs (right) showing mitotracker (red, mitochondrial ROS) and 8-hydroxy-2'-deoxyguanosine (green) staining in mouse spinal cord. In TM^{Pro/Pro} mice, co-localization (yellow, Icorr) is increased compared to wt mice. Blue, counterstain with DAPI. Scale bars: 20 µm. *$P < 0.05$; **$P < 0.01$; Student's t-test.

3.3 Altered mitochondrial morphology in TM^{Pro/Pro} mice

To explore potential causes of impaired mitochondrial function and increased mitochondrial ROS generation in the CNS of TM^{Pro/Pro} mice we next determined expression of porin (VDAC1), a mitochondrial marker-protein reflecting mitochondrial mass, and PGC1α, a transcription factor reflecting mitochondrial biogenesis [85-87]. Expression of both marker proteins was not altered in the spinal cord of TM^{Pro/Pro} mice as compared to wt mice (Fig. 3.3.1 A-D), indicating that neither mitochondrial mass nor mitochondrial biogenesis is impaired in TM^{Pro/Pro} mice.

A control

wt

TM^Pro/Pro

Porin positive cells [%]

B

Porin protein [% change]

Porin

GAPDH

control

C control

wt

TM^Pro/Pro

PGC1α positive cells [%]

control

D

PGC1α protein [% change]

PGC1α

GAPDH

control
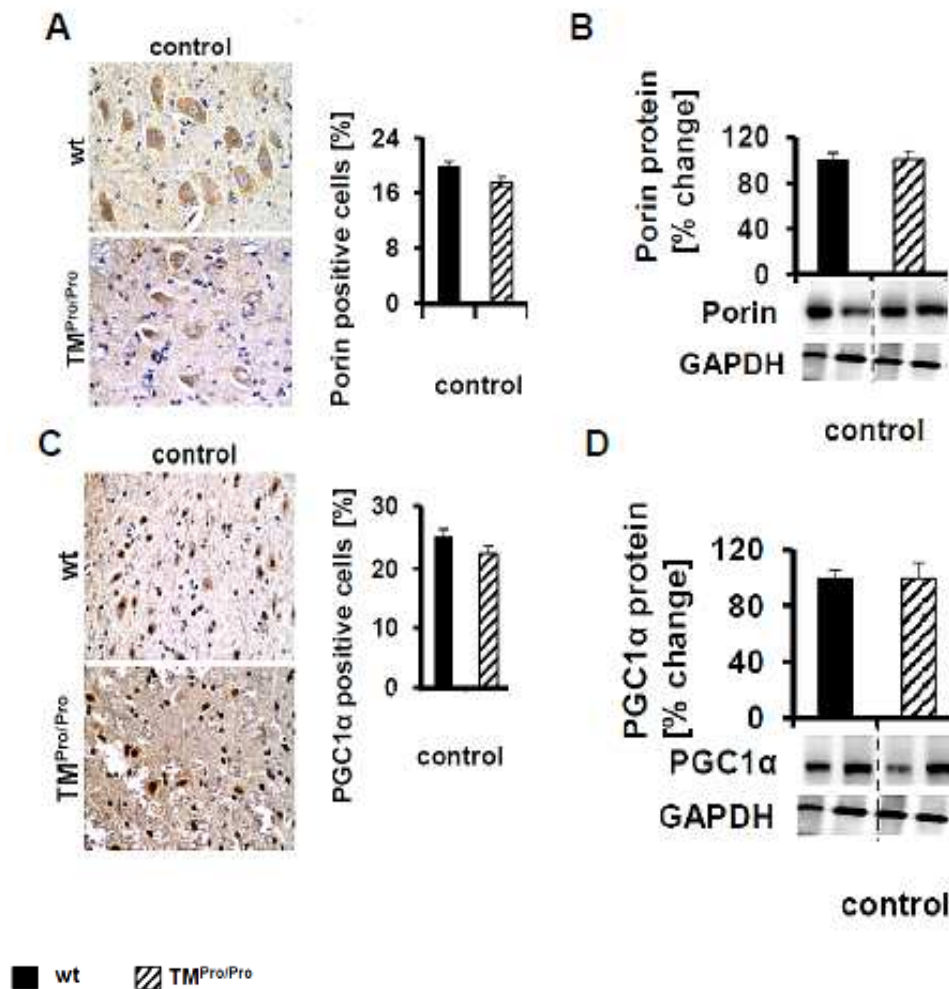
■ wt   ▨ TM^Pro/Pro

Fig. 3.3.1: mitochondrial mass and biogenesis are not impaired in TM^Pro/Pro mice

A-D: Expression of porin (A, B), reflecting mitochondrial mass, and PGC1α (C, D), reflecting mitochondrial biogenesis, in the upper spinal cord does not differ in wt and TM^Pro/Pro mice. Representative immunohistochemical images of porin (A, left) and PGC1α (C, left), bar graphs reflecting the frequency of positively stained cells (A, C, right), and representative immuno-blots (B, D, bottom) and bar graphs (B, D, top) summarising porin (B) or PGC1α (D) expression in mouse spinal cord tissue samples. Brown, porin (A) or PGC1α (C) positive cells detected by horseradish peroxidase-3,3´-diaminobenzidine reaction; blue, hematoxylin counterstain. Scale bars: 20 µm (A, C). Bar graphs represent the mean ± SEM of 6 (A-D) mice per group.

We next analysed mitochondria morphology using TEM. Total mitochondria from brain tissue of TM$^{Pro/Pro}$ mice showed frequently a distorted or "branching" morphology as compared to mitochondria from wt mice (Fig. 3.3.2). Hence, increased mitochondrial ROS generation in the CNS of TM$^{Pro/Pro}$ mice is associated with an altered mitochondrial function, but not with an altered mitochondrial number or biogenesis, consistent with a functional defect of mitochondria in the CNS of TM$^{Pro/Pro}$ mice.
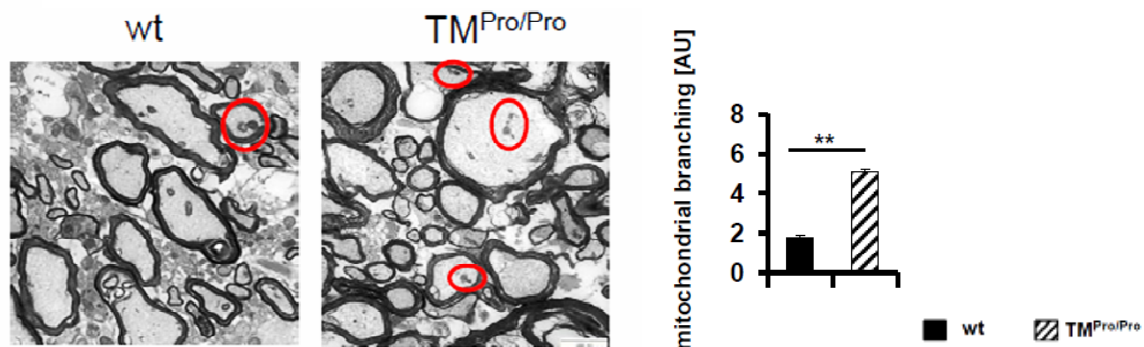
Fig. 3.3.2: Altered mitochondrial morphology in TM$^{Pro/Pro}$ mice

Left: TEM images of mouse spinal cord showing increased mitochondrial branching (red circle) in TM$^{Pro/Pro}$ mice as compared to wt mice. Scale bar: 500 nm. Right: Bar graphs represent the mean ± SEM of 3 mice per group; ** $P < 0.01$; Student´s t-test.

3.4 Impaired mitochondrial respiration and increased cardiolipin oxidation in TM$^{Pro/Pro}$ mice

To determine mitochondrial function we analysed mitochondrial respiration in isolated brain mitochondria from wt and TM$^{Pro/Pro}$ mice. Mitochondrial oxygen consumption was reduced in TM$^{Pro/Pro}$ derived mitochondria as compared to wt derived mitochondria, both following addition of glutamate and malate (probing for complex I/III activity) or succinate (probing for complex II/III) as substrates (Fig. 3.4.1 A). Thus, mitochondrial function is impaired in TM$^{Pro/Pro}$ derived mitochondria, and this defect appears to include an impaired function of complex III to V. We next determined levels of complexes I to V of the respiration chain using marker proteins for each complex. All marker proteins were either tentatively, but not significantly (NDUFB8, for complex I; complex IV subunit I) or significantly (marker proteins SDHB, UQCRC2 and ATP5α, reflecting complex II, complex III core protein and complex V alpha subunit) increased (Fig. 3.4.1 B). The increased expression of these markers protein argues against impaired activity of the respiratory chain due to a complex deficiency and indicates a functional defect.
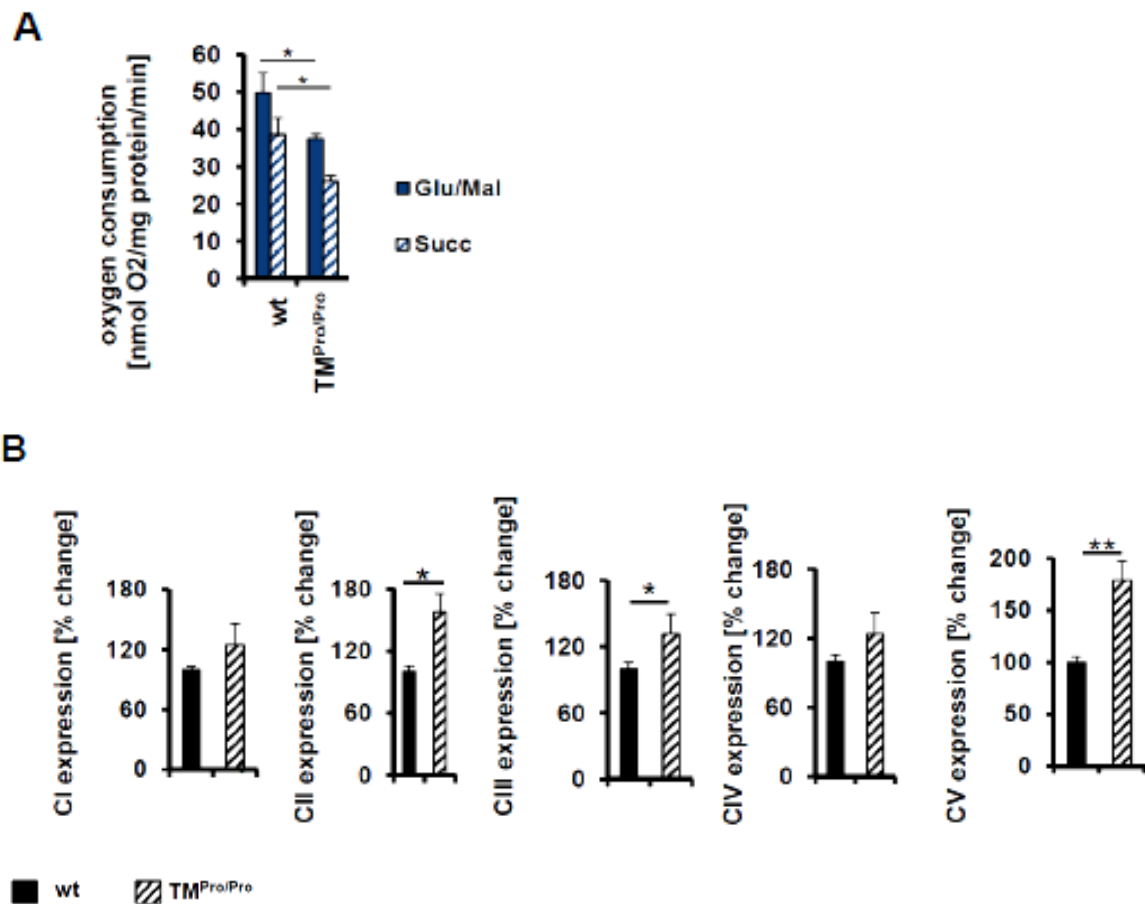
Fig. 3.4.1: Impaired mitochondrial respiration in TM^Pro/Pro mice
A: Oxygen consumption in TM^Pro/Pro derived mitochondria is reduced as compared to wt mitochondria. Mitochondria were isolated from the upper spinal cord and oxygen consumption was determined following stimulation of mitochondria with either 5 mM glutamate + 5 mM malate (Glu/Mal) or 10 mM succinate (Succ). **B:** Altered expression of mitochondrial respiratory chain marker proteins in upper spinal cord protein extracts of TM^Pro/Pro mice as compared to wt controls. Representative immune-blots (bottom) and bar graphs (top) reflecting relative expression (in %, relative to wt control) of the CI subunit NDFUFB8 (CI), CII-30kDa (CII), CIII-core protein 2 (CIII), CIV subunit I (CIV), and CV alpha subunit (CV). *P < 0.05; *P < 0.01; Student's t-test.

We next analysed cardiolipins in wt and TM^Pro/Pro mice as the function of the mitochondrial respiratory chain depends in part on the composition of cardiolipins (CL) [88]. Cardiolipins were isolated from mouse brain derived mitochondria and their fatty acid composition was analysed probing for the 17 most frequent CL-associated fatty acid species by HPLC/MS. Intriguingly, while the concentration of linoleic acid (C18:2) was increased, the concentration of palmitic acid (C16:0) was significantly and that of oleic acid (C18:1) slightly (but non-significantly) reduced in TM^Pro/Pro mice as compared to wt control mice (Fig 3.4.2 A). All other fatty acids showed no significant changes (Fig. 3.4.2 C). C18:2 is particular sensitive to oxidation and oxidised CLs impair the mitochondrial respiratory chain function [88-90]. Accordingly, we observed an increased oxidation of (C18:2)4 cardiolipins in TM^Pro/Pro derived mitochondria as compared to wt mitochondria (Fig. 3.4.2 B).

A

B

C
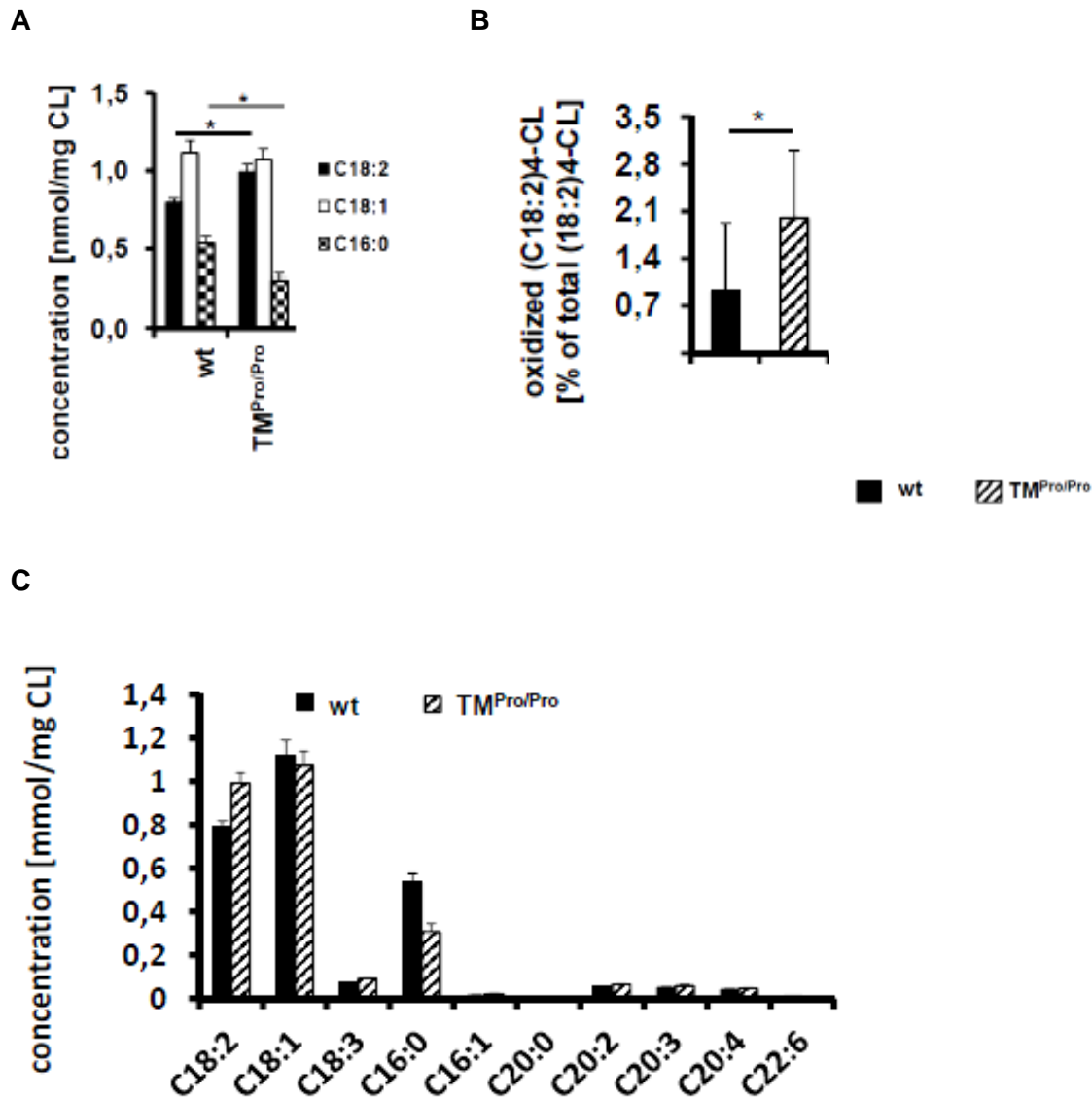
Fig. 3.4.2 A-C: Increased cardiolipin oxidation in TM^Pro/Pro^ mice

Analyses of cardiolipins (CL): the fatty acid composition of CL-species obtained from TM^Pro/Pro^ derived mitochondria is altered, with an increase of C18:2 and a reduction of C16:0 fatty acids, when compared with CL obtained from wt mitochondrial (C). The frequency of oxidised CL (C18:2) is increased in TM^Pro/Pro^ derived mitochondria as compared to wt controls (D). **E:** Mitochondrial cardiolipin of wt and TM^Pro/Pro^ mice. Representative bar graphs show concentrations of incoorported fatty acids into mitochondrial cardiolipins in mouse brain. Bar graphs summarise results obtained from six different mice in each group. *P < 0.05; Student's t-test.

As oxidation of CL is not only associated with an impaired activity of the mitochondrial respiratory chain, but also with an impaired stability of mitochondrial DNA [91] we analysed the D17-loop deletion, reflecting mitochondrial DNA damage. The D17-loop deletion was more frequent in TM$^{Pro/Pro}$ derived brain mitochondria as compared to wt mitochondria (Fig. 3.4.3). Taken together, these results establish the CL composition, CL oxidation, and mitochondrial function is impaired in mitochondria derived from neuronal tissues of TM$^{Pro/Pro}$ mice.
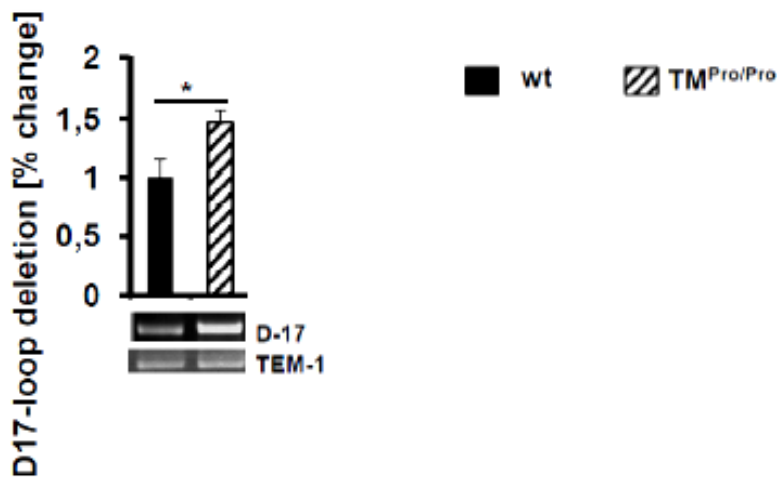
Fig. 3.4.3: Mitochondrial DNA damage, indicated by enhanced D17-loop deletion, is increased in TM$^{Pro/Pro}$ derived mitochondria as compared to wt controls. Bar graphs summarising results obtained from six different mice in each group; *$P < 0.05$; Student's t-test.

3.5 aPC reduces mitochondrial ROS in neuronal cells *in vitro*

Considering the low level of endogenous aPC generation in TM$^{Pro/Pro}$ mice and the established neuro-protective effects of aPC we next explored whether aPC cell-autonomously reduces mitochondrial ROS generation in rat neuronal PC12 cells. Exposure of PC12 cells to H$_2$O$_2$ time-dependently induces mitochondrial ROS generation (Fig. 3.5.1 A-B), with a significant induction 15 min and maximal levels 60 min after addition of H$_2$O$_2$. PC12 were left untreated (PBS control) or treated with aPC (20 nM; 1 h pre-incubation), stimulated with H$_2$O$_2$, and analysed after 15 and 60 min. Pre-treatment with aPC reduced mitochondrial ROS generation in neuronal PC12 cells at both time-points (Fig. 3.5.1 C-D). These findings demonstrate that aPC cell-autonomously restricts mitochondrial ROS production in neuronal cells.
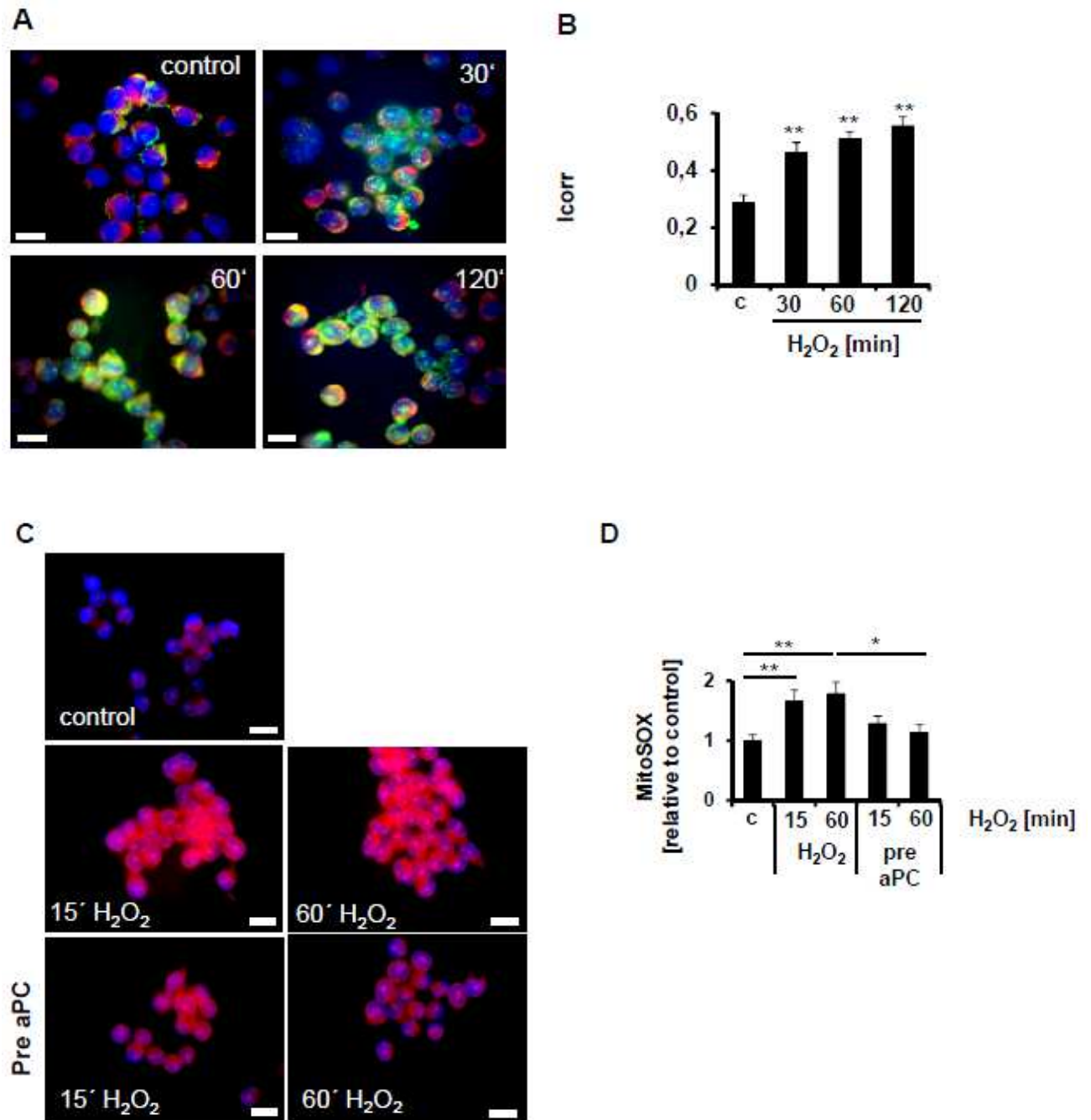
Fig. 3.5.1: aPC normalises mitochondrial ROS production in neuronal cells *in vitro*

A: Mitochondrial ROS production upon H_2O_2 stimulation. Representative images show immunofluorescence staining of rat neuronal PC12 cells. Red, mitotracker (mitochondrial marker); green, 8-hydroxy-2'-deoxyguanosine (ROS marker); yellow, merge; blue, nuclear DAPI counterstain; scale bars: 20µm. **B:** H_2O_2 stimulation increased ROS production in rat neuronal cells. Bar graphs summarising obtained results from 3 independent experiments. **$P < 0.01$, Students t-test. **C-D:** Rat neuronal PC12 cells were exposed to H_2O_2 (500 µM, 1hr) and cell were stained after indicated time-intervals with MitoSOX (red), detecting mitochondrial ROS (counterstain with DAPI, blue). Pre-treatment with aPC (20 nM) reduces mitochondrial ROS production. Representative fluorescent images (C) and bar graph (D) summarising results of 3 independent experiments; scale bars: 20 µm; *$P < 0.05$; **$P < 0.01$; Student's t-test.

3.6 aPC restores ROS generation, nociception and stabilises mitochondrial DNA in TM$^{Pro/Pro}$ mice

To determine whether restoring aPC can correct for the defects observed in TM$^{Pro/Pro}$ mice we next analysed TM$^{Pro/Pro}$ x hPC^{high} mice and TM$^{Pro/Pro}$ mice treated with aPC. Genetically restoring defective PC-activation in TM$^{Pro/Pro}$ mice by breeding with hPC^{high} mice reduced ROS production, as reflected by reduced peroxynitrite and 8-oxo-dG staining, in the CNS (Fig. 3.6.1 A-D). This suggests that the neuronal defects observed in mice with impaired TM-dependent PC activation may be reversible.
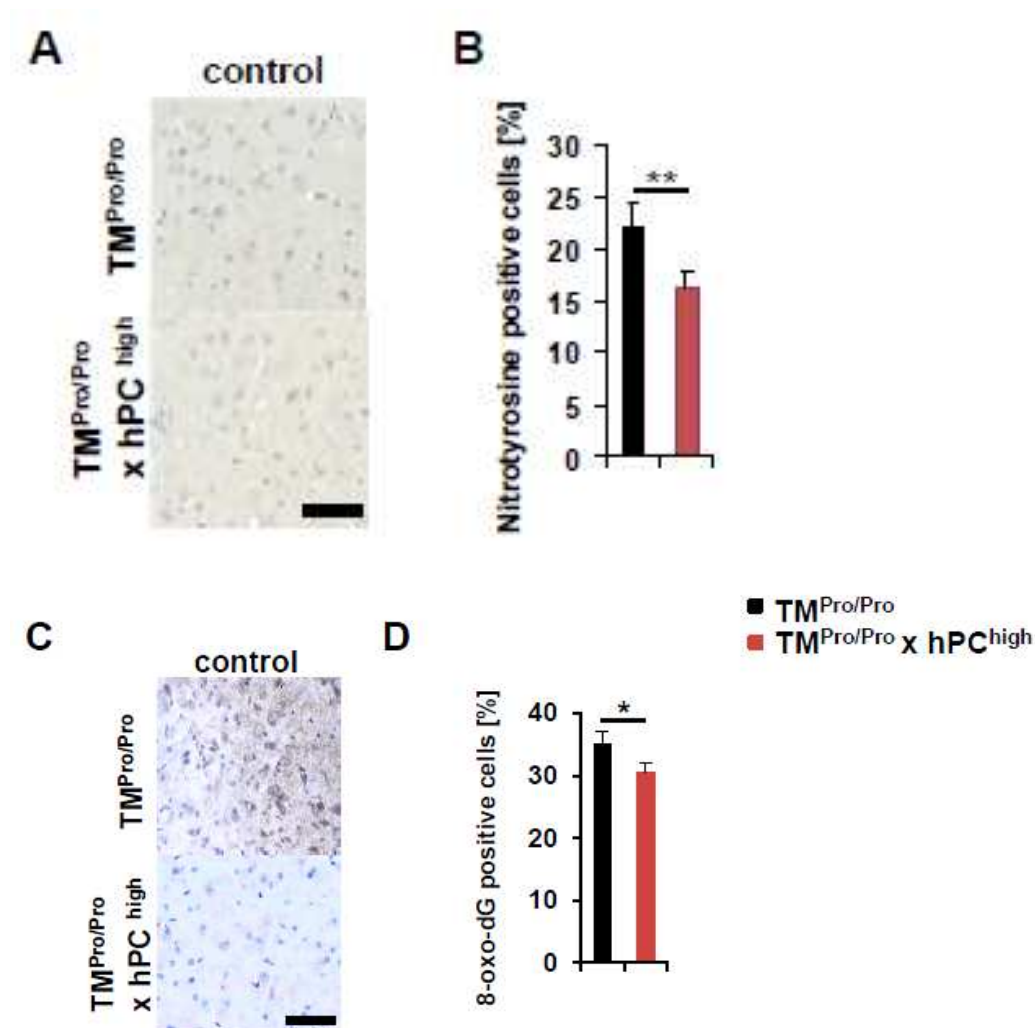
Fig. 3.6.1: aPC normalises ROS-generation

A-D: Representative images of immunohistochemically stained upper spinal cord sections (A, C) and bar graphs summarising results of eight mice per group (B, D). Restoring aPC in mice reduces nitrotyrosine (A, B) and 8-hydroxy-2'-deoxyguanosine (C, D) levels in TM$^{Pro/Pro}$ x hPC^{high} mice. Brown, nitrotyrosine (A) or 8-hydroxy-2'-deoxyguanosine (D) positive cells detected by horseradish peroxidase-3,3´-diaminobenzidine reaction; blue, haematoxylin counterstain. Scale bars: 20 µm; **$P < 0.01$; Student's t-test.

Next, we wanted to determine whether exogenous application of aPC is sufficient to restore impaired nociception and mitochondrial stability in TM$^{Pro/Pro}$ mice, so we treated TM$^{Pro/Pro}$ mice

with aPC (1 mg/kg body weight intraperitoneally, for 4 weeks). Pharmacological intervention aiming to restore defective aPC-generation in TM$^{Pro/Pro}$ mice was sufficient to normalise nociception, as reflected by a reduction of the latencies in the hot-plate and a faster reaction time in tail-flick assay (Fig. 3.6.2 A, B). Further, exogenous aPC administration was sufficient to stabilise mitochondrial DNA, as reflected by less frequent D17-loop deletions compared to TM$^{Pro/Pro}$ mice (Fig. 3.6.2 C-D). These results establish that impairment of TM-dependent PC activation, as observed in individuals with vascular or inflammatory diseases, is sufficient to cause neuronal dysfunction. Importantly, the neuronal defect induced by defective TM-mediated PC activation is reversible upon pharmacological substitution of aPC.
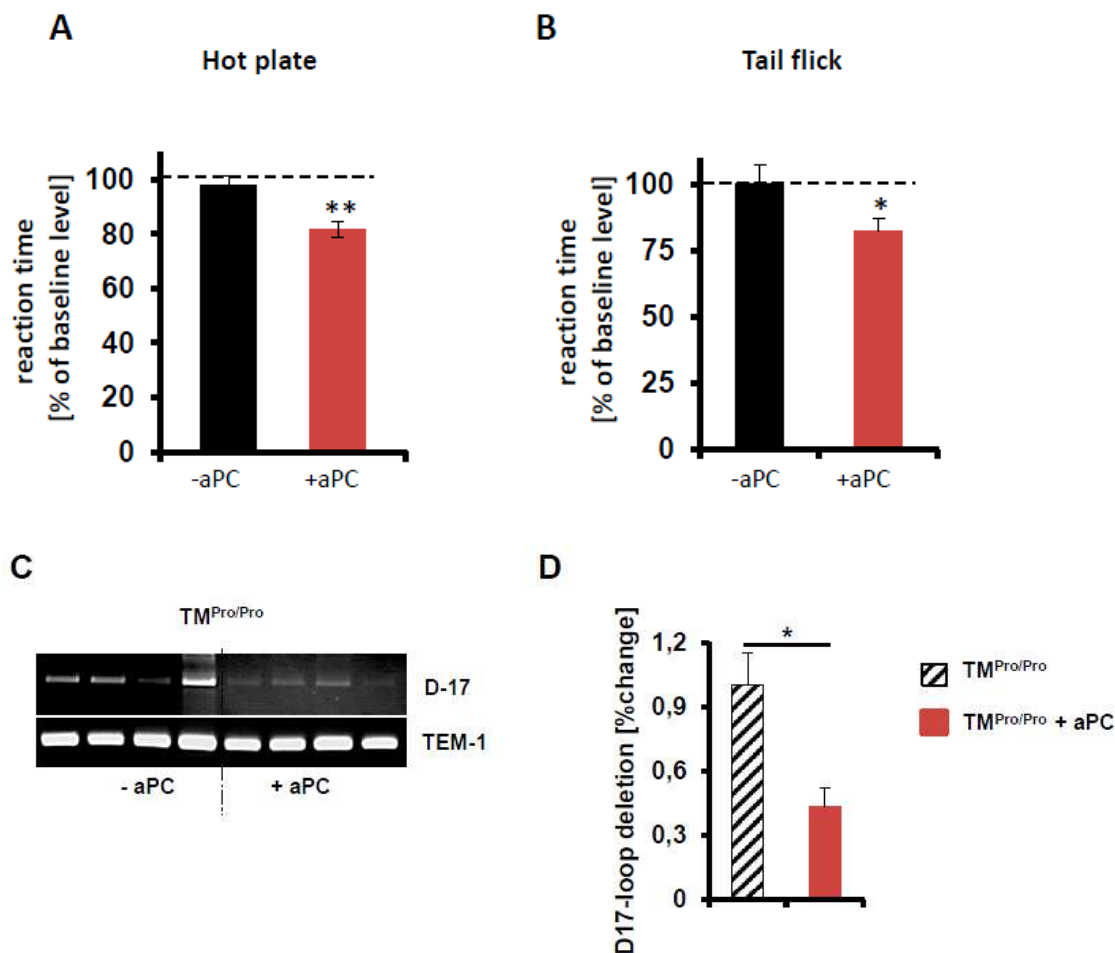
Fig. 3.6.2 A-D: aPC normalises nociception and reconstituted mitochondrial stability in TM$^{Pro/Pro}$ mice
A-B: Nociception (hot-plate assay, E; tail flick assay, F) is restored in TM$^{Pro/Pro}$ x hPC^{high} mice. Bar graphs summarise results of at least 8 mice per group (A, C) or of three repeat measurements in at least 8 (E-F) different mice per group. Spotted line shows baseline level (100 %) of reaction time. *P < 0.05; **P < 0.01; Student's t-test. **C-D:** Mitochondrial DNA damage, indicated by reduced D17-loop deletion, is ameliorated in TM$^{Pro/Pro}$ + aPC mice derived mitochondria as compared to TM$^{Pro/Pro}$ mice. Bar graphs summarising results obtained from six different mice in each group; *P < 0.05; Student's t-test.

Taken together, these data establish that the basal impaired nociception in aPC-deficient mice is not caused by a defect of the peripheral nerves, but linked with dysfunctional neurons in the CNS, caused by increased mitochondrial ROS production and altered mitochondrial function in neuronal cells. These results proved a hitherto unknown basal phenotype showing that impairment of TM-dependent PC activation, as observed in individuals with vascular or inflammatory diseases, is sufficient to cause neuronal dysfunction. Importantly, restoring the defective PC-activation ameliorated impaired neuronal function, establishing that the basal neuronal defect induced by defective TM-dependent PC activation is therapeutically amendable.

The above data uncover a new physiological function of the TM-dependent PC-activation for neuronal function and proper myelination in the CNS. This defect did not impair the function of peripheral nerves and did not accelerate – beyond the additive effect – peripheral neuropathy. However, we speculated that the impaired neuronal function and myelination within the CNS would predispose to demyelinating diseases of the CNS.

3.7 Loss of thrombomodulin-dependent protein C activation aggravates EAE

To determine the relevance of TM-dependent endogenous PC activation we used TM$^{Pro/Pro}$ mice. The disease onset was virtually identical in TM$^{Pro/Pro}$ and wild-type (wt) mice after induction of EAE (around day 11). However, the disease severity was markedly aggravated in TM$^{Pro/Pro}$ EAE mice, being significantly worse from day 14 onwards until the end of the observation period (day 30) (Fig. 3.7.1 A). Average EAE scores were calculated for each day and summed for the entire experiment to yield a Cumulative Disease Index (CDI), representing total disease load. WT mice had a CDI of 27.83±0.21, whereas TM$^{Pro/Pro}$ mice demonstrated a significantly higher CDI of 52.95±0.23 (Fig.3.7.1 B).
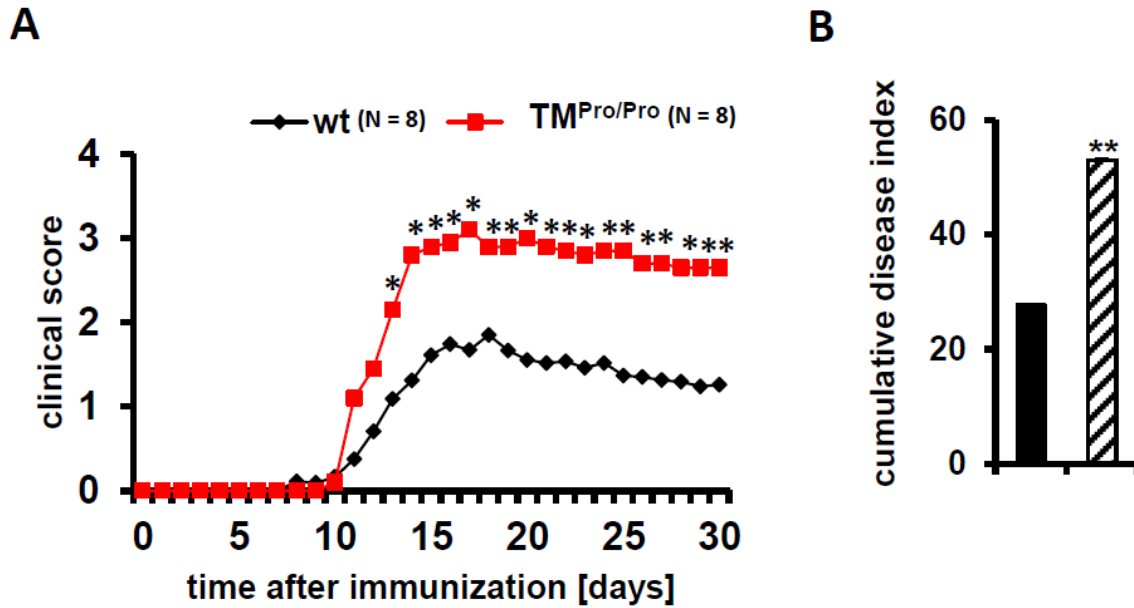
Fig. 3.7.1: Impaired endogenous PC activation aggravates EAE
A: Severity of EAE, based on a clinical score, in wt and TM$^{Pro/Pro}$ mice. Clinical disease score was aggravated in TM$^{Pro/Pro}$ mice compared to wt mice. **B:** The cumulative disease index for EAE TM$^{Pro/Pro}$ mice was significantly higher than EAE wt mice. (N = 8) *P < 0.05; Student´s t-test.

Histological analyses of cervical spinal cord using Luxol-Fast-Blue stained sections revealed no obvious difference between control wt and TM$^{Pro/Pro}$ control mice (Fig. 3.7.2). However, analyses of tissue samples obtained from mice 4 weeks after disease induction revealed an aggravated reduction of myelin in TM$^{Pro/Pro}$ EAE as compared to wt EAE mice (Fig 3.7.2).
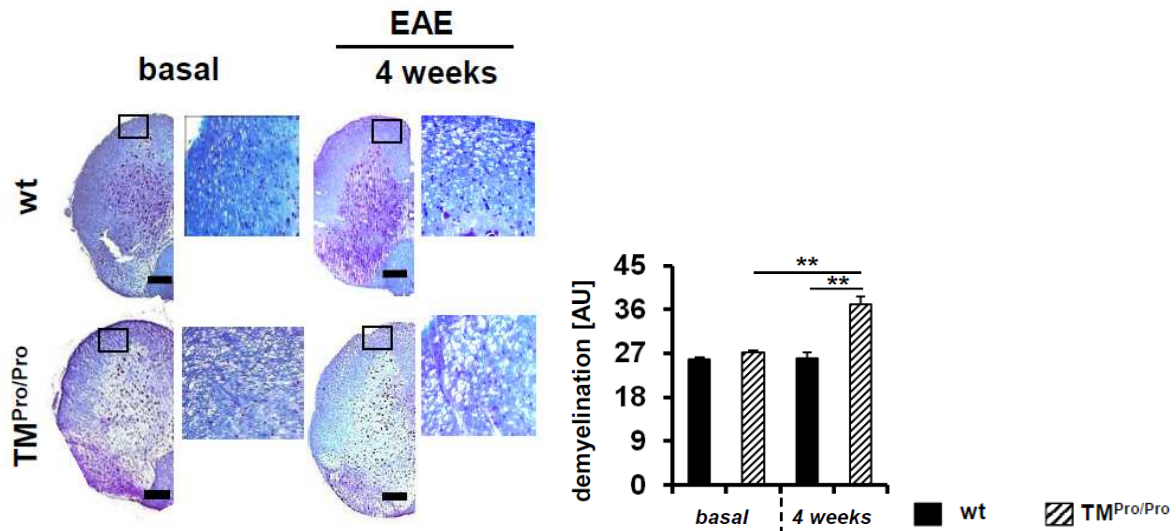
3.7.2: Aggravated demyelination in EAE TM^Pro/Pro mice

left: Myelin staining of mouse spinal cord by using Luxol-Fast-Blue (LFB). No difference was apparent at baseline (left), while demyelination was aggravated after 4 weeks EAE in TM^Pro/Pro EAE mice compared to wt EAE mice. Scale bars: 200 μm. right: Bar graphs showing counted demyelinated axons in LFB stained images (10 axons, $N = 5$), ** $P < 0.01$; Student´s t-test.

We next conducted ultrastructural analyses using TEM. In EAE wt mice, loosening of the myelin sheath or complete demyelination [note: arrow heads; figure legends] and pale axoplasm devoid of organelles [asterix] were visible (Fig. 3.7.3). These ultrastructural changes were aggravated in TM^Pro/Pro EAE mice (Fig. 3.7.3).
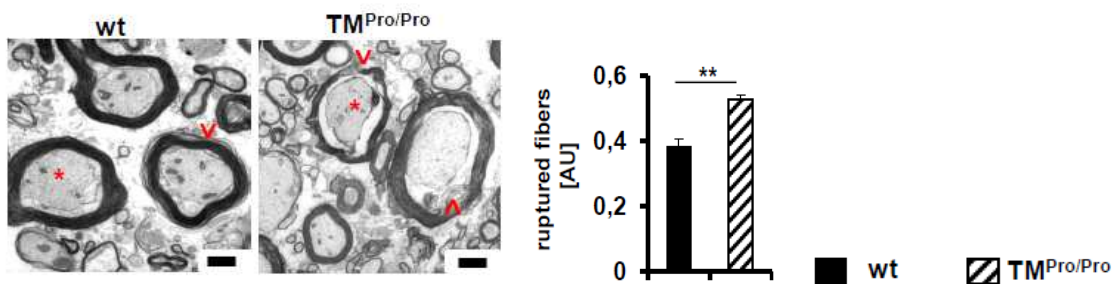
Fig. 3.7.3: Impaired myelin structure in EAE TM^Pro/Pro mice

left: TEM images of mouse spinal cord showed loosening of the myelin sheath or complete demyelination [arrow heads] and pale axoplasm devoid of organelles [asterix] in EAE mice. These ultrastructural changes were aggravated in TM^Pro/Pro EAE mice. right: Bar graphs summarising frequency of ruptured nerve fibers. Scale bars: 500 nm, N = 3. ** $P < 0.01$; Student´s t-test.

Taken together, based on a phenotypic and on histological analyses loss of endogenous PC activation aggravates EAE severity and associated neuronal demyelination.

3.8 Loss of endogenous PC activation increases markers of oxidative stress

Enhanced ROS generation contributes to neuro-degenerative diseases, including EAE. To determine whether impaired TM-dependent PC activation results in increased oxidative stress we analysed markers of ROS-generation, $ONOO^-$ and 8-oxo-dG. Using immunohistochemical analyses of spinal cord sections both markers were increased in EAE mice at 1 week after disease onset and at 4 weeks after disease induction (Fig. 3.8.1 A-B, D-E). The staining intensity was markedly increased in $TM^{Pro/Pro}$ mice at both time-points (Fig. 3.8.1 A-B, D-E), indicating enhanced ROS generation in mice with impaired PC activation.

Next, we used immunoblot analyses of spinal cord protein lysates to confirm the increased expression of $ONOO^-$. We found a corresponding expression pattern of $ONOO^-$ expression in EAE mice as shown in the immunohistochemical staining (Fig. 3.8.1 C). $ONOO^-$ was significantly increased in EAE mice in both wt and $TM^{Pro/Pro}$ mice after 1 week of disease onset and 4 weeks of disease induction. In $TM^{Pro/Pro}$ mice $ONOO^-$ expression was even aggravated compared to wt mice (Fig. 3.8.1 C). These data demonstrate that endogenously impaired PC activation enhances ROS during EAE disease course.
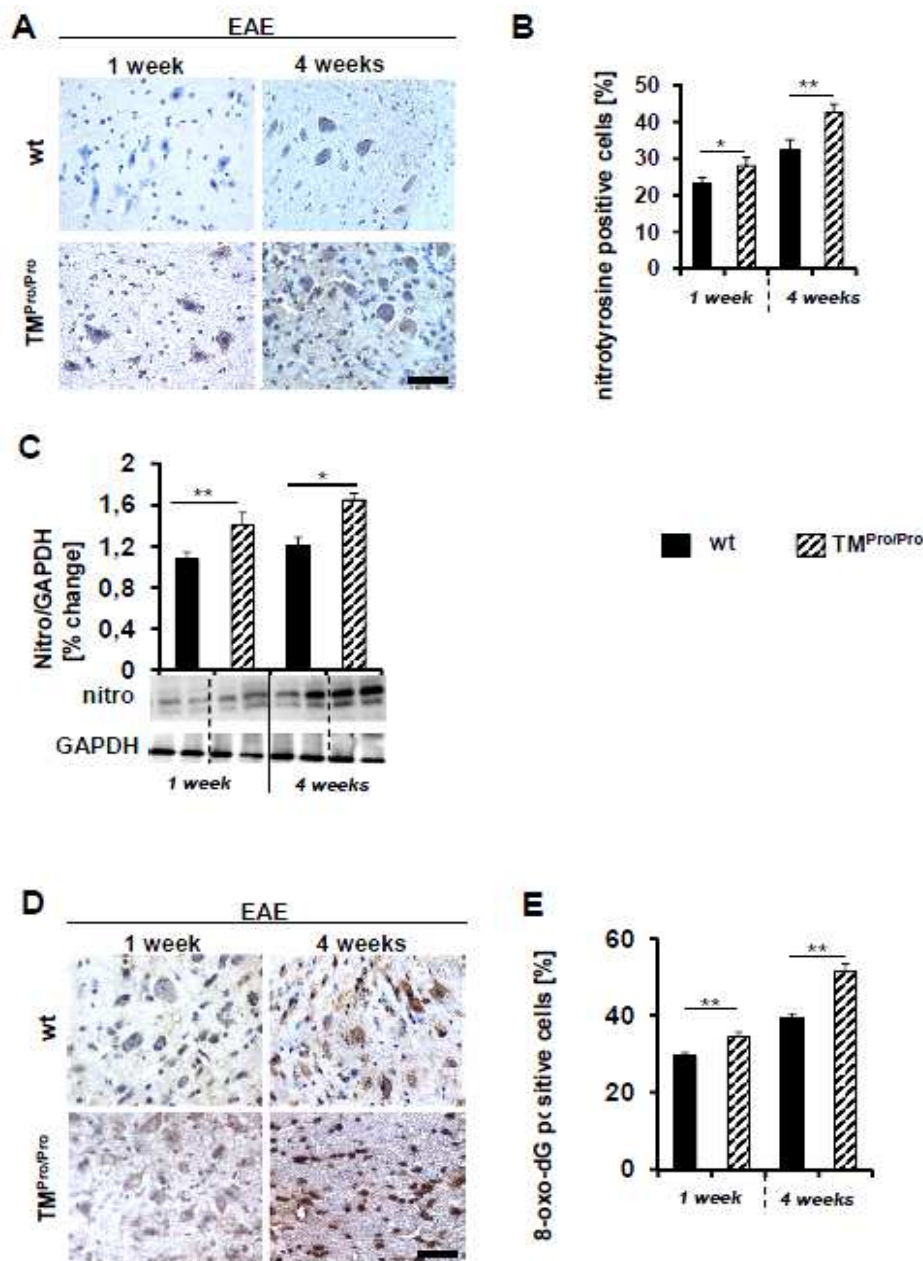
Fig. 3.8.1: Loss of endogenous PC activation increases markers of oxidative stress

A-B: Representative images (A) and bar graphs (B) showing immunohistochemical staining of mouse spinal cord. Nitrotyrosine is strongly expressed in EAE diseased mice after one week and expression is further increased after four weeks of EAE in both, wt and TM[Pro/Pro] mice. Brown, nitrotyrosine positive cells detected by horseradish peroxidase-3, 3´-diaminobenzidine reaction; blue, hematoxylin counterstain. Scale bars: 20 µm, N = 8. **C:** Representative western blots (bottom) and bar graphs (top) showing nitrotyrosine expression in mouse spinal cord tissue samples. Bar graphs summarise results obtained from eight different mice in each group. * $P < 0.05$, ** $P < 0.01$, Students t-test. **D-E:** Immunohistochemical staining for 8-hydroxy-2'-deoxyguanosine of mouse spinal cord. In EAE diseased mice, 8-hydroxy-2'-deoxyguanosine staining was aggravated after 4 weeks compared 1 week EAE in both groups, wt and TM[Pro/Pro] mice. In TM[Pro/Pro] mice staining intensity was increased compared to wt mice. Brown, 8-hydroxy-2'-deoxyguanosine positive cells detected by horseradish peroxidase-3, 3´-diaminobenzidine reaction; blue, hematoxylin counterstain. Scale bars: 20 µm, N = 8. * $P < 0.05$; ** $P < 0.01$; Student´s t-test.

3.9 Mitochondrial defect in TM$^{Pro/Pro}$ mice

To further evaluate whether the mitochondrial defect in TM$^{Pro/Pro}$ mice is aggravated during the EAE course we determined expression of the mitochondrial marker porin (VDAC1). After 1 week of EAE onset porin expression levels were slightly but not significantly reduced in the spinal cord of TM$^{Pro/Pro}$ mice as compared to wt mice (Fig. 3.9.1 A, B). But the expression was significantly decreased after 4 weeks of EAE induction in TM$^{Pro/Pro}$ mice compared to wt mice. Both in wt and TM$^{Pro/Pro}$ mice porin levels declined during the course of EAE. Immunoblot analyses of spinal cord lysates confirmed the decrease of porin expression in both wt and TM$^{Pro/Pro}$ diseased mice (Fig. 3.9.1 C). After 4 weeks of EAE induction there was significantly less porin expression detectable in TM$^{Pro/Pro}$ compared to wt EAE mice (Fig. 3.9.1 C). Next, we determined expression of the transcription factor PGC1α, which reflects mitochondrial biogenesis. A slight bot non-significant reduction became apparent in diseased TM$^{Pro/Pro}$ mice at 1 week after disease onset which became significantly after 4 weeks of EAE induction (Fig. 3.9.1 D, E). Again western blot analyses confirmed the reduction of PGC1α during disease course in both wt and TM$^{Pro/Pro}$ mice (Fig. 3.9.1 F).

Hence, mitochondrial ROS-generation precedes a defect in mitochondrial biogenesis in EAE TM$^{Pro/Pro}$ mice, indicating that loss of TM-dependent PC generation impairs primarily mitochondrial function and not mitochondrial biogenesis. However, during the EAE progression and the associated ROS generation mitochondrial biogenesis becomes eventually impaired.
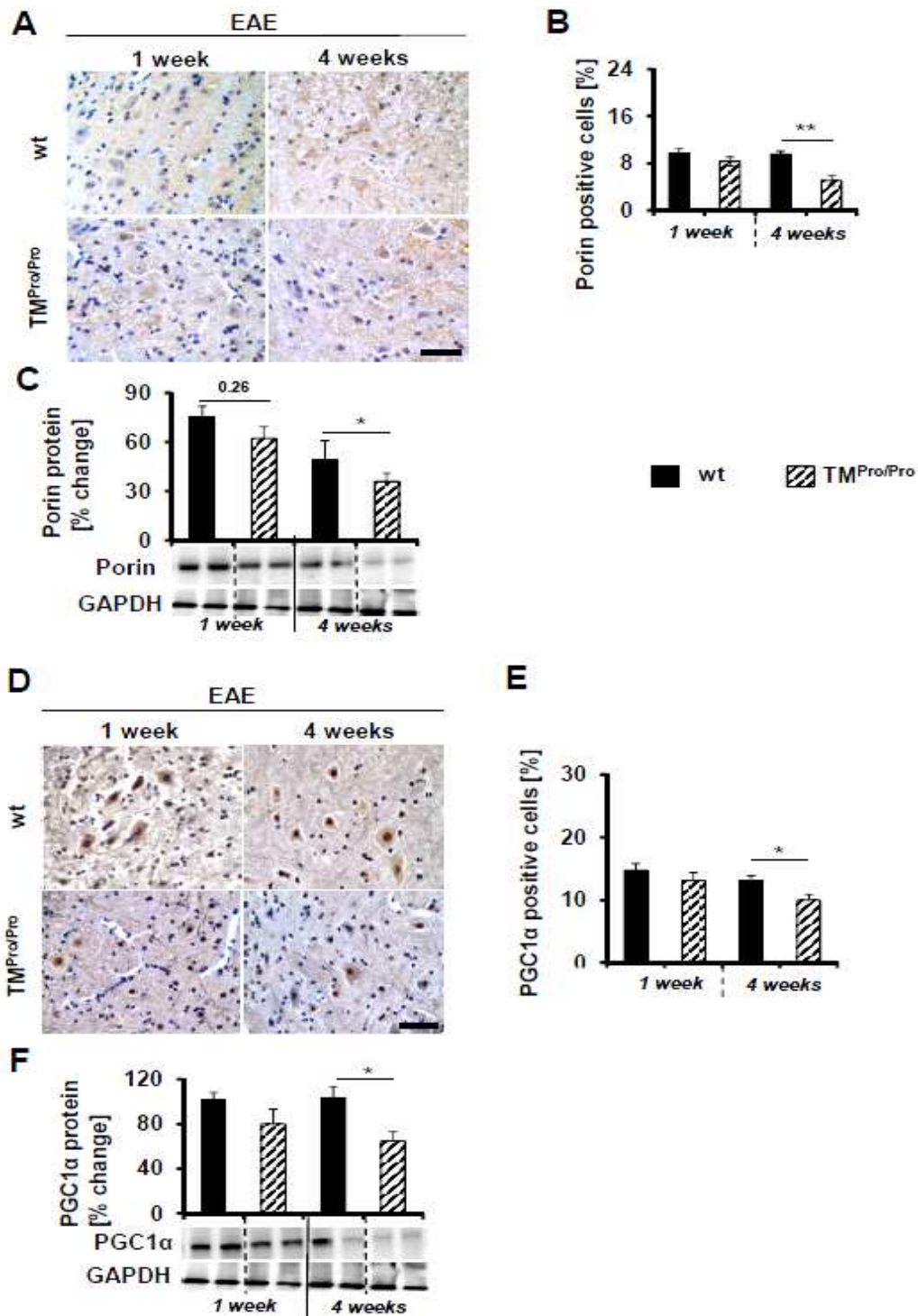
Fig. 3.9.1: Acquired mitochondrial deficiency in TM^Pro/Pro mice

A: Representative images showing immunohistochemical staining of mouse spinal cord. Four weeks after EAE onset, porin expression is decreased in EAE diseased mice in wt and TM^Pro/Pro mice. Brown, porin positive cells detected by horseradish peroxidase-3,3′-diaminobenzidine reaction; blue, hematoxylin counterstain. Scale bars: 20 µm. **B:** Bar graphs summarising the counting of porin positive cells from immunohistochemical staining. (N = 6). **P < 0.01; Student´s t-test. **C:** Representative western blots (bottom) and bar graphs (top) showing porin expression in mouse spinal cord tissue samples. Bar graphs summarize results obtained from six different mice in each group. *P < 0.05, Students t-test. **D:** Immunohistochemical staining for PGC1α of mouse spinal cord. PGC1α expression was decreased four

weeks after EAE onset in both groups, wt and TM$^{Pro/Pro}$ mice. Brown, PGC1α positive cells detected by horseradish peroxidase-3,3´-diaminobenzidine reaction; blue, hematoxylin counterstain. Scale bars: 20 µm. **E:** Bar graphs summarising the results of counting PGC1α positive cells. (N = 6) *P < 0.05, Students t-test. **F:** Representative western blots (bottom) and bar graphs (top) showing PGC1α expression in mouse spinal cord tissue samples. Bar graphs summarise results obtained from six different mice in each group. *P < 0.05; **P < 0.01; Student´s t-test.

3.10 Soluble TM is superior compared to p66^{Shc}-inhibtion or aPC-treatment in EAE TM$^{Pro/Pro}$ mice

To address potential mechanisms aggravating EAE in TM$^{Pro/Pro}$ mice various *in vivo* interventions were conducted. First, we tested the potential impact of impaired PC activation in TM$^{Pro/Pro}$ mice. To this end TM$^{Pro/Pro}$ mice were crossed with hPC^{high} mice. The latter express a mutant human PC, which can be efficiently activated by thrombin even in the absence of functional TM, resulting in increased plasma levels of aPC [21]. The initial disease course did not differ between TM$^{Pro/Pro}$ and TM$^{Pro/Pro}$ x hPC^{high} mice, e.g. the disease onset and the disease severity were virtually identical until day 19 (Fig. 3.10.1 A). However, after day 19 the disease severity was improved in TM$^{Pro/Pro}$ x hPC^{high} mice compared to TM$^{Pro/Pro}$ mice (Fig. 3.10.1 A), corroborating results in wt EAE mice treated intravenously with aPC [44]. Luxol-Fast-Blue staining of spinal cord sections showed a decreased demyelination in TM$^{Pro/Pro}$ x hPC^{high} EAE mice compared to TM$^{Pro/Pro}$ EAE mice 1 week after disease onset and 4 weeks after EAE induction (Fig. 3.10.1 B). Thus, aPC only partially corrects for impaired TM function in the context of EAE. In agreement with an antioxidant effect of aPC indices of excess ROS generation (ONOO$^-$, 8-oxo-dG) were markedly reduced in TM$^{Pro/Pro}$ x hPC^{high} mice (Fig. 3.10.2 A, B).

Next, we evaluated EAE and ROS-generation within the CNS in TM$^{Pro/Pro}$ mice with genetically superimposed p66^{Shc} deficiency (TM$^{Pro/Pro}$ x p66$^{Shc-/-}$) [19]. Genetically inactivation of the redox-protein p66^{Shc} has been shown to compensate for impaired TM function in TM$^{Pro/Pro}$ mice in the context of diabetic nephropathy, normalising indices of diabetic nephropathy and renal ROS markers. In the context of EAE genetically superimposed p66^{Shc} deficiency (TM$^{Pro/Pro}$ x p66^{Shc} mice) did not delay the disease onset, but improved the clinical EAE score throughout the entire observation period and diminishes tissue injury (Fig. 3.10 A). Again Luxol-Fast-Blue staining of spinal cord sections showed a decreased demyelination in TM$^{Pro/Pro}$ x p66^{Shc} EAE mice compared to TM$^{Pro/Pro}$ EAE mice 1 week after disease onset and 4 weeks after EAE induction (Fig. 3.10.1 B). The reduction of oxidative stress markers (nitrotyrosine and 8-oxo-dG) was likewise more pronounced in TM$^{Pro/Pro}$ x p66^{Shc} mice than in TM$^{Pro/Pro}$ x hPC^{high} mice (Fig. 3.10.1 A, B). Hence, p66^{Shc} deficiency is superior to restoring aPC levels in regard to EAE in TM$^{Pro/Pro}$ mice, indicating that TM

mediates a protective effect in the context of EAE, which may be partially independent of PC activation.

Soluble forms of TM have been evaluated in pre-clinical and clinical studies as an alternative mean to restore TM-dependent PC-activation as well as other potential cytoprotective effects of TM [49]. We used solulin, a soluble TM variant [49], to evaluate the therapeutic value of this approach in EAE. Strikingly, treatment of EAE TM$^{Pro/Pro}$ mice with solulin both delayed the disease onset (day 17 vs. day 10) and lessened the disease severity in comparison to PBS-treated EAE TM$^{Pro/Pro}$ mice (Fig. 3.10.1 A). The markedly improved outcome was associated with preserved myelination (LFB staining, Fig. 3.10.1 B) and reduced ROS-markers (ONOO$^-$, 8-oxo-dG) mice in both, 1 week after disease onset and 4 weeks after EAE induction (Fig. 3.10.2 A-B).
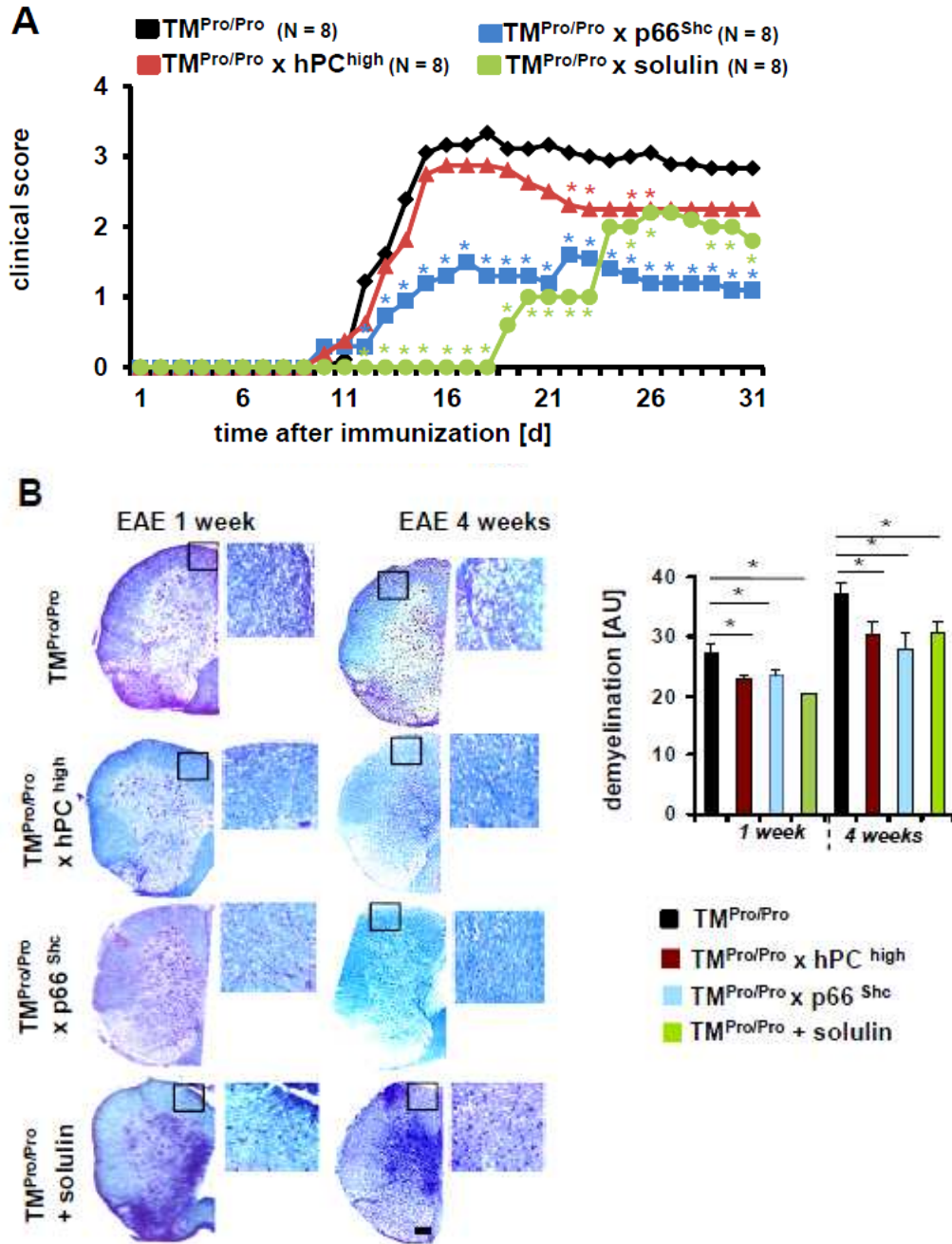
Fig. 3.10.1: Interventions with aPC, p66^Shc and soluble TM ameliorate EAE in TM^Pro/Pro mice

A: EAE was induced in C57Bl/6 wt, TM^Pro/Pro, double mutant TM^Pro/Pro mice with restored levels of hPC (TM^Pro/Pro x hPC^high mice) or abolished p66^Shc expression (TM^Pro/Pro x p66^Shc-/-), and TM^Pro/Pro treated with soluble thrombomodulin (solulin). Clinical disease scores were significantly ameliorated in TM^Pro/Pro mice treated with solulin compared to TM^Pro/Pro mice. Scores are plotted as mean (N = 8) *P < 0.05; Student´s t-test. **B:** left: Myelin staining of mouse spinal cord by using Luxol-Fast-Blue (LFB). Demyelination became apparent 1 week after EAE onset and was even more severe after 4 weeks of induction in EAE mice. In TM^Pro/Pro solulin treated and TM^Pro/Pro double mutant mice demyelination was reduced compared to TM^Pro/Pro mice. Scale bars: 200 μm. right: Bar graphs summarising demyelination of counted axons from Luxol-Fast-Blue stainings (10 countings, N = 6).
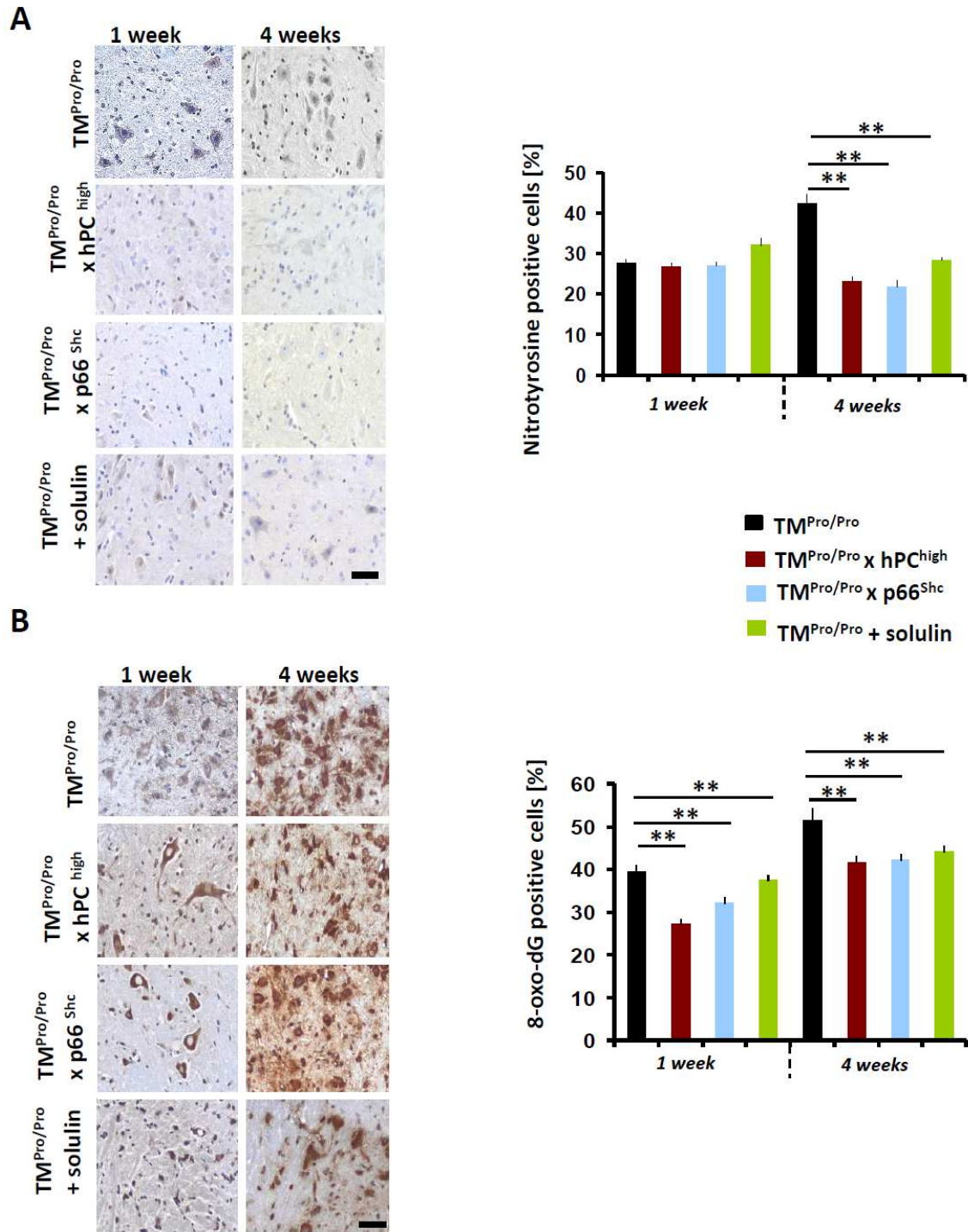
Fig. 3.10.2: Interventions with aPC, p66^Shc and soluble TM reduce oxidative stress in TM^Pro/Pro mice

A: Representative images (left) and bar graphs (right) showing immunohistochemical staining of mouse spinal cord for nitrotyrosine (A) and 8-hydroxy-2'-deoxyguanosine (B). Nitrotyrosine and 8-hydroxy-2'-deoxyguanosine are readily detectable after 1 week of EAE and are further increased after four weeks of EAE induction in TM^Pro/Pro mice. Nitrotyrosine and 8-hydroxy-2'-deoxyguanosine are ameliorated in TM^Pro/Pro double mutant mice and in TM^Pro/Pro mice treated with solulin. Brown, nitrotyrosine (A) or 8-hydroxy-2'-deoxyguanosine (B) positive cells detected by horseradish peroxidase-3, 3´-diaminobenzidine reaction; blue, hematoxylin counterstain. Bar graphs summarise results obtained from eight different mice in each group. Scale bars: 20 μm. N = 8. **P < 0.01; Student´s t-test.

Thus, soluble thrombomodulin more efficiently than genetically restoring aPC levels or inhibiting mitochondrial ROS-generation ameliorates the disease course of EAE. The potent protective effect of solulin suggests that this may be a potential therapeutic approach.

3.11 Soluble TM ameliorates EAE in wild type mice

To ascertain whether solulin does not only compensate for the genetically superimposed impairment of TM function in TM$^{Pro/Pro}$ mice, but may also be a potential therapeutic approach in mice expressing wild-type TM, we next evaluated the protective effect of solulin in EAE wt mice. Wt mice were treated with solulin following the induction of EAE, using the same protocol as above. In comparison to untreated or PBS-treated EAE wt mice solulin treatment delayed the disease manifestation and reduced the disease severity throughout the disease course (Fig. 3.11.1 A). In addition, solulin-treatment improved histological changes, reflecting myelin loss (Luxol-Fast-Blue), and normalised indices of ROS generation (ONOO$^-$, 8-oxo-dG, Fig. 3.11.1 B-D).
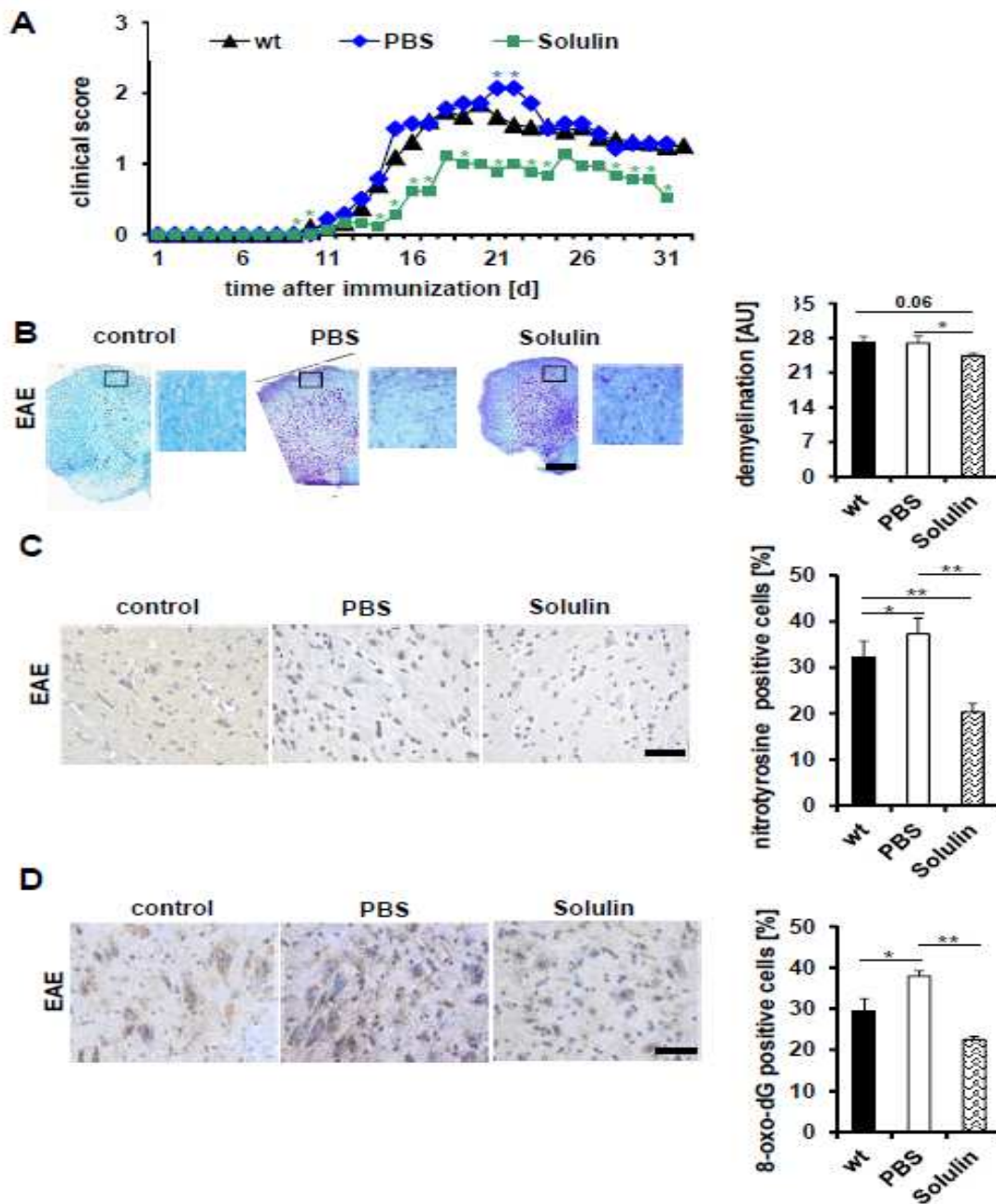
Fig. 3.11.1: Soluble TM ameliorates EAE in wild type mice

A: EAE was induced in C57/Bl6 wt mice and mice were left untreated or were treated with solulin or PBS for 30 days and clinical disease scores were determined. Solulin treatment significantly ameliorated EAE disease score in wt mice treated with solulin. Scores are plotted as mean (N = 8) *P < 0.05, students t-test. **B:** Myelin staining of mouse spinal cord by using Luxol-Fast-Blue (LFB). Demyelination was severe after 4 weeks in EAE mice. In solulin treated EAE wt mice demyelination was ameliorated compared to PBS-treated mice. Scale bars: 200 µm. right: Bar graphs summarising the demyelination of spinal cord sections (right, 10 countings, N = 6). **C:** Representative images (left C, D) and bar graphs (right C, D) showing nitrotyrosine (C) and 8-hydroxy-2'-deoxyguanosine immunohistochemical stainings of mouse spinal cord. Nitrotyrosine (C) and 8-hydroxy-2'-deoxyguanosine (D) staining is reduced in EAE wt mice treated with solulin compared to PBS treated mice. Brown, nitrotyrosine/8-hydroxy-2'-deoxyguanosine positive cells detected by horseradish peroxidase-3, 3´-diaminobenzidine reaction; blue, hematoxylin counterstain. Bar graphs summarise results obtained from eight different mice in each group. Scale bars: 20 µm. *P < 0.05; **P<0.01; Student´s t-test.

3.12 Solulin reduces mitochondrial ROS in neuronal cells *in vitro*

Considering the low level of endogenous aPC generation in $TM^{Pro/Pro}$ mice and the established neuro-protective effects of solulin we next explored whether solulin cell-autonomously reduces mitochondrial ROS generation in rat neuronal PC12 cells. PC12 were left untreated (PBS control) or treated with solulin (3 µg/ml; 1 h pre-incubation), stimulated with H_2O_2, and analysed after 15 and 60 min. Pre-treatment with solulin reduced mitochondrial ROS generation in neuronal PC12 cells at both time-points (Fig. 3.12.1 A-B). These findings demonstrate that solulin cell-autonomously restricts mitochondrial ROS production in neuronal cells.
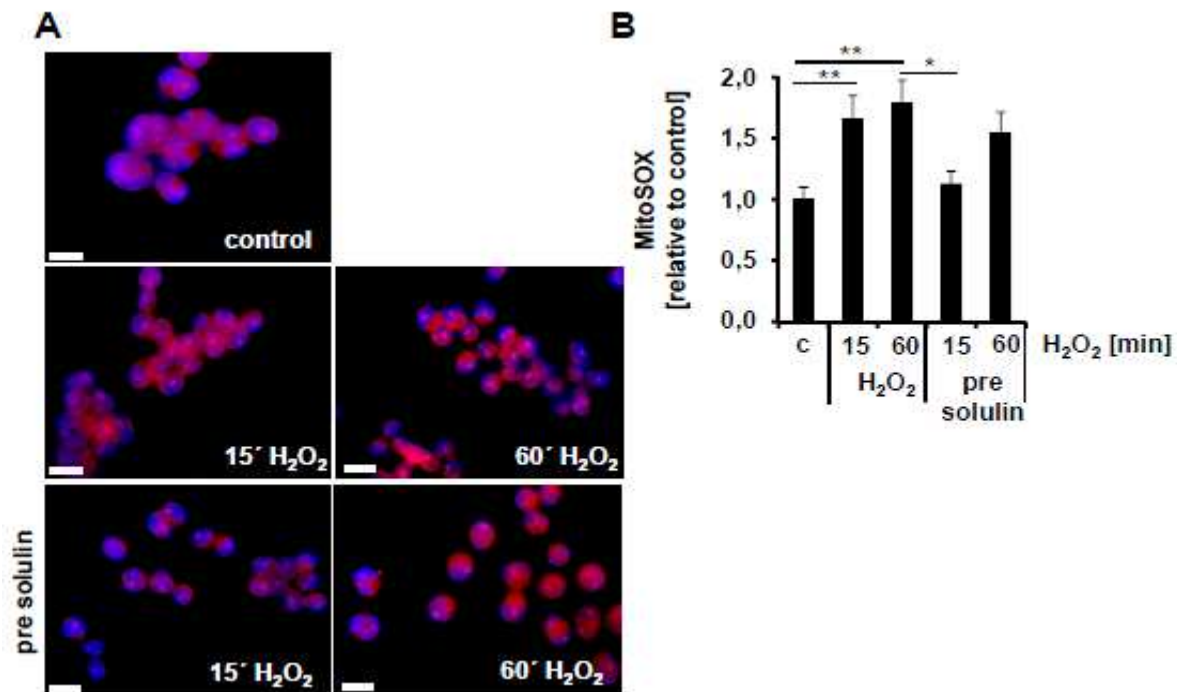
Fig. 3.12.1: Solulin decreased mitochondrial ROS *in vitro*
A: Rat neuronal PC12 cells were treated with H_2O_2 and stained for MitoSOX. In PC12 cells pre-treated with solulin mitochondrial ROS, as indicated by MitoSOX, was reduced. Red: MitoSOX, blue: DAPI. Scale bars: 20 µm. **B:** Summarising bar graphs obtained from 3 independent experiments. *$P < 0.05$; **$P < 0.01$; Student´s t-test.

3.13 Soluble TM ameliorates non-immunological induced neuronal demyelination

EAE is a disease primarily driven by an immunological reaction, but other mechanisms, such as increased ROS-generation, independently contribute to demyelination [92, 93]. The above data suggest that soluble TM conveys neuronal protection by reducing ROS-generation within the CNS and in neurons. To evaluate whether soluble TM convey a protective effect in a non-immunological demyelination model we analysed mice fed a cuprizone diet (0.2%) for 5 weeks. Cuprizone induced marked demyelination in wt and to a larger degree in $TM^{Pro/Pro}$

mice after 5 weeks (Fig. 3.13.1), establishing that TM protects neuronal myelin in a non-immunological demyelination model. Solulin treatment protected wt and – to a larger extend – TM$^{Pro/Pro}$ mice from demyelination (Fig. 3.13.1). Hence, the protective effect of solulin against EAE is at least partially independent of an immune-modulatory function.
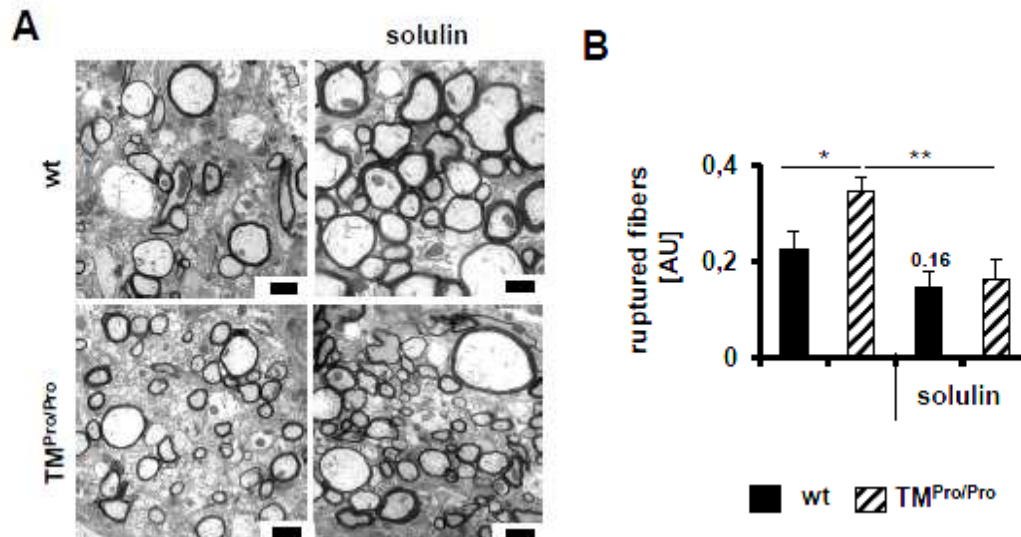
Fig. 3.13.1 Soluble TM ameliorates non-immunological induced neuronal demyelination
A: TEM images of mouse corpus callosum regions in the brain after feeding cuprizone diet for 5 weeks. Demyelination was aggravated in TM$^{Pro/Pro}$ mice. Solulin treatment impaired demyelination in both, wt and TM$^{Pro/Pro}$ mice. **B**: Bar graphs (down) summarising amount of ruptured nerve fibers. Scale bar: 1000 nm, N = 5. * $P < 0.05$; ** $P < 0.01$; Student´s t-test.

Taken together, these data demonstrate that basal endogenously impaired PC activation aggravates EAE, which is associated with increased ROS generation, impaired mitochondrial biogenesis, and impaired myelination in the CNS. These disease effects were partially reversible by restoring aPC or genetically restraining mitochondrial ROS generation, while treatment with solulin was more effective. The effects of TM on myelin are also apparent in a non-immunological model, revealing a function of TM in maintaining neuronal myelination independent of its immune-modulatory function.

4 Discussion

4.1 Thrombomodulin-mediated protein C activation maintains neuronal function and nociception

In the present study we demonstrate that TM-dependent PC activation constitutes a new endogenous pathway regulating nociception and neuron function within the CNS. The reduced nociceptive sensitivity in healthy mice with impaired PC-activation due to a point mutation in TM (TM^{Pro}) [71, 81] is related to a myelination defect in the CNS, while the function of peripheral nerves is unaffected. Disturbed myelination in the CNS of TM$^{Pro/Pro}$ mice is associated with increased mitochondrial ROS generation and mitochondrial dysfunction characterised by impaired activity of the electron transport chain, an altered CL-composition, increased oxidised CL, and an increased frequency of mitochondrial DNA mutations. Importantly, pharmacological or genetical approaches to compensate for defective PC activation in TM$^{Pro/Pro}$ mice correct these alterations and normalise the nociceptive sensitivity in TM$^{Pro/Pro}$ mice. These studies uncover a basal neurological defect in mice with disruption of the – primarily – endothelial derived cytoprotective TM-PC system.

Previously studies established a crucial neuroprotective function of PC in various disease models. Thus, aPC conveys protective effects in murine models of stroke, multiple sclerosis, amyotrophic lateral sclerosis (ALS) and neuronal apoptosis [11, 13, 45, 83, 94, 95]. *In vitro* aPC protects neurons from N-methyl-D-aspartate (NMDA) and staurosporine induced cell death [13]. Unlike in previous studies, in which the neuroprotective effect of aPC was only evaluated in the context in disease models, the current study establishes that TM-dependent PC activation is physiologically required for neuronal function. This suggests that impaired TM-function, as observed in various disease conditions such as atherosclerosis, diabetes, or sepsis [96-99], is sufficient to impair neuronal function, independently of additional disease related factors such as hyperglycemia or inflammation. Hence, we propose that impaired aPC generation is an independent and sufficient cause of impaired neurological function.

Functional TM-deficiency, either due to targeted endothelial deletion (TM$^{LoxP/LoxP}$ x Tie2^{Cre}) or the TM^{Pro} mutation, promotes fibrin deposition in various organs, but not in the brain [81, 100]. These observations suggested already that TM-dependent PC-activation might modulate CNS function at least partially independent of fibrin-formation. Congruently, a cytoprotective PC mutant with markedly reduced anticoagulant function (3K3A-APC) provides potent neuroprotection [101, 102]. The observation that TM-dependent PC activation maintains myelin integrity, stabilises mitochondrial function, and restricts mitochondrial ROS generation in the CNS provides new insights into the mechanisms

through which aPC conveys neuroprotection. Intriguingly, disease models previously used to evaluate the neuro-protective effect of aPC are all linked with increased ROS generation [37, 101, 103, 104]. The protective effects of aPC in neuronal disease models linked with increased ROS generation [37, 101, 103, 104] and the increased cerebral ROS generation in mice with impaired aPC generation (this study) are entirely congruent with aPC's antioxidant effects in other *in vitro* and *in vivo* models [19, 44, 69, 105]. Impaired mitochondrial function is apparent in numerous diseases, including severe inflammation and sepsis [106-110], and hence stabilising of mitochondrial function may be a general phenomenon contributing to aPC's cytoprotective effects. In the context of diabetic nephropathy loss of aPC generation can be compensated for by a concomitant loss of p66^{Shc} expression, a mitochondrial targeted pro-oxidant redox-protein [19]. Both p66^{Shc} deficiency and aPC convey neuro-protective effects in neuronal disease models such as EAE or stroke and neuronal apoptosis [13, 14, 111-113], suggesting an interaction of p66^{Shc} and aPC also in the context of neuronal disease. Alternatively, aPC's antioxidant effect may be related to its ability to suppress superoxide dismutase-1 expression in the CNS [83]. Whether the neuro-protective effects of aPC are related to reduced expression of p66^{Shc}, SOD1, or both remains to be evaluated.

Neurons do not express TM [100] and hence TM expressed by other cells, most likely endothelial cells, must activate aPC, which is then transported across the BBB by endothelial EPCR [12, 36]. The EPCR facilitated transport of aPC across the BBB under physiological conditions is entirely congruent with aPC's requirement for normal neuronal function, but at the same time implies that impaired EPCR mediated aPC transport across the BBB will induce neuronal defects similar to that observed in TM$^{Pro/Pro}$ mice. Accordingly, aPC's ability to reduce SOD1 expression in neuronal tissues is lost in mice with markedly reduced EPCR expression [83]. Endothelial dysfunction with reduced TM and EPCR function might hence endanger neuronal function through two independent and potentially additive effects: impaired PC-activation and impaired transport of aPC across the BBB. This may render the CNS particular vulnerable to diseases associated with reduced TM and EPCR function, such as vascular or inflammatory diseases.

The myelination defect associated with aPC deficiency (this study) implies that aPC's effects within the CNS depend at least partially on oligodendrocytes. Furthermore, the altered cerebral CL-profiled and (non-significant) alterations in the peripheral lipid profile in TM$^{Pro/Pro}$ mice [114] suggest that aPC may modulate cellular function by altering the lipid profile. This may affect prostaglandin metabolism and thus indirectly interfere with nociception, as previously demonstrated for PAR agonists [34, 115]. Further studies are needed to define the different cell population within the CNS that are regulated by aPC and the mechanisms and receptors involved.

All four PARs are expressed in the nervous system [9]. As in other tissues, the role of PARs in the nervous system is context dependent [116]. The baseline conduction velocity of peripheral nerves obtained from TM$^{Pro/Pro}$ mice was not different from that in wt mice. This does not exclude a role of PARs in regulating the function and nociception of peripheral nerves under disease conditions, as previously shown [117, 118], but establishes that under normal, non-diseased conditions loss of TM-dependent PC-activation primarily affects the function and ultrastructure of neurons within the CNS. The neuroprotective effect of aPC depends on PAR-3 both *in vivo* and *in vitro* [13, 83]. Of note, PAR-3 likewise conveys cytoprotective and antioxidant effects in renal cells [19, 22], suggesting that PAR-3 may regulate mitochondrial function in both brain and kidney. In regard to nociception studies hitherto focused on the role of PARs in afferent sensory neurons, linking the role of PARs to both pain-perception and inflammation [116, 119]. Importantly, loss of TM-dependent PC-activation is sufficient to impair nociception and cause neuronal dysfunction within the CNS even in the absence of additional disease promoting stimuli. Congruently PAR1 or PAR4 stimulation at sub-inflammatory doses increases the nociceptive threshold [35, 120]. The receptors conveying impaired nociception in TM$^{Pro/Pro}$ mice remain to be established. Principally, increased PAR1 and / or PAR4 by thrombin or impaired PAR3 activation due to low aPC levels may contribute to the observed phenotype. *In vivo* studies with cell-specific deletion of receptors will be required to define the receptor mechanisms involved.

Based on the current and previous results modulation of PAR signalling may provide a new therapeutic approach for peripheral neuropathies without provoking inflammation [121]. Such therapies will, however, not only affect nociception by modulating dorsal root ganglia [35, 120], but may have additional effects on secondary neurons relaying signals to the brain. The preclinical evaluation of therapeutic approaches directly targeting PAR-signalling hence has to carefully address potential effects on the ultrastructure of central neurons.

Importantly, restoring aPC in mice with defective aPC-generation reverses the neuronal dysfunction and normalises morphological alterations. Hence, pharmacological targeting the neuro-protective effect of aPC may constitute a save therapeutic approach to neuropathy and without causing structural and potentially harmful side-effects. Clinical studies evaluating the neuro-protective effect of the 3K3A-aPC mutant demonstrated a good safety profile in patients with acute stroke. Treatment of peripheral neuropathy would, however, require long-term treatment, potentially for months or years. Potential side-effect during long-term treatment can not be excluded and need to be evaluated. Importantly, mice with constitute high aPC levels due to a transgene expressing a human hyper-activatable PC-mutant (aPC^{high} mice) [21] have normal behaviour and lack symptoms indicative of neuronal impairment even at high age, suggesting that pharmacological targeting of aPC-mediated neuro-protection may be feasible and safe.

4.2 The thrombomodulin protein C system protects from myelin loss in EAE

After establishing a physiological role of TM-dependent PC activation for myelination we next evaluated whether TM-dependent PC activation aggravates the disease progression of demyelination models. Using mice with genetically enforced impaired TM-dependent PC activation we demonstrate a pathomechanistic relevance of reduced endogenous PC-activation in EAE. Compensating for impaired PC activation reduces ROS generation within the CNS, maintains myelination, and improves the disease outcome. Of note, soluble TM has superior efficacy, delaying the disease onset and reducing the disease severity. The myelin-protective effect is at least partially independent of the immune response, demonstrating that the TM-PC system conveys neuroprotective effects in EAE independent of its known immune-modulatory function.

Considering the above data demonstrating that endogenous TM stabilises mitochondrial function and the myelin-sheet in the absence of an inflammatory disease process and the established functional interaction of mitochondrial dysfunction and myelination these observations suggest that loss of TM function alters myelin-axon interaction and promotes a primary cyto-degenerative process in resident CNS cells, which predisposes to demyelinating diseases. A pathogenetic relevance of coagulation regulators, including TM, is supported by a recent transcriptomic meta-analysis of MS and its experimental models suggested [122]. Based on these data we propose that alterations within the TM-PC system cause primary alterations of mitochondrial function in the CNS predisposing to demyelination diseases. This hypothesis, which is congruent with the "inside-out" theory in the pathogenesis of MS [123], awaits further experimental evaluation.

Like aPC and solulin the thrombin-mutant W215A/E217A reduces demyelination in EAE-mice, which, however, was attributed to an anti-inflammatory effect [40]. The ability of solulin and aPC to directly protect primary CNS cells such as neurons and astrocytes [37, 124], the impaired myelination in TM-deficient mice (section 3.1, 3.7), and the myelin protective effect of solulin in a non-immune demyelination model (section 3.13) suggest that TM-PC based therapeutic strategies may independently target two important pathomechanisms in MS: inflammation and demyelination. This dual therapeutic tactic may provide a rationale for the astonishing efficacy of TM-PC based therapeutic strategies in neuronal disease models [125-127].

In particular in regard to demyelinating diseases such as MS the myelin-protective effect of soluble thrombomodulin – and potentially of aPC and W215A/E217A thrombin – may provide superior efficacy when compare to current anti-inflammatory strategies. Soluble TM and aPC mutants lacking anticoagulant function (3K3A-APC) are being evaluated in clinical studies [49, 128, 129] and given the current results and the urgent need of new therapeutic

approaches for patients with multiple sclerosis we propose that these substances should be considered for clinical studies. Importantly, 3K3A-APC is largely devoid of an endogenous anticoagulant function and solulin mimics the "on-demand" anticoagulant properties of endogenous thrombomodulin, reducing the risk of haemorrhage and hence increasing the safety of these newly developed therapeutics [49].

The myelin-protective effect observed here is associated with reduce mitochondrial ROS generation within the CNS. Enhanced ROS generation is a well-established factor aggravating EAE and is thought to promote multiple sclerosis in humans. An anti-oxidant effect of aPC and solulin has been previously established in other disease models [130] [19, 50, 95, 131] [82]. Furthermore, aPC protects from ROS-induced experimental ALS and reduces neuronal-cell death in stroke models by suppressing mitochondrial dysfunction [11, 19]. Indeed, aPC inhibits p66[Shc]-mediated mitochondrial ROS-generation and cell death in the context of diabetic nephropathy [19, 21] and EAE (as demonstrated). Furthermore, we uncovered a mitochondria-stabilizing effect of aPC. Similar to aPC p66[Shc] modulates the outcome of neurological diseases such as stroke, dementia, and EAE [59, 112, 132] and neuronal cell death [113, 133, 134]. These similarities imply that TM-dependent PC activation suppresses p66[Shc]-dependent ROS-generation and neuronal damage not only in EAE, but also in other neurological diseases.

Soluble thrombomodulin did not only improve the disease course in TM[Pro/Pro] mice, but also in wild-type mice. The efficacy of soluble TM in mice primarily expressing functional TM is most likely explained by an inflammation induced loss of TM-function in EAE-wt mice, a typical finding in humans with and animal models of inflammatory diseases [17, 95, 135, 136]. We failed to detect increased aPC generation using an established protocol in mice following soluble TM injection [21, 81, 100]. This observation supports direct neuro-protective effects of soluble TM independently of PC-activation [137]. Yet it needs to be pointed out that we determined *in vivo* PC-generation 24 h after the last injection of soluble TM and hence an intermittent increase of TM-mediated aPC generation, which is sufficient for cytoprotective effects [19, 83], cannot be excluded.

Inhibition of endogenous aPC using antibodies surprisingly resulted in protection from EAE [45], a finding ad odds with the current observation and those made by Han et al. [44] and Verbout et al. [40]. While Han and Verbout initiated treatment with aPC or W215A/E217A, respectively, at the time of maximal disease onset, Alabanza injected the inhibitory antibodies directly after induction of EAE, suggesting that the different timing may account for the observed disparities. However, in the current study genetic approaches were used, which mimic loss of aPC-generation or rescue of impaired TM-dependent PC-activation before disease onset, and solulin was injected starting on the 1st day of the disease induction. The current observations do not support the view that the disparities observed by Han, Verbout,

and Alabanza reflect the different timing of drug administration. Hence, other mechanisms must account for the observed disparities, such as hitherto unspecified effects of the PC-Ab complexes on the EAE-associated immune-response.

Previously several neuro-protective mechanisms of the TM-PC system have been proposed, including reduced leukocyte infiltration into or diminished cell death within the CNS and stabilization of the blood-brain barrier [83, 138]. We identify a hitherto unknown mitochondria- and myelin-stabilizing effect of the TM-PC system, which may provide TM-PC based therapeutics with superior properties compared to current anti-inflammatory therapies. In addition, we demonstrate that solulin, a soluble TM variant, conveys superior protection from EAE. These results encourage the analyses of solulin or other therapeutic strategies employing mechanisms targeted by the TM-PC system in future translational studies.

5 Conclusion

In this study we demonstrate that impairment of TM-dependent PC activation is sufficient to cause neuronal dysfunction in the absence of disease related processes, uncovering a hitherto unknown physiological function of TM-dependent PC activation for neuronal integrity. This newly discovered basal phenotype is associated with enhanced ROS production and mitochondrial dysfunction in the CNS. Importantly, these neuronal defects are reversible upon genetic or pharmacological substitution of aPC, establishing that this pathomechanisms is therapeutically amendable. These neuro-protective effects may provide TM-PC based therapeutics with superior properties compared to current anti-inflammatory therapies in demyelinating diseases as well as – potentially – in other neurodegenerative diseases.

Loss of the physiological CNS-stabilising function of the TM-PC system aggravates the disease course of EAE. Importantly, the neuronal consequences of impaired TM-dependent PC activation accelerate demyelinating diseases independent of the immunological reaction, supporting the "inside-out" model of MS. Restoring aPC levels or genetically restraining mitochondrial ROS production partially reversed the clinical disease onset and disease symptoms. Soluble thrombomodulin has pronounced protective properties, which are superior to therapeutic application of aPC itself, and was able to markedly improve the clinical EAE symptoms. These results provide new impetus for future studies exploring the involved mechanisms in greater detail and for translational studies evaluating TM-PC-based therapeutic strategies in patients with demyelinating diseases.

6 References

1. Spronk, H.M., J.W. Govers-Riemslag, and H. ten Cate, *The blood coagulation system as a molecular machine.* Bioessays, 2003. **25**(12): p. 1220-8.

2. Wang, W., et al., *Elements of the primary structure of thrombomodulin required for efficient thrombin-activable fibrinolysis inhibitor activation.* J Biol Chem, 2000. **275**(30): p. 22942-7.

3. Tsiang, M., S.R. Lentz, and J.E. Sadler, *Functional domains of membrane-bound human thrombomodulin. EGF-like domains four to six and the serine/threonine-rich domain are required for cofactor activity.* J Biol Chem, 1992. **267**(9): p. 6164-70.

4. Suzuki, K., et al., *Structure and expression of human thrombomodulin, a thrombin receptor on endothelium acting as a cofactor for protein C activation.* EMBO J, 1987. **6**(7): p. 1891-7.

5. Lu, R.L., et al., *The active site of the thrombin-thrombomodulin complex. A fluorescence energy transfer measurement of its distance above the membrane surface.* J Biol Chem, 1989. **264**(22): p. 12956-62.

6. Vu, T.K., et al., *Molecular cloning of a functional thrombin receptor reveals a novel proteolytic mechanism of receptor activation.* Cell, 1991. **64**(6): p. 1057-68.

7. Coughlin, S.R. and E. Camerer, *PARticipation in inflammation.* J Clin Invest, 2003. **111**(1): p. 25-7.

8. Bahou, W.F., *Protease-activated receptors.* Curr Top Dev Biol, 2003. **54**: p. 343-69.

9. Luo, W., Y. Wang, and G. Reiser, *Protease-activated receptors in the brain: receptor expression, activation, and functions in neurodegeneration and neuroprotection.* Brain Res Rev, 2007. **56**(2): p. 331-45.

10. Weiler, H. and B.H. Isermann, *Thrombomodulin.* J Thromb Haemost, 2003. **1**(7): p. 1515-24.

11. Griffin, J.H., et al., *Activated protein C and ischemic stroke.* Crit Care Med, 2004. **32**(5 Suppl): p. S247-53.

12. Deane, R., et al., *Endothelial protein C receptor-assisted transport of activated protein C across the mouse blood-brain barrier.* J Cereb Blood Flow Metab, 2009. **29**(1): p. 25-33.

13. Guo, H., et al., *Activated protein C prevents neuronal apoptosis via protease activated receptors 1 and 3.* Neuron, 2004. **41**(4): p. 563-72.

14. Andreou, A.P., et al., *Protective effects of non-anticoagulant activated protein C variant (D36A/L38D/A39V) in a murine model of ischaemic stroke.* PLoS One, 2015. **10**(4): p. e0122410.

15. Weijer, S., et al., *A thrombomodulin mutation that impairs activated protein C generation results in uncontrolled lung inflammation during murine tuberculosis.* Blood, 2005. **106**(8): p. 2761-8.

16. Kager, L.M., et al., *A thrombomodulin mutation that impairs active protein C generation is detrimental in severe pneumonia-derived gram-negative sepsis (melioidosis).* PLoS Negl Trop Dis, 2014. **8**(4): p. e2819.

17. Rajashekhar, G., et al., *Soluble thrombomodulin reduces inflammation and prevents microalbuminuria induced by chronic endothelial activation in transgenic mice.* Am J Physiol Renal Physiol, 2012. **302**(6): p. F703-12.

18. Li, W., et al., *Decreased activated protein C levels are inversely associated with the urinary albumin excretion rate in patients with type 2 diabetes.* Clin Lab, 2014. **60**(2): p. 261-6.

19. Bock, F., et al., *Activated protein C ameliorates diabetic nephropathy by epigenetically inhibiting the redox enzyme p66Shc.* Proc Natl Acad Sci U S A, 2013. **110**(2): p. 648-53.

20. Gil-Bernabe, P., et al., *Exogenous activated protein C inhibits the progression of diabetic nephropathy.* J Thromb Haemost, 2012. **10**(3): p. 337-46.

21. Isermann, B., et al., *Activated protein C protects against diabetic nephropathy by inhibiting endothelial and podocyte apoptosis.* Nat Med, 2007. **13**(11): p. 1349-58.

22. Madhusudhan, T., et al., *Cytoprotective signaling by activated protein C requires protease-activated receptor-3 in podocytes.* Blood, 2012. **119**(3): p. 874-83.

23. Soh, U.J. and J. Trejo, *Activated protein C promotes protease-activated receptor-1 cytoprotective signaling through beta-arrestin and dishevelled-2 scaffolds.* Proc Natl Acad Sci U S A, 2011. **108**(50): p. E1372-80.

24. Bae, J.S., et al., *The ligand occupancy of endothelial protein C receptor switches the protease-activated receptor 1-dependent signaling specificity of thrombin from a permeability-enhancing to a barrier-protective response in endothelial cells.* Blood, 2007. **110**(12): p. 3909-16.

25. Hafer-Macko, C.E., et al., *Thrombomodulin deficiency in human diabetic nerve microvasculature.* Diabetes, 2002. **51**(6): p. 1957-63.

26. Haslbeck, M., *[New options in the treatment of various forms of diabetic neuropathy].* MMW Fortschr Med, 2004. **146**(21): p. 47-50.

27. Dyck, P.J., et al., *The Rochester Diabetic Neuropathy Study: reassessment of tests and criteria for diagnosis and staged severity.* Neurology, 1992. **42**(6): p. 1164-70.

28. Nathan, D.M., *Long-term complications of diabetes mellitus.* N Engl J Med, 1993. **328**(23): p. 1676-85.

29. Ramchandren, S., et al., *Peripheral nerve vasculitis presenting as complex regional pain syndrome.* J Clin Neuromuscul Dis, 2008. **10**(2): p. 61-4.

30. Chaudhry, V., J. Russell, and A. Belzberg, *Decompressive surgery of lower limbs for symmetrical diabetic peripheral neuropathy.* Cochrane Database Syst Rev, 2008(3): p. CD006152.

31. Vance, K.M., R.C. Rogers, and G.E. Hermann, *PAR1-activated astrocytes in the nucleus of the solitary tract stimulate adjacent neurons via NMDA receptors.* J Neurosci, 2015. **35**(2): p. 776-85.

32. Kim, Y.H., et al., *Protease-activated receptor 2 activation inhibits N-type Ca2+ currents in rat peripheral sympathetic neurons.* Mol Cells, 2014. **37**(11): p. 804-11.

33. Zhao, P., et al., *Neutrophil Elastase Activates Protease-activated Receptor-2 (PAR2) and Transient Receptor Potential Vanilloid 4 (TRPV4) to Cause Inflammation and Pain.* J Biol Chem, 2015. **290**(22): p. 13875-87.

34. Vergnolle, N., et al., *Proteinase-activated receptor-2 and hyperalgesia: A novel pain pathway.* Nat Med, 2001. **7**(7): p. 821-6.

35. Asfaha, S., et al., *Proteinase-activated receptor-1 agonists attenuate nociception in response to noxious stimuli.* Br J Pharmacol, 2002. **135**(5): p. 1101-6.

36. Maggio, N., et al., *The anticoagulant activated protein C (aPC) promotes metaplasticity in the hippocampus through an EPCR-PAR1-S1P1 receptors dependent mechanism.* Hippocampus, 2014. **24**(8): p. 1030-8.

37. Gorbacheva, L., et al., *NF-kappaB-dependent and -independent pathways in the protective effects of activated protein C in hippocampal and cortical neurons at excitotoxicity.* Neurochem Int, 2013. **63**(2): p. 101-11.

38. Maggio, N., et al., *Thrombin regulation of synaptic plasticity: implications for physiology and pathology.* Exp Neurol, 2013. **247**: p. 595-604.

39. Compston, A. and A. Coles, *Multiple sclerosis.* Lancet, 2008. **372**(9648): p. 1502-17.

40. Verbout, N.G., et al., *Thrombin mutant W215A/E217A treatment improves neurological outcome and attenuates central nervous system damage in experimental autoimmune encephalomyelitis.* Metab Brain Dis, 2015. **30**(1): p. 57-65.

41. Gallo, P. and B. Van Wijmeersch, *Overview of the management of relapsing-remitting multiple sclerosis and practical recommendations.* Eur J Neurol, 2015. **22 Suppl 2**: p. 14-21.

42. Skundric, D.S., W.W. Cruikshank, and J. Drulovic, *Role of IL-16 in CD4+ T cell-mediated regulation of relapsing multiple sclerosis.* J Neuroinflammation, 2015. **12**: p. 78.

43.   Jamshidian, A. and M. Gharagozloo, *Can plasma exchange therapy induce regulatory T lymphocytes in multiple sclerosis patients?* Clin Exp Immunol, 2012. **168**(1): p. 75-7.

44.   Han, M.H., et al., *Proteomic analysis of active multiple sclerosis lesions reveals therapeutic targets.* Nature, 2008. **451**(7182): p. 1076-81.

45.   Alabanza, L.M., et al., *Inhibition of endogenous activated protein C attenuates experimental autoimmune encephalomyelitis by inducing myeloid-derived suppressor cells.* J Immunol, 2013. **191**(7): p. 3764-77.

46.   Cantwell, A.M. and E. Di Cera, *Rational design of a potent anticoagulant thrombin.* J Biol Chem, 2000. **275**(51): p. 39827-30.

47.   Tsukada, N., et al., *Thrombomodulin in the sera of patients with multiple sclerosis and human lymphotropic virus type-1-associated myelopathy.* J Neuroimmunol, 1995. **56**(1): p. 113-6.

48.   Festoff, B.W., et al., *Soluble thrombomodulin levels in plasma of multiple sclerosis patients and their implication.* J Neurol Sci, 2012. **323**(1-2): p. 61-5.

49.   van Iersel, T., et al., *Phase I study of Solulin, a novel recombinant soluble human thrombomodulin analogue.* Thromb Haemost, 2011. **105**(2): p. 302-12.

50.   Su, E.J., et al., *The thrombomodulin analog Solulin promotes reperfusion and reduces infarct volume in a thrombotic stroke model.* J Thromb Haemost, 2011. **9**(6): p. 1174-82.

51.   Lin, J.H., et al., *Modulation of glycosaminoglycan addition in naturally expressed and recombinant human thrombomodulin.* J Biol Chem, 1994. **269**(40): p. 25021-30.

52.   Xu, J., et al., *Endogenous activated protein C signaling is critical to protection of mice from lipopolysaccaride-induced septic shock.* J Thromb Haemost, 2009. **7**(5): p. 851-6.

53.   Borissoff, J.I., et al., *Genetic and pharmacological modifications of thrombin formation in apolipoprotein e-deficient mice determine atherosclerosis severity and atherothrombosis onset in a neutrophil-dependent manner.* PLoS One, 2013. **8**(2): p. e55784.

54.   Zhou, D., et al., *A method for detecting and preventing negative RNA interference in preparation of lentiviral vectors for siRNA delivery.* RNA, 2009. **15**(4): p. 732-40.

55.   Dutta, R., et al., *Mitochondrial dysfunction as a cause of axonal degeneration in multiple sclerosis patients.* Ann Neurol, 2006. **59**(3): p. 478-89.

56.   Mahad, D., et al., *Mitochondrial defects in acute multiple sclerosis lesions.* Brain, 2008. **131**(Pt 7): p. 1722-35.

57.   Craner, M.J., et al., *Co-localization of sodium channel Nav1.6 and the sodium-calcium exchanger at sites of axonal injury in the spinal cord in EAE.* Brain, 2004. **127**(Pt 2): p. 294-303.

58.   Craner, M.J., et al., *Molecular changes in neurons in multiple sclerosis: altered axonal expression of Nav1.2 and Nav1.6 sodium channels and Na+/Ca2+ exchanger.* Proc Natl Acad Sci U S A, 2004. **101**(21): p. 8168-73.

59.   Su, K.G., et al., *Genetic inactivation of the p66 isoform of ShcA is neuroprotective in a murine model of multiple sclerosis.* Eur J Neurosci, 2012. **35**(4): p. 562-71.

60.   Su, K.G., et al., *Axonal degeneration in multiple sclerosis: the mitochondrial hypothesis.* Curr Neurol Neurosci Rep, 2009. **9**(5): p. 411-7.

61.   Bernardi, P., et al., *The mitochondrial permeability transition from in vitro artifact to disease target.* FEBS J, 2006. **273**(10): p. 2077-99.

62.   Rasola, A. and P. Bernardi, *The mitochondrial permeability transition pore and its involvement in cell death and in disease pathogenesis.* Apoptosis, 2007. **12**(5): p. 815-33.

63.   Migliaccio, E., et al., *The p66shc adaptor protein controls oxidative stress response and life span in mammals.* Nature, 1999. **402**(6759): p. 309-13.

64.   Giorgio, M., et al., *Electron transfer between cytochrome c and p66Shc generates reactive oxygen species that trigger mitochondrial apoptosis.* Cell, 2005. **122**(2): p. 221-33.

65.   Pinton, P., et al., *Protein kinase C beta and prolyl isomerase 1 regulate mitochondrial effects of the life-span determinant p66Shc.* Science, 2007. **315**(5812): p. 659-63.

66.   Camici, G.G., et al., *Genetic deletion of p66(Shc) adaptor protein prevents hyperglycemia-induced endothelial dysfunction and oxidative stress.* Proc Natl Acad Sci U S A, 2007. **104**(12): p. 5217-22.

67.   Furugohri, T. and Y. Morishima, *Paradoxical enhancement of the intrinsic pathway-induced thrombin generation in human plasma by melagatran, a direct thrombin inhibitor, but not edoxaban, a direct factor Xa inhibitor, or heparin.* Thromb Res, 2015. **136**(3): p. 658-62.

68.   Sperandio, O., et al., *Identification of novel small molecule inhibitors of activated protein C.* Thromb Res, 2014. **133**(6): p. 1105-14.

69.   Dong, W., et al., *Activated Protein C Ameliorates Renal Ischemia-Reperfusion Injury by Restricting Y-Box Binding Protein-1 Ubiquitination.* J Am Soc Nephrol, 2015.

70.   Karlsson, U. and R.L. Schultz, *Fixation of the Central Nervous System from Electron Microscopy by Aldehyde Perfusion. I. Preservation with Aldehyde Perfusates Versus Direct Perfusion with Osmium Tetroxide with Special Reference to Membranes and the Extracellular Space.* J Ultrastruct Res, 1965. **12**: p. 160-86.

71.   Weiler-Guettler, H., et al., *A targeted point mutation in thrombomodulin generates viable mice with a prethrombotic state.* J Clin Invest, 1998. **101**(9): p. 1983-91.

72.   Nemoto, S. and T. Finkel, *Redox regulation of forkhead proteins through a p66shc-dependent signaling pathway.* Science, 2002. **295**(5564): p. 2450-2.

73.   Giorgio, M., et al., *The p66Shc knocked out mice are short lived under natural condition.* Aging Cell, 2012. **11**(1): p. 162-8.

74.   Chen, M.K., et al., *Peripheral benzodiazepine receptor imaging in CNS demyelination: functional implications of anatomical and cellular localization.* Brain, 2004. **127**(Pt 6): p. 1379-92.

75.   Airaksinen, M.S., et al., *Specific subtypes of cutaneous mechanoreceptors require neurotrophin-3 following peripheral target innervation.* Neuron, 1996. **16**(2): p. 287-95.

76.   Price, M.P., et al., *The mammalian sodium channel BNC1 is required for normal touch sensation.* Nature, 2000. **407**(6807): p. 1007-11.

77.   Walter, P., H.A. Lardy, and D. Johnson, *Antibiotics as tools for metabolic studies. X. Inhibition of phosphoryl transfer reactions in mitochondria by peliomycin, ossamycin, and venturicidin.* J Biol Chem, 1967. **242**(21): p. 5014-8.

78.   Robb-Gaspers, L.D., et al., *Coupling between cytosolic and mitochondrial calcium oscillations: role in the regulation of hepatic metabolism.* Biochim Biophys Acta, 1998. **1366**(1-2): p. 17-32.

79.   Robb-Gaspers, L.D., et al., *Integrating cytosolic calcium signals into mitochondrial metabolic responses.* EMBO J, 1998. **17**(17): p. 4987-5000.

80.   Bradford, M.M., *A rapid and sensitive method for the quantitation of microgram quantities of protein utilizing the principle of protein-dye binding.* Anal Biochem, 1976. **72**: p. 248-54.

81.   Weiler, H., et al., *Characterization of a mouse model for thrombomodulin deficiency.* Arterioscler Thromb Vasc Biol, 2001. **21**(9): p. 1531-7.

82.   Yamaji, K., et al., *Activated protein C, a natural anticoagulant protein, has antioxidant properties and inhibits lipid peroxidation and advanced glycation end products formation.* Thromb Res, 2005. **115**(4): p. 319-25.

83.   Zhong, Z., et al., *Activated protein C therapy slows ALS-like disease in mice by transcriptionally inhibiting SOD1 in motor neurons and microglia cells.* J Clin Invest, 2009. **119**(11): p. 3437-49.

84.   Esmon, C.T. and J.D. Glass, *The APCs of neuroprotection.* J Clin Invest, 2009. **119**(11): p. 3205-7.

85.   Kim, J., et al., *Mitochondrial loss, dysfunction and altered dynamics in Huntington's disease.* Hum Mol Genet, 2010. **19**(20): p. 3919-35.

86. Sawada, N., et al., *Endothelial PGC-1alpha mediates vascular dysfunction in diabetes.* Cell Metab, 2014. **19**(2): p. 246-58.

87. Cui, L., et al., *Transcriptional repression of PGC-1alpha by mutant huntingtin leads to mitochondrial dysfunction and neurodegeneration.* Cell, 2006. **127**(1): p. 59-69.

88. Martens, J.C., et al., *Oxidation of cardiolipin is involved in functional impairment and disintegration of liver mitochondria by hypoxia/reoxygenation in the presence of increased Ca(2)(+) concentrations.* Mol Cell Biochem, 2014. **394**(1-2): p. 119-27.

89. Pope, S., J.M. Land, and S.J. Heales, *Oxidative stress and mitochondrial dysfunction in neurodegeneration; cardiolipin a critical target?* Biochim Biophys Acta, 2008. **1777**(7-8): p. 794-9.

90. Mulligan, C.M., et al., *Dietary linoleate preserves cardiolipin and attenuates mitochondrial dysfunction in the failing rat heart.* Cardiovasc Res, 2012. **94**(3): p. 460-8.

91. Wu, C.Y., et al., *A persistent level of Cisd2 extends healthy lifespan and delays aging in mice.* Hum Mol Genet, 2012. **21**(18): p. 3956-68.

92. van der Goes, A., et al., *Reactive oxygen species are required for the phagocytosis of myelin by macrophages.* J Neuroimmunol, 1998. **92**(1-2): p. 67-75.

93. Starossom, S.S., et al., *Platelets Play Differential Role During the Initiation and Progression of Autoimmune Neuroinflammation.* Circ Res, 2015.

94. Wang, Y., et al., *Activated protein C analog protects from ischemic stroke and extends the therapeutic window of tissue-type plasminogen activator in aged female mice and hypertensive rats.* Stroke, 2013. **44**(12): p. 3529-36.

95. Geiger, H., et al., *Pharmacological targeting of the thrombomodulin-activated protein C pathway mitigates radiation toxicity.* Nat Med, 2012. **18**(7): p. 1123-9.

96. Rezaie, A.R. and L. Yang, *Mutagenesis studies toward understanding the mechanism of the cofactor function of thrombomodulin.* Biophys Chem, 2005. **117**(3): p. 255-61.

97. Dargaud, Y., et al., *Characterization of an autosomal dominant bleeding disorder caused by a thrombomodulin mutation.* Blood, 2015. **125**(9): p. 1497-501.

98. Wang, H., et al., *The lectin-like domain of thrombomodulin ameliorates diabetic glomerulopathy via complement inhibition.* Thromb Haemost, 2012. **108**(6): p. 1141-53.

99. Li, Y.H., et al., *Thrombomodulin plays an important role in arterial remodeling and neointima formation in mouse carotid ligation model.* Thromb Haemost, 2006. **95**(1): p. 128-33.

100. Isermann, B., et al., *Endothelium-specific loss of murine thrombomodulin disrupts the protein C anticoagulant pathway and causes juvenile-onset thrombosis.* J Clin Invest, 2001. **108**(4): p. 537-46.

101. Guo, H., et al., *Neuroprotective activities of activated protein C mutant with reduced anticoagulant activity.* Eur J Neurosci, 2009. **29**(6): p. 1119-30.

102. Mosnier, L.O., et al., *Influence of the 3K3A-activated protein C variant on the plasma clot lysis activity of t-PA and of t-PA on the variant's anticoagulant activity.* J Thromb Haemost, 2013. **11**(11): p. 2059-62.

103. Guo, H., et al., *An activated protein C analog stimulates neuronal production by human neural progenitor cells via a PAR1-PAR3-S1PR1-Akt pathway.* J Neurosci, 2013. **33**(14): p. 6181-90.

104. Petraglia, A.L., et al., *Activated protein C is neuroprotective and mediates new blood vessel formation and neurogenesis after controlled cortical impact.* Neurosurgery, 2010. **66**(1): p. 165-71; discussion 171-2.

105. Sopel, M.J., et al., *Treatment with activated protein C (aPC) is protective during the development of myocardial fibrosis: an angiotensin II infusion model in mice.* PLoS One, 2012. **7**(9): p. e45663.

106. Errea, O., et al., *The disruption of mitochondrial axonal transport is an early event in neuroinflammation.* J Neuroinflammation, 2015. **12**(1): p. 152.

107. Kim, H.R., et al., *Mitochondrial DNA aberrations and pathophysiological implications in hematopoietic diseases, chronic inflammatory diseases, and cancers.* Ann Lab Med, 2015. **35**(1): p. 1-14.

108. De Felice, F.G. and S.T. Ferreira, *Inflammation, defective insulin signaling, and mitochondrial dysfunction as common molecular denominators connecting type 2 diabetes to Alzheimer disease.* Diabetes, 2014. **63**(7): p. 2262-72.

109. Protti, A., et al., *Mitochondrial changes in platelets are not related to those in skeletal muscle during human septic shock.* PLoS One, 2014. **9**(5): p. e96205.

110. d'Avila, J.C., et al., *Sepsis induces brain mitochondrial dysfunction.* Crit Care Med, 2008. **36**(6): p. 1925-32.

111. Wang, Y., et al., *Neurotoxicity of the anticoagulant-selective E149A-activated protein C variant after focal ischemic stroke in mice.* Blood Cells Mol Dis, 2013. **51**(2): p. 104-8.

112. Spescha, R.D., et al., *Post-ischaemic silencing of p66Shc reduces ischaemia/reperfusion brain injury and its expression correlates to clinical outcome in stroke.* Eur Heart J, 2015. **36**(25): p. 1590-600.

113. Zhu, M., et al., *Propofol protects against angiotensin II-induced mouse hippocampal HT22 cells apoptosis via inhibition of p66Shc mitochondrial translocation.* Neuromolecular Med, 2014. **16**(4): p. 772-81.

114. Seehaus, S., et al., *Hypercoagulability inhibits monocyte transendothelial migration through protease-activated receptor-1-, phospholipase-Cbeta-, phosphoinositide 3-*

kinase-, and nitric oxide-dependent signaling in monocytes and promotes plaque stability. Circulation, 2009. **120**(9): p. 774-84.

115. van Dijk, G., et al., *Integrative neurobiology of metabolic diseases, neuroinflammation, and neurodegeneration.* Front Neurosci, 2015. **9**: p. 173.

116. Vergnolle, N., *Protease-activated receptors as drug targets in inflammation and pain.* Pharmacol Ther, 2009. **123**(3): p. 292-309.

117. Lu, J., et al., *Pain in experimental autoimmune encephalitis: a comparative study between different mouse models.* J Neuroinflammation, 2012. **9**: p. 233.

118. Kurejova, M., et al., *An improved behavioural assay demonstrates that ultrasound vocalizations constitute a reliable indicator of chronic cancer pain and neuropathic pain.* Mol Pain, 2010. **6**: p. 18.

119. Ding-Pfennigdorff, D., B. Averbeck, and M. Michaelis, *Stimulation of PAR-2 excites and sensitizes rat cutaneous C-nociceptors to heat.* Neuroreport, 2004. **15**(13): p. 2071-5.

120. Asfaha, S., et al., *Protease-activated receptor-4: a novel mechanism of inflammatory pain modulation.* Br J Pharmacol, 2007. **150**(2): p. 176-85.

121. Vergnolle, N., et al., *Proteinase-activated receptors: novel signals for peripheral nerves.* Trends Neurosci, 2003. **26**(9): p. 496-500.

122. Raddatz, B.B., et al., *Transcriptomic meta-analysis of multiple sclerosis and its experimental models.* PLoS One, 2014. **9**(1): p. e86643.

123. Witte, M.E., et al., *Mitochondrial dysfunction contributes to neurodegeneration in multiple sclerosis.* Trends Mol Med, 2014. **20**(3): p. 179-87.

124. Niego, B., et al., *Thrombin-induced activation of astrocytes in mixed rat hippocampal cultures is inhibited by soluble thrombomodulin.* Brain Res, 2011. **1381**: p. 38-51.

125. Huseby, E.S., et al., *Role of T cell-glial cell interactions in creating and amplifying central nervous system inflammation and multiple sclerosis disease symptoms.* Front Cell Neurosci, 2015. **9**: p. 295.

126. Turner, M.J., et al., *Reduction of inflammation and preservation of neurological function by anti-CD52 therapy in murine experimental autoimmune encephalomyelitis.* J Neuroimmunol, 2015. **285**: p. 4-12.

127. Walker-Caulfield, M.E., J.K. Hatfield, and M.A. Brown, *Dynamic changes in meningeal inflammation correspond to clinical exacerbations in a murine model of relapsing-remitting multiple sclerosis.* J Neuroimmunol, 2015. **278**: p. 112-22.

128. Williams, P.D., et al., *Preclinical safety and pharmacokinetic profile of 3K3A-APC, a novel, modified activated protein C for ischemic stroke.* Curr Pharm Des, 2012. **18**(27): p. 4215-22.

129. Lyden, P., et al., *Phase 1 safety, tolerability and pharmacokinetics of 3K3A-APC in healthy adult volunteers.* Curr Pharm Des, 2013. **19**(42): p. 7479-85.

130. Bock, F., et al., *Activated protein C based therapeutic strategies in chronic diseases.* Thromb Haemost, 2014. **111**(4): p. 610-7.

131. Foley, J.H., et al., *Solulin increases clot stability in whole blood from humans and dogs with hemophilia.* Blood, 2012. **119**(15): p. 3622-8.

132. Kanninen, K., et al., *Nuclear factor erythroid 2-related factor 2 protects against beta amyloid.* Mol Cell Neurosci, 2008. **39**(3): p. 302-13.

133. Andoh, T., S.Y. Lee, and C.C. Chiueh, *Preconditioning regulation of bcl-2 and p66shc by human NOS1 enhances tolerance to oxidative stress.* FASEB J, 2000. **14**(14): p. 2144-6.

134. Spescha, R.D., et al., *Deletion of the ageing gene p66(Shc) reduces early stroke size following ischaemia/reperfusion brain injury.* Eur Heart J, 2013. **34**(2): p. 96-103.

135. Yoshimura, J., et al., *Benefit profile of recombinant human soluble thrombomodulin in sepsis-induced disseminated intravascular coagulation: a multicenter propensity score analysis.* Crit Care, 2015. **19**: p. 78.

136. Xu, T., et al., *Protective effects of thrombomodulin on microvascular permeability after subarachnoid hemorrhage in mouse model.* Neuroscience, 2015. **299**: p. 18-27.

137. Festoff, B.W., et al., *Neuroprotective effects of recombinant thrombomodulin in controlled contusion spinal cord injury implicates thrombin signaling.* J Neurotrauma, 2004. **21**(7): p. 907-22.

138. Cheng, T., et al., *Activated protein C blocks p53-mediated apoptosis in ischemic human brain endothelium and is neuroprotective.* Nat Med, 2003. **9**(3): p. 338-42.

7 List of publications

Publications

Activated Protein C Ameliorates Renal Ischemia-Reperfusion Injury by Restricting Y-Box Binding Protein-1 Ubiquitination.
Dong W, Wang H, Shahzad K, Bock F, Al-Dabet MM, Ranjan S, **Wolter J**, Kohli S, Hoffmann J, Dhople VM, Zhu C, Lindquist JA, Esmon CT, Gröne E, Gröne HJ, Madhusudhan T, Mertens PR, Schlüter D, Isermann B.
J Am Soc Nephrol. 2015 May 26. pii: ASN.2014080846. [Epub ahead of print],
Impact factor: 9,34

Defective podocyte insulin signalling through p85-XBP1 promotes ATF6-dependent maladaptive ER-stress response in diabetic nephropathy.
Madhusudhan T, Wang H, Dong W, Ghosh S, Bock F, Thangapandi VR, Ranjan S, **Wolter J**, Kohli S, Shahzad K, Heidel F, Krueger M, Schwenger V, Moeller MJ, Kalinski T, Reiser J, Chavakis T, Isermann B.
Nat Commun. 2015 Mar 10;6:6496. doi: 10.1038/ncomms7496.
Impact factor: 11,47

Nlrp3-inflammasome activation in non-myeloid-derived cells aggravates diabetic nephropathy.
Shahzad K, Bock F, Dong W, Wang H, Kopf S, Kohli S, Al-Dabet MM, Ranjan S, **Wolter J**, Wacker C, Biemann R, Stoyanov S, Reymann K, Söderkvist P, Groß O, Schwenger V, Pahernik S, Nawroth PP, Gröne HJ, Madhusudhan T, Isermann B.
Kidney Int. 2015 Jan;87(1):74-84. doi: 10.1038/ki.2014.271. Epub 2014 Jul 30.
Impact factor: 8,56

Activated protein C ameliorates diabetic nephropathy by epigenetically inhibiting the redox enzyme p66Shc.
Bock F, Shahzad K, Wang H, Stoyanov S, **Wolter J**, Dong W, Pelicci PG, Kashif M, Ranjan S, Schmidt S, Ritzel R, Schwenger V, Reymann KG, Esmon CT, Madhusudhan T, Nawroth PP, Isermann B.
Proc Natl Acad Sci U S A. 2013 Jan 8;110(2):648-53.
Impact factor: 9,81

The lectin-like domain of thrombomodulin ameliorates diabetic glomerulopathy via complement inhibition.
Wang H, Vinnikov I, Shahzad K, Bock F, Ranjan S, **Wolter J**, Kashif M, Oh J, Bierhaus A, Nawroth P, Kirschfink M, Conway EM, Madhusudhan T, Isermann B.
Thromb Haemost. 2012 Dec;108(6):1141-53.
Impact factor: 4,98

Nuclear factor erythroid-derived 2 (Nfe2) regulates JunD DNA-binding activity via acetylation: a novel mechanism regulating trophoblast differentiation.
Kashif M, Hellwig A, Hashemolhosseini S, Kumar V, Bock F, Wang H, Shahzad K, Ranjan S, **Wolter J**, Madhusudhan T, Bierhaus A, Nawroth P, Isermann B.
J Biol Chem. 2012 Feb 17;287(8):5400-11.

Minocycline reduces plaque size in diet induced atherosclerosis via p27(Kip1).
Shahzad K, Thati M, Wang H, Kashif M, **Wolter J**, Ranjan S, He T, Zhou Q, Blessing E, Bierhaus A, Nawroth PP, Isermann B.

Atherosclerosis. 2011 Nov;219(1):74-83.
Impact factor: 3,99

p45NF-E2 represses Gcm1 in trophoblast cells to regulate syncytium formation, placental vascularization and embryonic growth.
Kashif M, Hellwig A, Kolleker A, Shahzad K, Wang H, Lang S, **Wolter J**, Thati M, Vinnikov I, Bierhaus A, Nawroth PP, Isermann B.
Development. 2011 Jun;138(11):2235-47.
Impact factor: 6,46

8 Curriculum vitae

Personal data:

Name: Juliane Wolter
Gender: Female
Date of Birth: 30.10.1981
Place of Birth: Salzwedel
Nationality: German
Marital status: Single
Address: Jutta-Balk-Straße 4, 39104 Magdeburg
                   Tel.: 0176 29 00 80 43
                   e-mail: juliane.wolter@gmx.de

Education:

08/2011 – 10/2015	PhD student AG Prof. Dr. med. Berend Isermann Department of Clinical Chemistry and Pathobiochemistry University Hospital Magdeburg
02/2009 – 07/2011	PhD student AG Prof. Dr. med. Berend Isermann Medical Clinic I University Hospital Heidelberg
10/2003 - 12/2008	Diplom degree in Biology Georg-August-University Göttingen
03/2003 – 09/2003	Dental assistant Dental surgery Dr. Trakis/Dr. Hahn in Wolfsburg
08/2000 – 02/2003	Apprenticeship as dental assistant Dental surgery Dr. Trakis/Dr. Hahn in Wolfsburg
09/1996 – 07/2000	Visit of Gymnasium Beetzendorf
09/1992 - 08/1996	Käthe-Kollwitz-Gymnasium in Dähre

(Juliane Wolter)

9   Declaration

Hiermit erkläre ich, dass ich die von mir zur Promotion eingereichte Dissertation mit dem Titel

A novel function of the endothelial thrombomodulin-protein C system for cellular function in the CNS

im Institut für Klinische Chemie und Pathobiochemie

mit Unterstützung durch Prof. Dr. med. Berend Isermann

selbständig verfasst und ohne sonstige Hilfe durchgeführt und bei der Abfassung der Dissertation keine anderen als die dort aufgeführten Hilfsmittel benutzt habe.

Weiterhin erkläre ich, dass ich weder diese noch eine andere Arbeit zur Erlangung des akademischen Grades doctor rerum naturalium (Dr. rer. nat.) an anderen Einrichtungen eingereicht habe.

Magdeburg, den 26.10.2015

Juliane Wolter

10 Acknowledgement

I would like to thank Prof. Rohini Kuner and especially Dr. Martina Kurejova (for nerve-skin-preparations), who trained me how to perfom fancy experiments.

Finally, I would like to appreciate my beloved family for their sustained considerations and great confidence in me throughout all these years. Without your support and encouragement it would have been unimaginable for me to indulge my passion for this long "trip". I love you.

A big thank you for your support to all the people I may have forgotten to mention, as well as expressing my apology that I could not mention personally one by one.

May the force be with you!